MECHANISMS OF CELL PENETRATION BY SSRNA BACTERIOPHAGES

A Dissertation

by

LAITH ABDELQADER HARB

Submitted to the Graduate and Professional School of
Texas A&M University
in partial fulfillment of the requirements for the degree of

DOCTOR OF PHILOSOPHY

Chair of Committee,	Jean-Philippe Pellois
Committee Members,	Lanying Zeng
	Ryland F. Young
	Jason Gill
Head of Department,	Josh Wand

May 2022

Major Subject: Biochemistry

ABSTRACT

Bacteriophages are being reevaluated for their therapeutic potential, however, the pathways and mechanisms guiding genome transfer from the phage capsid to the host cytoplasm, a critical step in the phage infection cycle, remain unclear. Phages ensure their viral genome enters the host by traversing the host cell envelope. Phages infecting gram-negative bacteria, therefore, must contest the outer membrane, a periplasmic peptidoglycan meshwork, and the inner membrane to accomplish this task. While several canonical phages have evolved dedicated proteins and interaction pathways to facilitate penetration, less is known about how the smaller, simpler single-stranded (ss)RNA phages manage to penetrate the cell. The ssRNA phages universally infect their hosts by exploiting the mechanics of diverse, host-encoded retractile pili. These pili can facilitate significant biological functions, such as transfer of genetic material between cells, bacterial motility, and persistence. The purpose of the work outlined in this dissertation is to understand the function and role of pili and their respective machinery in guiding cell penetration among ssRNA phages. Genetic and fluorescence microscopy approaches yielded a foundational result: initial penetration of the viral payload causes a severance and release of surface pili from the host cell. This phenomenon was present in several paradigm phages, including the ssRNA coliphages MS2 and Qβ, interacting with conjugative F-pili, as well as PP7, a phage infecting *Pseudomonas aeruginosa* through type IV motility pili. For MS2, it was revealed that passage through the cell envelope requires the host-encoded coupling protein, TraD. For PP7, forces generated by an

auxiliary retraction protein, PilU, was essential for cell penetration. Additionally, an experimental evolution approach was used to select for MS2 variants with improved plaquing to better understand how MS2 utilizes TraD for cell penetration. A single mutation in the maturation protein, responsible for pilus recognition, permitted plaquing in a cell background producing only basal levels of TraD. As well, the nucleotide binding activity of TraD was found to be essential for cell penetration by MS2. Lastly, quantitative analysis of F-pili secretion and dynamics was performed using several F-pilus machinery mutants to better understand how each gene affects the formation of conjugative pili. Many subunits of the pilus machine were found to be essential for pilus formation, while others promote pilus length and frequency. Overall, the work presented here provides a thorough examination of pilus-phage systems, exploring the pathways underlying pilus synthesis, function, and their role as facilitators of ssRNA phage cell penetration.

DEDICATION

This dissertation is dedicated to my mother, Rula, and my undergraduate mentors from James Madison University: Drs. Louise Temple-Rosebrook, Ronald Raab, Yanjie Zhang, and Eric Pappas. Thank you for believing in me.

ACKNOWLEDGEMENTS

I would like to thank my advisor, Dr. Lanying Zeng for her support and encouragement throughout my graduate career. I appreciate her patience, expertise, and the freedom she affords me to explore my own ideas in the laboratory. I am also thankful for her willingness to share her perspective and valuable insights about research and the inner workings of academia. Her guidance helped strengthen my understanding and appreciation of science. I'd also like to thank my advisory committee for helpful discussions, idea generating, and helping me identify and prioritize experiments. Although my experiments have not always panned out, they have consistently demonstrated a level of enthusiasm for my work and helped me stay motivated and focused. I am very appreciative for their willingness to serve and their efforts towards improving my capacity as a scientist.

I'd like to acknowledge my friends and colleagues, who have played instrumental roles throughout my academic career. First, my fellow lab mates, both past and present, who understand so well what it takes to succeed and so graciously and willingly assisted and continue to assist me even to this day. Drs. Qiuyan Shao, Jimmy Trinh, Jingwen Guan, and Kailun Zhang, thank you for making me feel welcome, trusting me, and taking the time to teach me both basic and advanced techniques. I appreciate your efforts and your contributions have greatly influenced my development as a scientist.

Thank you to my current lab mates, Matthew Theodore and Zihao Yu. I appreciate your insight, thoughtfulness, emotional support, and friendship. I look

forward to our early morning laughs, sharing delicious food, and learning as much as I can from your diverse backgrounds. Thank you for working with me to overcome challenges, both inside and outside the laboratory. I am very grateful that you chose to join our lab and wish you success moving forward.

I want to acknowledge specific members of the Center for Phage Technology, both past and present, for their assistance in helping me reach my goals. I'd like to acknowledge Dr. Junjie Zhang. I appreciate his expertise, enthusiasm for our projects, and skilled laboratory personnel. His contributions have significantly improved my understanding of our system. I'd also like to thank Drs. Karthik Chamakura and Karl Gorzelnik for personally introducing me to the world of ssRNA phage. Thank you for being willing to teach me. Thanks for addressing my questions and concerns (even sometimes at weird hours of the day), helping me develop protocols, find resources, use correct language, and lending me books and papers to help along the way. I'd like to thank Jirapat Thongchol for his advice, assistance with experiments, and willingness to share reagents. I enjoy our phone chats about ssRNA phage and theory crafting with you. I also want to thank Dr. Mei Liu, for graciously allowing me to work within her laboratory space. Thank you, Jay Clark, and Tram Le for teaching me how to operate the equipment within that space.

I'd like to thank Rafael Almanzar, who went above and beyond his duties to ensure my success in the program. I'd also like to thank my friend Carl Thompson, who chatted with me almost every day. Thank you for helping me stay balanced and focused on the mission.

Lastly, I'd like to acknowledge my fiancé, Kristianna Bowles. Thank you for your honesty, attention, patience, guidance, friendship, and love. I am truly blessed to have you. You've been at my side throughout my westward journey, physically and at times in spirit, while I battled through some of the most challenging times of my life. Your positivity and encouragement motivated me to keep moving forward. Your kindness, empathy, and dedication, displayed in both your work and personal life, have inspired some of my greatest achievements. Thank you for supporting me.

CONTRIBUTORS AND FUNDING SOURCES

Contributors

This work was supervised by a dissertation committee consisting of Dr. Lanying Zeng, Dr. Jean-Philippe Pellois, Dr. Ryland F. Young, and the late Dr. James C. Hu of the Department of Biochemistry and Biophysics and Dr. Jason Gill of the Department of Animal Science.

The lab of Dr. Peter J. Christie of the Department of Microbiology and Molecular Genetics at the University of Texas Medical School at Houston contributed conjugation data, the *traD* mutant strains described in chapters 2 and 4, and the *tra*/*trb* strains used in chapter 5. The laboratory of Dr. Zemer Gitai of the Department of Molecular Biology at Princeton University provided the *Pseudomonas aeruginosa* strains used in chapter 3. The turbidostat used in chapter 4 was constructed by Dr. Karthik Chamakura of the Department of Biochemistry and Biophysics at Texas A&M University.

All other work conducted for the dissertation was completed by the student independently.

Funding Sources

This work was made possible by the National Science Foundation (NSF) under grant number MCB-1902392, the National Institutes of Health (NIH) under grant number R21AI156846, and the Texas A&M University X-Grant number 290386. Its contents are solely the responsibility of the authors and do not necessarily represent the official views of Texas A&M University, the NSF, or the NIH.

TABLE OF CONTENTS

Page

ABSTRACT II

DEDICATION IV

ACKNOWLEDGEMENTS V

CONTRIBUTORS AND FUNDING SOURCES VIII

TABLE OF CONTENTS IX

LIST OF FIGURES XII

LIST OF TABLES XIV

CHAPTER I INTRODUCTION AND LITERATURE REVIEW 1

Characteristics of non-tailed phages 5
ssDNA Phages 5
ssDNA phages: The *Inoviridae* 6
dsRNA phages: The *Cystoviridae* 9
ssRNA Phages 13
Adsorption and Cell Penetration 15
Gene expression, Replication, Assembly, and Lysis 17
Fiersviridae that infect bacteria other than *E. coli* 22
F-Pili: Structure, Synthesis, and Function 23
Structure of F-pili 23
Synthesis of F-pili 27
Function of F-pili in Conjugation 30
Non-conjugative pili in other systems 31
Type IV Pili Structure 31
Synthesis of Type IV Pili 35
Functions of Type IV Pili in Motility 38
Dissertation Overview 41

CHAPTER II SSRNA PHAGE PENETRATION TRIGGERS DETACHMENT OF THE F-PILUS* 44

Introduction 44

Materials and Methods 46
Bacterial Strains, Phages, Plasmids, and Primers 46
Construction of Coat-sfGFP 49
Preparation of MS2 lysates 49
Pilus detachment assay 50
Construction of pOX38 Δ*traD* 51
Conjugation assay 52
Phage sensitivity assay 52
RNA ejection assay 53
RNA smFISH 53
Fluorescence microscopy imaging 57
Results 57
Detection of F-pili by fluorescent labeling of MS2 particles 57
Early infection by ssRNA phages leads to F-pilus detachment 60
F-pilus retraction is required for phage-triggered detachment 62
MS2-resistant mutant Δ*traD* inhibits gRNA entry 66
MS2 triggers detachment of F-pili elaborated by Δ*traD* mutant cells 71
Discussion 74

CHAPTER III SSRNA PHAGE PENETRATION CAUSES DETACHMENT OF TYPE IV MOTILITY PILI 79

Introduction 79
Materials and Methods 81
Bacterial Strains and Phages 81
Preparation of PP7 Lysates 82
Sample Preparation for Labeling T4P 82
Pilus Detachment Assay 83
Live-cell Observation of Motility and T4P Dynamics 83
RNA smFISH 84
Fluorescence Microscopy Imaging 86
Results 88
PP7 Binds and Cleaves PAO1 T4P during Pilus Retraction 88
PP7 Infection causes a Reduction in T4P Dynamics and Motility 92
The Auxiliary Retraction ATPase, PilU, is required for Pilus Detachment 96
PilU is required for the cytosolic penetration of PP7 gRNA 98
Discussion 101

CHAPTER IV GENETIC ANALYSIS OF DETERMINANTS OF SSRNA BACTERIOPHAGE CELL PENETRATION BY EXPERIMENTAL EVOLUTION. 106

Introduction 106
Materials and Methods 108
Bacterial strains, Phages, Plasmids, Primers 108

Evolution Experiment....111
Purification of Evolved MS2 lysate....111
RNA Extraction....112
Recapitulation of Identified Mutants....113
RNA smFISH....113
Results....117
Experimental adaptation of MS2 towards TraD independence....117
Mutation in *mat* is sufficient for plaquing on basal levels of TraD....119
TraD C-terminal domains and ATPase activity promote efficient infection....123
Discussion....131

CHAPTER V ANALYSIS OF GENETIC DETERMINANTS INVOLVED IN F-PILUS SECRETION....135

Introduction....135
Materials and Methods....137
Bacterial strains, Phages, Plasmids, Primers....137
Detection and quantification of F-pili using MS2-GFP....139
PCR and plasmid construction....139
Construction of LZ2662....140
Live-cell observation of F-pili dynamics....140
Results....141
Phenotypic characterization of pOX38 deletion mutants....141
Quantification of F-pilus synthesis from misexpression of pOX38 genes....144
Direct visualization of F-pili dynamics....146
Discussion....150

CHAPTER VI CONCLUSIONS....152

The role of F-pili in facilitating ssRNA phage penetration....152
Pilus detachment is present in diverse pilus-phage systems....154
Function of coupling proteins in ssRNA phage penetration....155

REFERENCES....159

LIST OF FIGURES

Page

Figure 1.1 The infection cycle of a tailed, virulent bacteriophage. 4

Figure 1.2 The M13 phage genome and gene functions. 8

Figure 1.3 Diagram of the dsDNA phage Φ6 life cycle. 12

Figure 1.4 Genome architecture of model *Fiersviridae*. 14

Figure 1.5 Role of RNA secondary structure in controlling MS2 gene expression. 19

Figure 1.6 Cryo-ET density map from *in situ* structures of F-pilus T4SS. 26

Figure 1.7 Schematic of the F-T4SS. 28

Figure 1.8 Diagram of the T4P transmembrane channel in *P. aeruginosa*. 33

Figure 1.9 The T4P basal body from *M. xanthus*. 34

Figure 1.10 Schematic of twitching motility facilitated by T4P. 39

Figure 2.1 Fluorescent capsid labeling of MS2 virions to detect F-pili. 59

Figure 2.2 MS2-GFP interacting with *tra* mutants. 60

Figure 2.3 Schematic of pilus enumeration assay. 61

Figure 2.4 Infection by ssRNA phages leads to pilus detachment. 64

Figure 2.5 Length distribution of F-pili associated with HfrH cells in the absence of phage infection 65

Figure 2.6 The change in the average number of cell-associated pili over time in uninfected (-) and infected samples from pOX38 and Δ*traD* cells. 68

Figure 2.7 MS2 resistant mutant Δ*traD* inhibits MS2 gRNA entry. 70

Figure 2.8 MS2 resistant mutant Δ*traD* releases pili after infection with MS2. 72

Figure 2.9 Length distribution of cell associated F-pili from pOX38 and Δ*traD*. 73

Figure 2.10 Model for pilus-detachment facilitated gRNA entry of ssRNA phage MS2 76

Figure 3.1 PP7 cleaves PAO1 T4P through pilus retraction. 91
Figure 3.2 Microscopic Twitching Motility is largely Inhibited by PP7 Infection. 93
Figure 3.3 T4P Dynamic Activity is Inhibited by PP7 Infection. 95
Figure 3.4 PilU promotes T4P detachment during PP7 infection. 97
Figure 3.5 PilU is required for cell penetration of PP7 RNA.....99
Figure 3.6 Pilus retraction is required for cell penetration of PP7 RNA.....100
Figure 4.1 Experimental adaptation of MS2 using turbidostat setup. 118
Figure 4.2 Evolved MS2 has improved plaquing with basal TraD. 119
Figure 4.3 Mutations found in the evolved MS2 genome. 120
Figure 4.4 Plaquing phenotypes of individual evolved MS2 mutant lysates. 121
Figure 4.5 Structure of MS2 Mat protein with A355S mutation highlighted. 122
Figure 4.6 Organization of TraD Mutants for Complementation Studies.....125
Figure 4.7 TraD Nucleotide Binding is Required for MS2 Cell Penetration. 126
Figure 4.8 Pairwise Alignment of TraD gene products from pOX38 and pED208. 128
Figure 4.9 Plaquing phenotypes of MS2 on different TraD mutants. 130
Figure 5.1 Quantification of F-pilus synthesis from F-T4SS deletion strains. 143
Figure 5.2 Quantification of F-pilus synthesis during overexpression of pOX38 genes. 145
Figure 5.3 Direct labeling of cysteine modified F-pili. 147
Figure 5.4 Live-cell visualization and quantification of F-pili dynamics. 149

LIST OF TABLES

Page

Table 2.1 Bacterial strains, phages, plasmids, and primers used in this work. 47

Table 2.2 Sequences of smFISH probes used to detect MS2 RNA, oriented 5’ to 3’. 56

Table 2.3 Phenotypic characterization of the Δ*traD* mutation.....68

Table 3.1 Bacterial strains and phages used in this work.....81

Table 3.2 Sequences of smFISH probes used to detect PP7 RNA, oriented 5' to 3'. 87

Table 3.3 Efficiency of Plating of different PAO1 mutants used in this study. 88

Table 4.1 Bacterial Strains, Phages, Plasmids, and Primers used in this work. 108

Table 4.2 Sequences of smFISH probes used to detect MS2 RNA, oriented 5’ to 3’. ..116

Table 4.3 EOP of MS2 by Complementation of TraD Mutants.....129

Table 5.1 Bacterial strains, plasmids, and primers used in this work. 137

CHAPTER I

INTRODUCTION AND LITERATURE REVIEW

Bacteriophages are vast in both number and diversity and make strong contributions to several critical processes across ecosystems, such as directing bacterial evolution (1, 2) facilitating horizontal gene transfer (3), and modulating the composition of microbial communities (4). Many of these interactions are contingent upon successful phage infection, which is a multistep process that differs significantly across bacteria-phage systems. Generally, the infection cycle can be divided into several key stages: adsorption, cell penetration, replication, and host cell lysis (Figure 1.1).

The tailed phages of the order *Caudovirales* are the most abundant and best-studied phages, responsible for the bulk of our understanding of the infection cycle. These tailed phages contain genomic double-stranded DNA (dsDNA) of variable sizes, ranging from 18 to over 500 kb (5). The DNA is encapsidated in a proteinaceous, icosahedral head which is attached to a specialized tail that typically incorporates other receptor binding proteins (RBPs), such as tail fibers and spikes, used to recognize the host. Host recognition through phage adsorption is the first stage in the infection cycle. RBPs can recognize a variety of host components present on the cell surface, such lipopolysaccharides, wall teichoic acids, capsules, cell appendages (e.g., pili, flagella), and membrane proteins such as porins (6). The initial interaction with the host receptor is typically reversable before a separate, irreversible interaction occurs, either with the same or a secondary receptor. The interaction between phage RBPs and their respective

host receptor is typically highly specific, and the ability for a phage to infect a host is often determined by the presence or absence of a complementary phage receptor.

Once the phage recognizes the host, it must then traverse the host cell envelope. This relies on the safe and efficient transport of the phage genomic material from the phage particle to the host cytoplasm, a process referred to as cell penetration. The charged genomic material must contend with several barriers to penetration, including impermeable membranes, a peptidoglycan meshwork, and periplasmic nucleases. In *Caudovirales*, many phages utilize specialized tail complexes to overcome these barriers and deliver their DNA. Some utilize a pore-forming spike protein to puncture the outer membrane (7). The tail complexes may also contain proteins with enzymatic activity, such as lysozymes, to cleave glycosidic bonds found in peptidoglycan (8). Once the physical barriers are dealt with, the tail then acts as a conduit which allows the DNA to pass through. However, this is one of the least understood aspects of cell penetration among *Caudovirales*. Some phages encode tape measure proteins (TMPs), typically housed within the tail sheath, that have been implicated in cell penetration (9). Conformational changes resulting from RBP-receptor interactions can lead to the ejection of the TMPs which form a channel that may facilitate DNA translocation (9).

After the genomic material has entered the host cytoplasm, if the phage is virulent, the phage may initiate lytic development. The phage hijacks host cell machinery to facilitate replication of its own DNA and expression of genes necessary for assembly and maturation of the virus particle, including head and tail assembly proteins and proteins responsible for DNA packaging. The progeny continues to accumulate

within the infected cell until a programmed cell burst, or lysis event, occurs, governed by the timed accumulation of lysis proteins designed to compromise the cell envelope from within. The virus particles are then released from the host cell and are free to find and adsorb to new hosts to begin the infection cycle again.

The mechanisms described above are generalizations regarding tailed, dsDNA phages, whose genome size allows them to encode many specialized tools to permit host recognition, cell penetration and host lysis. However, for the smaller, non-tailed phages, whose genome sizes are much more limited, they often rely on the mechanics of host-complexes for adsorption and delivery of genetic material. The remainder of this work will focus on describing the phage-host interactions among non-tailed phages, specifically those that utilize extracellular host appendages, their mechanisms of cell penetration, and the functions of host cell machinery utilized by non-tailed phages to permit infection.

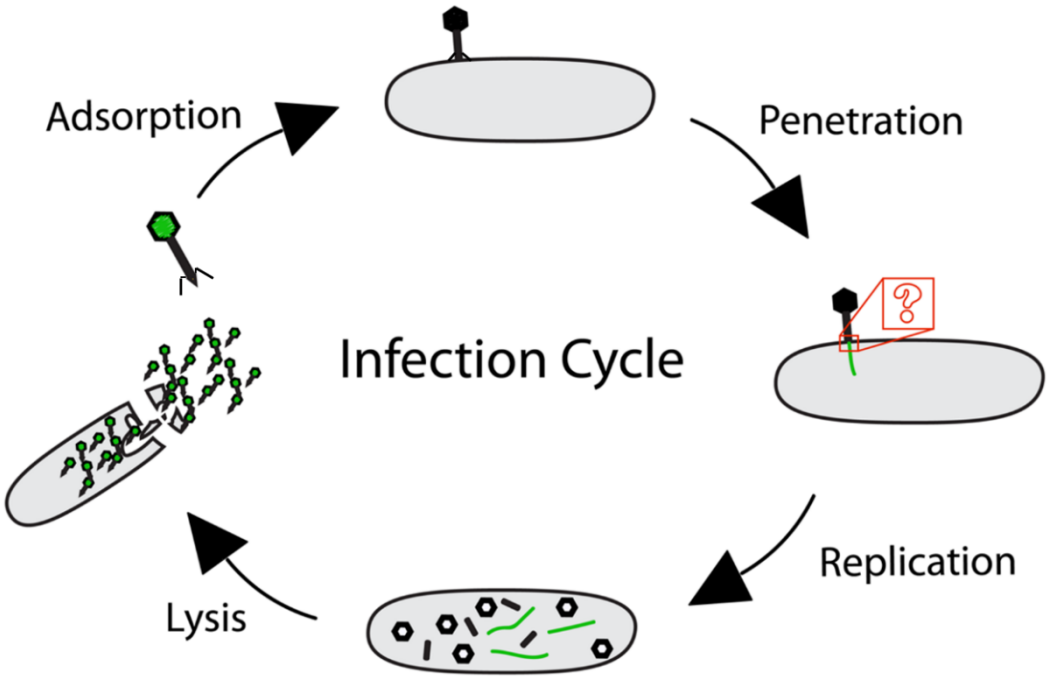

Figure 1.1 The infection cycle of a tailed, virulent bacteriophage.
First, the infectious virion recognizes the host using its RBP. Following this interaction, cell penetration through lesser-known mechanisms occurs, resulting in the phage genomic material entering the host cytoplasm. Afterwards, the phage uses the host machinery to create phage proteins, replicate the genomic material, and ultimately create more phage particles. Lastly, the phage utilizes lysis proteins to cause cell death and release of phage particles which continue the cycle in a new host.

Characteristics of non-tailed phages

The non-tailed phages are among the smallest and simplest phages, typically composed of only a few different structural proteins encapsidating a relatively small genome. They may contain either single-stranded (ss)DNA, ssRNA, or dsRNA genomes which determine how they are generally classified.

ssDNA Phages

The ssDNA phages can be divided into two dominant families based on their morphologies: the filamentous *Inoviridae* and the icosahedral or "cubic" *Microviridae*. The *Inoviridae* (e.g., M13, f1, fd) have a characteristic filamentous shape, typically appearing as long, thin filaments in electron micrographs. They are ~6 nm in diameter and can be between 1 – 2 μm in length (10). The virions are typically composed of 5 different proteins used to create the capsid, which houses the ssDNA, and the pilot protein used for pilus-mediated host recognition.

The *Microviridae* (e.g., ΦX174) are aptly named due to their small genome and particle sizes. Their genomes range from 4-6 kb while the particles are typically ~25 nm in diameter with T=1 symmetry (11). Like the *Inoviridae*, they also are comprised of only a few proteins: the major capsid protein, the major spike protein, a small DNA binding protein, and the DNA pilot protein (H). These phages utilize the H protein to facilitate DNA translocation through conduit formation upon binding to a secondary receptor (12). Since these phages are not known to require an extracellular host appendage for infection, they will not be covered in detail in this dissertation.

ssDNA phages: The Inoviridae

The *Inoviridae* phages can be characterized by their unique filamentous morphologies and their circular ssDNA genomes. Most of our understanding about *Inoviridae* stems from research conducted on the Ff group of filamentous phages (F-specific filamentous), which infect bacteria (typically *E. coli*) containing the conjugative F-plasmid. The best-studied of the Ff phages are the closely related f1, fd, and M13 coliphages. These phages were isolated independently yet share sequence identity of 98.5% and have all been used interchangeably in molecular biology research (13). M13 has become one of the more popular Ff phage, mostly due to its suitability as a cloning vector, as well as uses in phage display (14), nanotechnologies (15), and directed evolution (16).

M13 carries a 6,407 bp circular genome containing 9 genes. However, it can produce 11 different proteins, given that two internal translation start sites exist within genes *gp2* and *gp1*, which lead to the production of gp10 and gp11, respectively (Figure 1.2A) (17). The ssDNA is encapsidated in about 2700 copies of the major coat protein, gp8, which is arranged in a helical structure (18). The ends of the filament contain 5-7 copies of different minor coat proteins. One end possesses gp3 and gp6 while the other has gp7 and gp9. The minor coat protein, gp3 (sometimes referred to as the pilot protein), acts as the RBP, binding exclusively to the tip of conjugative F-pili. The gp6 protein works together with gp3 to aid in the stability of the virion and terminates assembly. Gp7 and gp9 are thought to be targeted by a packaging signal which aids them in identifying the ssDNA to be packaged (19).

M13 and the other Ff phages recognize long, dynamic, filamentous structures known as F-pili as their primary receptor. M13 also uses the highly conserved inner membrane protein complex, TolQRA, as its secondary receptor. The TolQRA proteins are all integral inner membrane proteins which complex together to ensure membrane integrity and promote outer membrane constriction during cell division (20). Adsorption is facilitated by one of the two N-terminal domains (N2) of the gp3 protein which orient the virion at the tip of the F-pilus. Adsorption to the F-pilus causes a conformational change in the N2 domain, which exposes the TolA binding site on the N1 domain (21). The TolQRA complex, as well as the gp3 protein, are essential for infection to occur (22, 23). Therefore, the F-pilus, which is known to undergo cycles of extension and retraction (24), likely retracts to bring the filamentous phage to the cell surface for internalization in a TolQRA-dependent manner. Gp3 must move across the outer membrane, allowing the N1 domain to interact with the periplasmic domain of TolA (25). However, the details and subsequent stages of this mechanism are not well understood.

After cell penetration, the ssDNA initiates DNA replication. The negative-sense strand begins synthesis at the origin of replication from the positive-sense ssDNA through the synthesis of an RNA primer by RNA polymerase (26). This primer is used by DNA polymerase III to complete synthesis of the negative-sense strand. The positive-sense ssDNA is then synthesized with the aid of cytoplasmic phage proteins gp2, gp5, and gp10, which mediate rolling circle replication. While replication ensues, phage proteins gp1, gp4, and gp11 come together to form a transmembrane export complex and the major and minor coat proteins become inserted into the membrane. The replicated

positive-sense ssDNAs are escorted to the export complex by the phage packaging protein, gp5, for assembly and secretion of the mature phage virions. Notably, infection does not induce cell lysis, nor does it kill the cell. Instead, the phage particles are steadily produced and secreted while the cells continue to grow and divide (Figure 1.2B) (27).

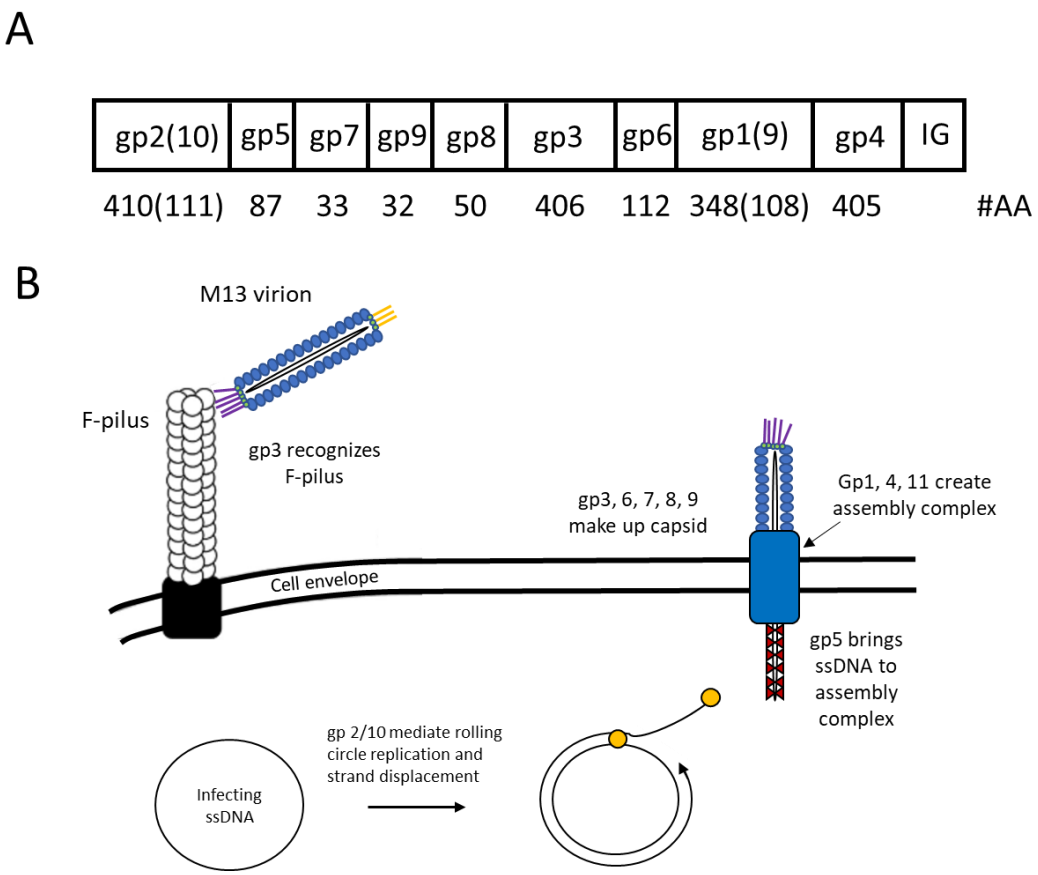

Figure 1.2 The M13 phage genome and gene functions.
(A) M13 genome and gene product sizes. Parentheses indicate genes with internal start sites. The non-coding intergenic region (IG) is indicated. Adapted from (28). (B) Function of M13 proteins in different stages of the life cycle. Adapted from (29).

dsRNA phages: The Cystoviridae

The first and most notable member of the *Cystoviridae* is phage Φ6, an obligately lytic phage originally isolated from the plant pathogen *Pseudomonas syringae* pv. *phaseolicola* (Pph) (30, 31). Φ6 is characterized by having a dsRNA genome consisting of 3 linear segments, termed L, M, and S, with lengths of ~6kb, ~4kb, and ~3kb, respectively (32). The dsRNA is encapsidated in a polyhedral capsid comprised of 5 different proteins, each with their own function. Protein P1 forms the procapsid (33), P2 provides the active site for the RNA-dependent RNA polymerase (34), P4 functions as an NTPase involved in packaging (35, 36), P7 stabilizes the RNA during packaging (34), and P8 encodes the coat protein which forms the capsid (37) and is enveloped in a lipid layer in the mature virion (30). The lipid layer contains the host-attachment complex, which is composed of two proteins: the attachment protein, P3, and a hydrophobic P6 protein, which associates P3 with the lipid layer (38).

Φ6 stands out among other *Cystoviridae* in part due to its host receptor. While *Cystoviridae* phages Φ8, Φ12, and Φ13 (whose host strain is also sensitive to Φ6) recognize host lipopolysaccharides as their primary receptors, Φ6 recognizes type IV motility pili (T4P) (39). These T4P mediate twitching motility, and therefore undergo cycles of extension and retraction to drive directional movement. Pph cells that are resistant to Φ6 either lack T4P entirely, or tend to be hyperpiliated, suggesting a defect in retraction which enriches for surface pili (40). After attachment, it is thought that T4P retraction brings the Φ6 virion to the cell surface where membrane fusion occurs between the lipid layer and the outer membrane of the host (41). This supposedly

provides the phage lytic transglycosylase P5 (42, 43), located between the lipid layer and the capsid (44), access to the peptidoglycan layer for local degradation and subsequent cell penetration (Figure 1.3) (45).

Notably, replication of the genomic dsRNA is reliant on the successful packaging of all 3 RNA segments into the procapsid. The positive-sense strands are packaged into the procapsid in order by segment: first segment S, then M followed by L (46). This requires the hydrolysis of NTP, which is facilitated by the hexameric NTPase P4 (47, 48). Once packaged, the positive-sense RNA is used as a template to produce dsRNA by the phage encoded RNA-dependent RNA polymerase, P2. A high-quality crystal structure of P2 has been solved and was used to draw several inferences regarding its polymerase function (49). Elongation begins through the pairing of a NTP, usually GTP, with the template strand. This causes the template to ratchet backwards, creating a new site for productive base-pairing. This binding and ratcheting cycle continues, with the dsRNA product being shunted out of the complex. The negative-sense strands produced can also be used as templates to produce more positive-sense strands, which are released from the procapsid into the cytoplasm to serve as mRNAs or packaged in new procapsids. Differences in the 3’ base composition of the S, M, and L segments of the genome determines the expression level of each segment. The negative-sense strand of the S and M segments possess a 3’-CCUUU, while the L segment has a 3’-CAUUU. This single difference leads to 10-20 times higher expression from the S and M segments compared to L, exemplifying one means of gene regulation (38).

During assembly, the procapsids serve as scaffolds for the coat protein, P8. The progeny must then acquire the lipid layer to form the mature virion. Although the mechanism is known, expression of the membrane protein P9 induces cytoplasmic vesicle formation, and the stability of these vesicles is reliant on the protein P12, which may act as a chaperone (50).

Release of the viral progeny is achieved by host cell lysis. While the exact mechanism is unknown, two proteins with lytic functions have been identified for Φ6: P5 and P10. P5 is a lytic transglycosolase which has been implicated in causing peptidoglycan degradation during cell penetration. It is possible that P5 also works to compromise the host peptidoglycan layer from within during lysis (45). Another protein, P10, is also required for lysis. It was thought that P10 may act as a holin by creating membrane lesions that give P5 access to the peptidoglycan, as P5 expression alone is incapable of inducing cell lysis (51).

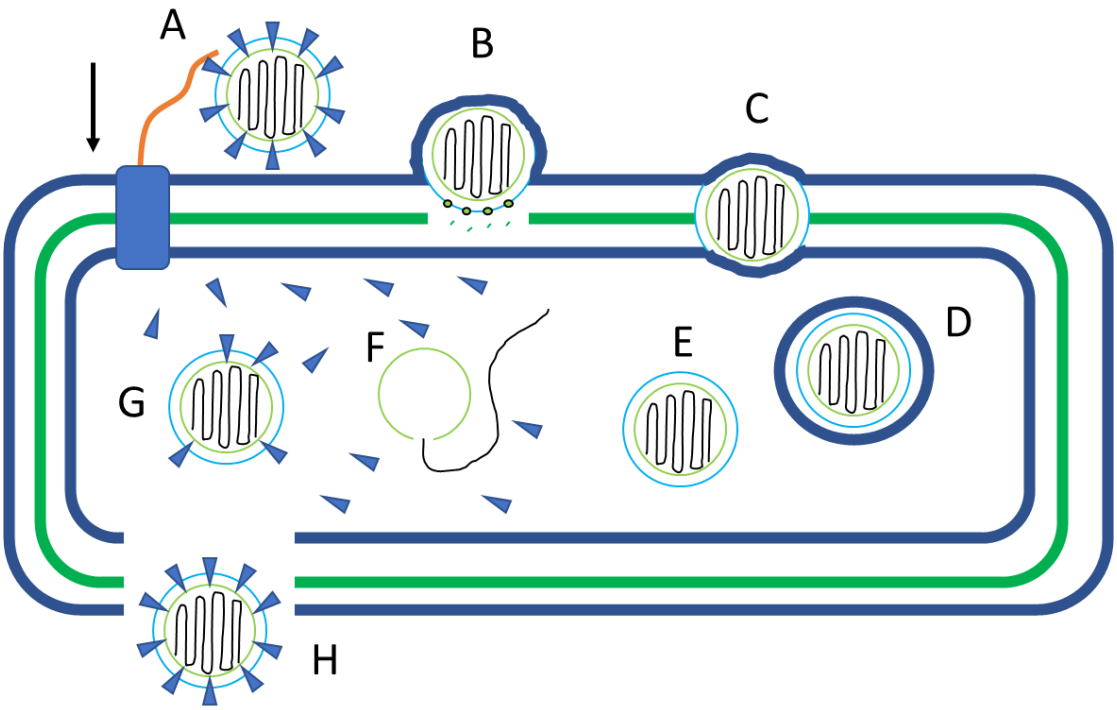

Figure 1.3 Diagram of the dsDNA phage Φ6 life cycle.
(A) The infectious Φ6 virion binds to the type IV pilus receptor. Retraction likely brings the virion to the cell surface. (B) Membrane fusion between lipid layer and host outer membrane. Peptidoglycan degradation occurs by the P5 protein. (C-D) Cell uptakes virion into cytoplasm. (E) Transcription occurs from nascent RNA. (F) ssRNA packaging and replication begins within nucleocapsid shell. (G) Nucleocapsid shell recruits host-attachment proteins and develops lipid layer. (H) Host lysis occurs and releases progeny. Adapted from (11).

ssRNA Phages

The ssRNA phages form the family *Fiersviridae* and represent the smallest and simplest group of the non-tailed phages. Generally, *Fiersviridae* contain linear, positive-sense ssRNA genomes between 3.5 – 4.3 kB in size (11). They typically encode 4 gene products: a maturation protein (Mat), used for host-recognition, a coat protein(s), a lysis protein, and a RNA-dependent RNA polymerase (Rep). The virions appear spherical and are typically around 25 nm in diameter with an icosahedral, T=3 symmetry. The mature particles typically contain 178 copies (89 dimers) of the coat protein and a single maturation protein. The two most notable genera, *Emesvirus* and *Qubevirus* contain the paradigm phages MS2 and Qβ, respectively. These genera were renamed from *Levivirus and Allolevivirus* in 2020 following the identification of 1,015 near-complete ssRNA phage genomes from metatransciptome analysis of environmental samples (52).

The genomes are usually arranged with the *mat* at the 5' end, followed by *coat* and *rep* (Figure 1.4). The lysis gene can either overlap with the *coat* or *rep* genes in a separate reading frame (53) or be in a separate ORF entirely (54). The *Qubeviruses* differ by containing a bifunctional Mat that also serves as the lysis protein (55), and therefore do not encode a separate gene for this function. They encode a read-through protein (A_1), via a leaky stop codon at the end of the *coat*. This read-through protein is an essential minor coat protein (56).

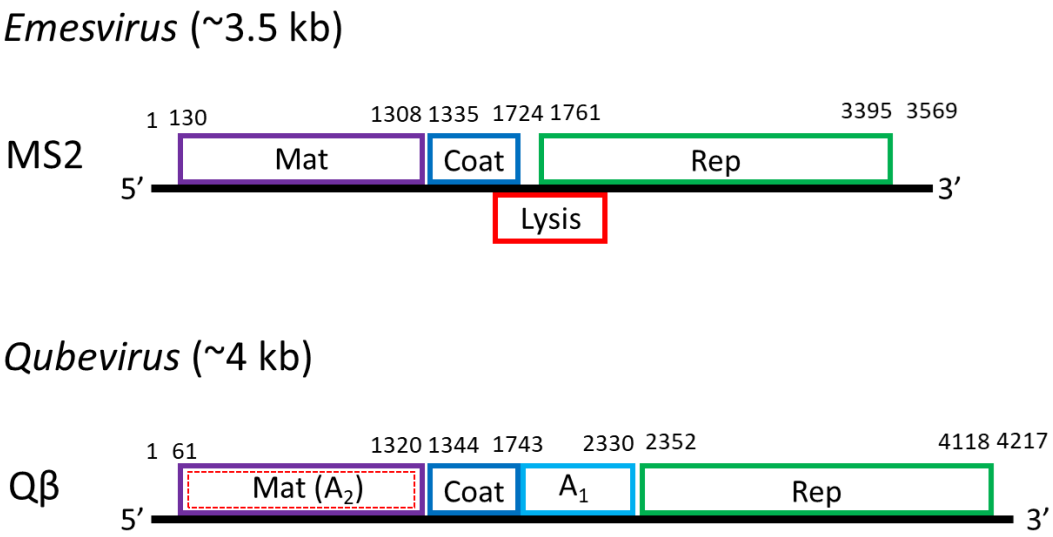

Figure 1.4 Genome architecture of model *Fiersviridae*.
The genomes of *Emesviruses* and *Qubeviruses* are organized similarly and both contain the 3 core ssRNA phage proteins: Mat, Coat, and Rep. However, while the lysis protein start site of *Emesviruses* MS2 is embedded in the c*oat* gene, the Mat of *Qubeviruses* Qβ allows exhibits a lytic function. Additionally, Qβ encodes an essential, read-through minor coat protein, A_1.

Adsorption and Cell Penetration

The ssRNA phages universally infect their hosts via retractile pili and have thus far only been isolated in gram-negative bacteria. Pili are thin, flexible, filamentous host appendages that help facilitate several important and diverse host processes, such as gene transfer, motility, and biofilm formation (57). Phage-pilus interactions have been studied in a variety of hosts with different pili types, however, the interactions between coliphages infecting via conjugative F-pili are by far the best studied.

Much of our knowledge about the early stages of ssRNA phage infection stems from studies conducted using the paradigm phage MS2 and its relatives (e.g., R17, f2). Initially, MS2 binds to the side of the F-pilus using its Mat. This interaction occurs between the β-region of Mat and the N- and C- termini of four pilin subunits through a series of electrostatic interactions between residues at the Mat-pilin interface (58). Eliminating charged pilin residues at the interface grants resistance to F-specific ssRNA phages (59). The binding of MS2 to piliated cells at 4 °C or free F-pili at 4-37 °C is reversible and does not lead to loss of infectivity in the viral particles (60).

After adsorption, the ssRNA phage must penetrate the cell envelope to deliver its genomic RNA (gRNA) into the cytoplasm. While this penetration step is arguably the least understood aspect of the infection process, several experimental observations have been established. Under infectious conditions, the interaction between MS2 and piliated cells (but not free F-pili) leads to a series of events that presumably take place during cell penetration. This involves the rapid and irreversible sensitization of the virus particles to exogenous RNAse, implying a disassociation of the viral capsid from the

RNA (61). Since this reaction occurs with piliated cells at 37°C, this suggests that the reaction may require energy. Cell penetration also triggers the sudden loss of cellular nucleoside triphosphates (62) and is promoted by the presence of divalent cations (63). In addition, penetration leads to the cleavage of the 44 kDa Mat into two, about equally sized peptides, which are thought to remain associated with the cell (64).

The role of conjugative pili in the transfer of gRNA is not well understood. Various models have been proposed to explain the mechanism of nucleoprotein transport by conjugative pili, each with little supporting evidence. The pilus conduction model was initially proposed by Brinton (1965), which suggested that the F-pilus is a hollow tube that facilitates the transport of the gRNA through the interior of the pilus (65). This model was supported by the finding that the pilus lumen contains basic residues which may interact with the negatively charged gRNA (66). However, the pilus retraction model serves as a more favored explanation for cell penetration. Since the F-pili are naturally involved in conjugation, a process requiring intimate contact between donor and recipient cells brought together through pilus retraction, it seems intuitive that the pilus bound phage is brought to the cell surface through pilus retraction, leading to the internalization of the gRNA. Early support for this model came from the finding that *P. aeruginosa* cells infected with the ssRNA phage PP7 have a 50% reduction in overall T4P lengths, and that phages were often seen at the bases of pili, as observed by electron microscopy (67).

Gene expression, Replication, Assembly, and Lysis

After cell penetration, the gRNA then acts as a mRNA transcript to be used in protein synthesis. There are several known regulatory mechanisms that take advantage of secondary structure, translational coupling, read-through events and RNA binding proteins to control gene expression (Figure 1.5). The *coat* gene is the only RNA region immediately accessible to ribosomes in its folded state (68). Translation of *coat* partially unfolds the secondary structure which permits translation of *rep* and allows RNA replication to occur. Rep provides the catalytic subunit for the RNA-dependent RNA polymerase holoenzyme (RdRp); the other subunits are host proteins: elongation factors, EF-Tu and EF-Ts (69), and ribosomal protein S1 (70). Replication forms a hairpin intermediate in the structure of the 5' end of the gRNA which exposes the RBS of the *mat* gene to allow for its translation (71). Coupling translation of *mat* with replication initiation allows for tight regulation of Mat expression, ensuring that Mat is usually translated only once per replication event (68).

Expression of Coat is regulated entirely by the interactions between the ribosomal S1 protein and a region of the gRNA located immediately upstream of *coat* called the S site. This site has high affinity for S1 proteins, therefore, both ribosomes and the RdRp essentially compete for the same binding sequence. Since replication and translation proceed in opposite directions and cannot successfully occur simultaneously, competition for the S site controls the switch between replication and translation (68). Lack of translation due to gRNA replication is the only known mechanism of *coat* regulation.

Rep expression occurs through translational coupling with the *coat* gene. Translation of *coat* causes a long-distance disruption of an RNA stem structure found upstream of the Rep start site, termed MJ. Unfolding of MJ liberates the *rep* start site, allowing ribosomes to begin translation of *rep*. Additionally, expression of Rep is also controlled by the level of intracellular Coat proteins. The *rep* start site is incorporated into the operator hairpin loop, which has high affinity for Coat proteins. At sufficiently high concentrations, dimerized Coat proteins bind to the operator hairpin loop and sterically inhibit ribosome binding.

In MS2, expression of the lysis protein, L, is controlled by the translational termination of the *coat* gene. Since *L* overlaps with the *coat* gene and therefore lacks its own RBS, it cannot be translated on its own. Instead, the ribosome occasionally fails to disassociate from the RNA after translational termination of the *coat* gene. This is thought to cause the ribosome to move backward and initiate translation of the L protein (72). This strategy allows L synthesis to be tightly controlled and prevents premature cell death.

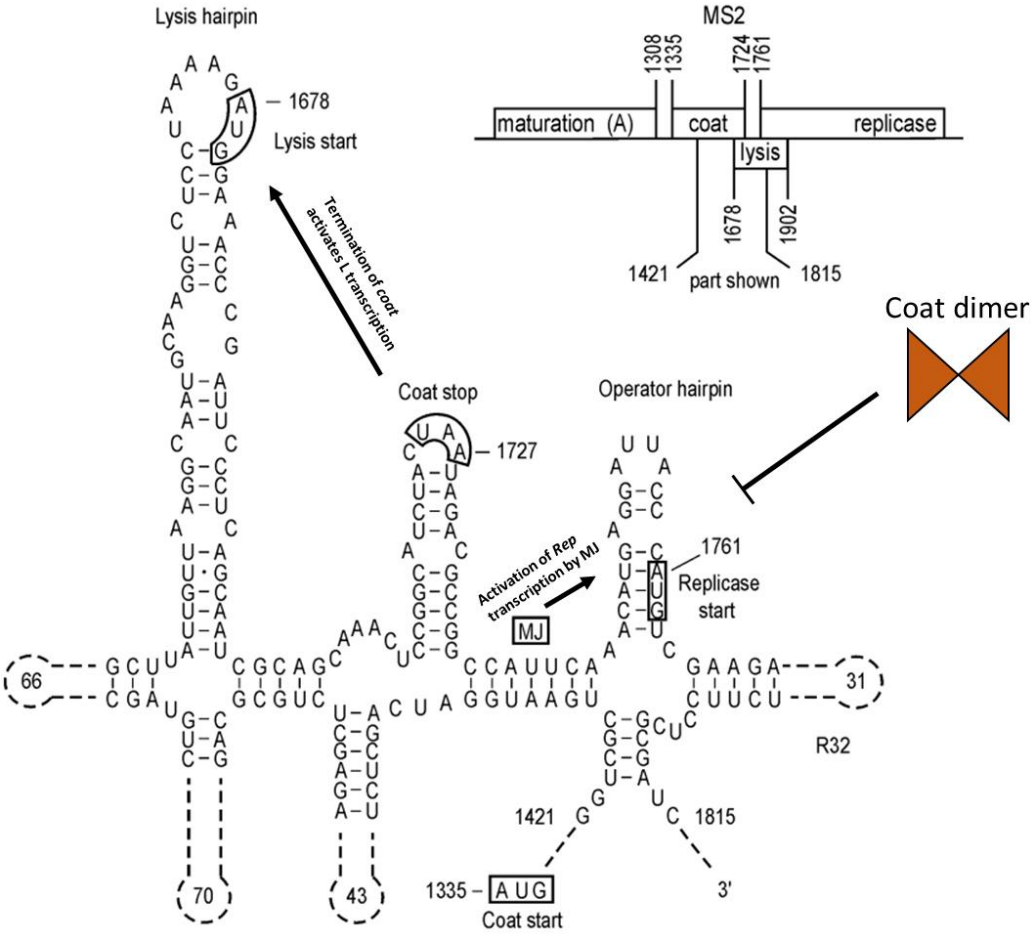

Figure 1.5 Role of RNA secondary structure in controlling MS2 gene expression. Start codons and long-range interactions (MJ) are boxed. Numbers in dashed regions indicated the number of nucleotides present but not shown. Interactions are described in the text. Adapted from (68).

Most of our understanding regarding the molecular mechanism of ssRNA phage replication comes from work done using the Rep purified from Qβ. This was mostly due to the ease of purification compared to the notoriously difficult MS2 Rep. After Rep is translated, RNA replication can occur. In Qβ, the RdRp consists of the EF-Tu, EF-Ts, and Rep at a 1:1:1 ratio, with S1 being associated less consistently (68). EF-Tu is thought to be responsible for binding the RNA to the polymerase. EF-Ts plays a role in chain elongation by facilitating the release of newly synthesized RNA from the replicase (73). S1 works to prevent the formation of dsRNA intermediates and plays a role in replication termination (74). Initial synthesis of the negative-sense strand begins at the penultimate nucleotide, the 3' end being -CCCA. This creates a negative-sense strand containing a -GGG at the 5' end. Rep resolves this discrepancy by incorporating a single A residue at the 3' end. The negative-sense strand then serves as a template to produce more positive-sense strands by the RdRp.

Assembly of the viral particles is guided by several protein-RNA interactions between the Coat and Mat proteins and conserved secondary structures located throughout the gRNA. Cryo-EM *in-situ* reconstructions of the ssRNA genome identified over 50 contacts between Coat proteins and RNA stem-loops (75). High-resolution mapping was achieved for 16 different stem-loops, which showed that 15 of the stem loops are bound tightly to a Coat dimer. Since the interactions of these 15 stem-loops were observed with significantly higher resolution than the others, it was proposed that they play a more central role in nucleating capsid assembly. Three of these stem loops group together in a way that attracts three Coat dimers to assemble, with the center stem-

loop being previously proposed as the assembly initiation site (76, 77). The other stem-loop is found at the 3' end, bound to one copy of Mat, which is thought to help stabilize the RNA during assembly. The high affinity stem-loops sequester enough Coat dimers to fully encapsidated the Mat-bound gRNA to form the mature virion.

Lastly, the newly assembled virions are released from host cells through a lysis event. *Fiersviridae* are known to elicit host cell lysis through a single gene, whose function in lysis varies significantly depending on the phage (78). The function of the MS2 lysis protein, L, is not clearly defined. However, colonies that survived induction of L were found to have mutations affecting the heat shock chaperone, dnaJ (79). Specifically, a P330Q missense mutation located in the conserved, CTD of dnaJ, was found to inhibit complex formation between dnaJ and L. Suppressors of L that could overcome this P330Q mutation appeared to have truncations in the NTD, suggesting that the NTD of L is functionalized by the action of dnaJ. Additionally, mutational analysis of L revealed several single missense mutations that led to lysis defects (80). Most of these mutations were in the LS dipeptide motif and nearby residues. The missense changes were conservative, suggesting that the LS motif is likely important for establishing heterotypic protein-protein interactions with the target of L in the membrane. In contrast, the Mat protein of Qβ, called A_2, in addition to recognizing host F-pili, also targets a host peptidoglycan synthesis enzyme, MurA. Direct binding between A_2 and MurA, likely at the substrate binding site on MurA, inhibits its function and causes arrest of cell wall synthesis and ultimately lysis through the formation of septal blebs in dividing cells (55).

Fiersviridae that infect bacteria other than E. coli

Although ssRNA phages have only been identified among some pilus-producing gram-negative bacteria, presumably any bacterial strain that produces a pilus may support infection by a native ssRNA phage. In fact, several ssRNA phages have been identified that infect a diverse range of hosts, including *P. aeruginosa* (81, 82), *Cauolobacter spp.* (83), and *Acinetobacter spp*. (54). The polar pili produced from these strains are significantly different in structure and function compared to F-pili, yet the ssRNA phages that are unique to these systems are thought to infect using similar strategies. Although the pili systems are diverse, the ssRNA phages themselves share striking similarities in terms of particle size, structure, and means of infection. The ssRNA phages identified thus far typically have particles sizes ranging from 21 – 26 nm in diameter and maintain icosahedral morphology.

The ssRNA phages infecting the *Cauolobacter* genus can be distinguished based on the species they infect, such as *crescentus* (ΦCb5), *bacteroides* (ΦCb8r), or *fuseformis* (ΦCb23r) (83). ΦCb5, the best studied of the *Cauolobacter* ssRNA phages, recognizes host tight adherence (Tad) pili, which help facilitate surface attachment (84). However, *Pseudomonas* ssRNA phages have only been identified for *P. aeruginosa* (e.g., 7s, PP7 and LeviOr01). These phages recognize the highly dynamic T4P used in twitching motility (85). Similarly, the *Acinetobacter* ssRNA phage, AP205, also utilizes T4P for infection (86). This list is not exhaustive, and potentially thousands more ssRNA phages may be characterized given the prevalence of ssRNA genomes identified in metatranscriptome analyses (52).

F-Pili: Structure, Synthesis, and Function

Several bacterial species employ large, multi-component, transmembrane complexes called Type IV Secretion Systems (T4SSs) to facilitate the transfer of DNA or protein effectors via direct cell contact between cells. Contact-dependent transfer of macromolecules can be mediated by extracellular host structures called pili. These are typically long, thin, filamentous appendages composed of thousands of individual monomers arranged in a helical pattern.

The T4SS encoded on the conjugative F-plasmid is one of the best studied T4SSs and has served as a mechanistic and structural model for many other pili-secreting complexes. The F-plasmid encodes a transferrable T4SS containing all the necessary machinery to produce dynamic F-pili, which extend and retract to facilitate donor-recipient contact during conjugation. These F-pili also serve as the native receptor for several coliphages, including ssRNA phages MS2, Qβ, and the ssDNA phage M13. Studies of the structure and function of the F-T4SS and its associated F-pili have further enriched our understanding of how pilus specific phages recognize their hosts and deliver their genetic material.

Structure of F-pili

The F-pilus is typically between 1-2 μm in length and has reported diameters ranging from 8-11 nm (87). Individual cells are often multipiliated in rich media (between 1-5 F-pili) and F-pili can be distributed anywhere on the cell surface (88). However, de-repressed F-plasmid variants (e.g., pED208) can produce upwards of 20 pili per cell (89). Cryo-EM reconstructions using these highly expressed pili have

yielded the highest resolution structures of conjugative pili to date (66). The pilus has a diameter of 8.7 nm with an internal lumen of 2.8 nm. The filament is composed of pilin-phosphatidylglycerol monomers arranged in stacked pentameric complexes that are slightly offset, giving rise to a helical structure with an axial rise of 1.2 nm. Each pilin subunit contains 3 α-helices, arranged with the loop connecting α2 and α3 facing inward towards the lumen, keeping the N- and C-termini accessible for ssRNA phage adsorption (58).

Recent *in situ* Cryo-ET studies of the F-plasmid encoded T4SS have provided several insights into the structure of the pilus secretion machinery (Figure 1.6) (90). Tomographic reconstructions of the structures identified in the envelope of *E. coli* minicells allowed for clear visualization of the transmembrane T4SS complex, including the channel that presumably forms the mating bridge during conjugation. The outer and inner membrane both house ring-shaped structures that are connected by a cylindrical filament spanning the periplasm. The outer membrane ring is 25 nm in diameter and 11.5 nm in height and appeared to have 13 knobs encompassing a central channel 13 nm in diameter that allows the pilus to pass through. This complete transmembrane complex was termed F1. Beyond the F1 structure, three other structures were found at the cell surface (Figure 1.6B). First, the F1 structure with an extracellular density corresponding to the pilus was observed, termed F2. This observation suggests that pilus maturation occurs at the outer membrane, in contrast to the T4P secretion machines which synthesize pili at the inner membrane to be shunted across to the outer membrane (91). However, this structure only represented ~5% of the total structures observed. Another

structure, termed F3, shows a thin, ~12 nm filament that connects the inner and outer membranes, with a ring and a mature pilus both visible on the outer membrane. This was the most abundant structure visible (~60% of all structures). Lastly, the F4 structures were simply the mature F-pili attached to the outer membrane (~5%). It is thought that the F1 and F2 structures interchange, with the pili-less F1 structures occurring during mating, while F2 is reserved to donor cells seeking out recipients using pili dynamics. It is possible that pili can either fully retract to be recycled in the inner membrane, or be deposited on the cell surface, giving rise to the F3 and F4 structures. However, the precise nature of these structures, as well as the reason for their frequency, is still unclear.

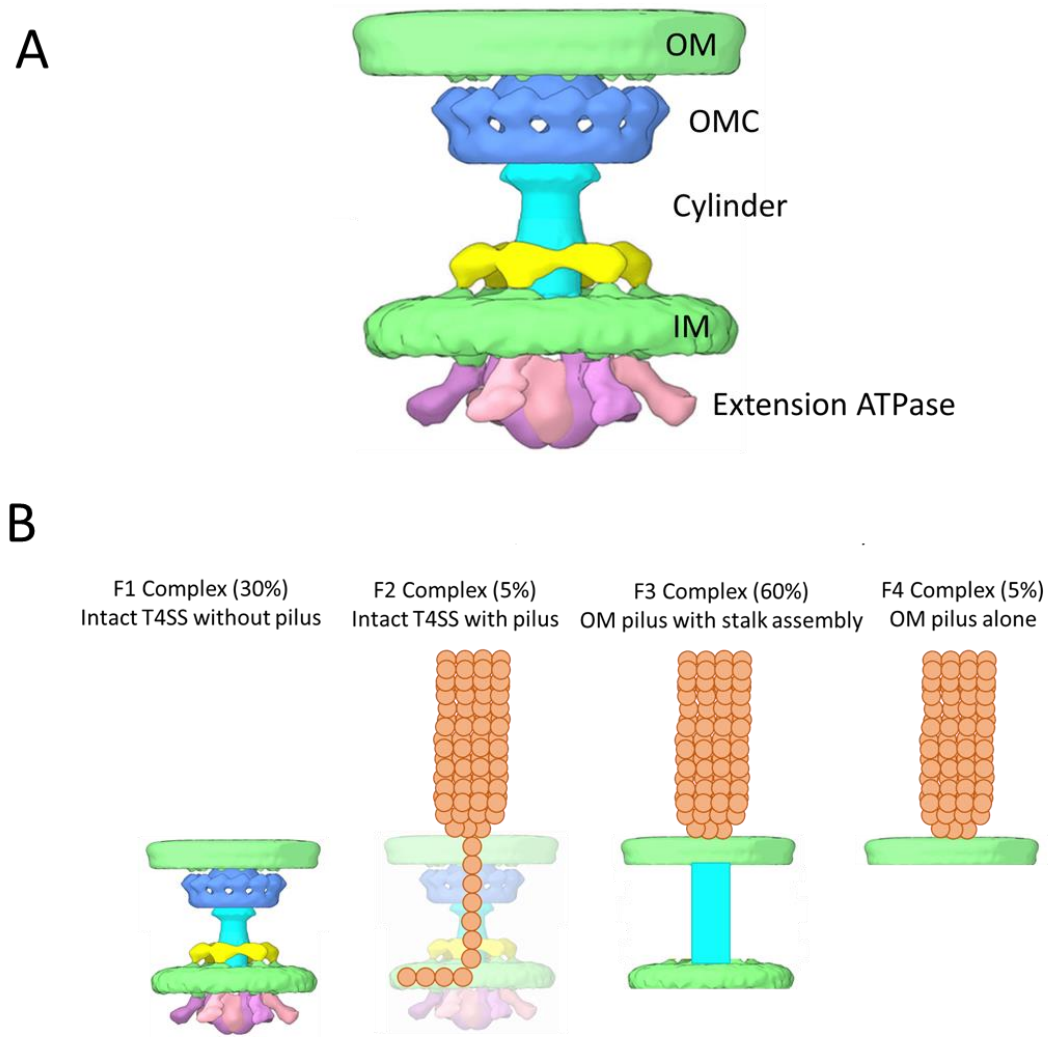

Figure 1.6 Cryo-ET density map from *in situ* structures of F-pilus T4SS.
(A) Density map of F1 complex with major components labeled. Recreated from electron microscopy databank IDs: EMD-9344 and EMD-9347. (B) Schematics and relative distributions of different pilus-T4SS subcomplexes. Adapted from (90).

Synthesis of F-pili

Production of functional F-pili and T4SSs rely on gene expression from the transfer (or *tra*) region of the F-plasmid. The F-pilus is composed of monomers of pilin, which is produced from a processed version of the pro-pilin peptide, TraA. Processing is performed in part by the TraQ and TraX proteins. TraQ acts as a chaperone for the 121 amino acid propilin, allowing it to accumulate in the inner membrane (92). The propilin is cleaved by the host leader peptidase B (LepB) and the N-terminus is acetylated by TraX, resulting in a 70 amino acid pilin (93, 94). The mature pilin monomers are sequestered in the inner membrane prior to assembly by several host proteins of the transfer region: TraE, -K, -B, -V, -C, -W, -G, -F, -H, -L, and TrbC (Figure 1.7) (95). Mutational analysis assigned certain functions for these proteins. The assembly of the tip is conducted by TraE, -K, -C, -G, and -L. TraB, -V, -W, -F, and -H are responsible for pilus elongation. More specifically, the transmembrane channel is composed of TraB, -V, and -K (96). TraL and TraE are anchored in the inner membrane and act as a scaffold for TraC, which is an ATPase responsible for shunting TraA monomers into the channel during pilus extension. While the exact function of each *tra* gene is not known, the remaining genes have several proposed functions based on homology, cellular localization, and interacting partners. TraW, -G, -H, -F, and TrbC are thought to play a role in conjugative pore formation, with TraF and TraH interacting directly with each other (97).

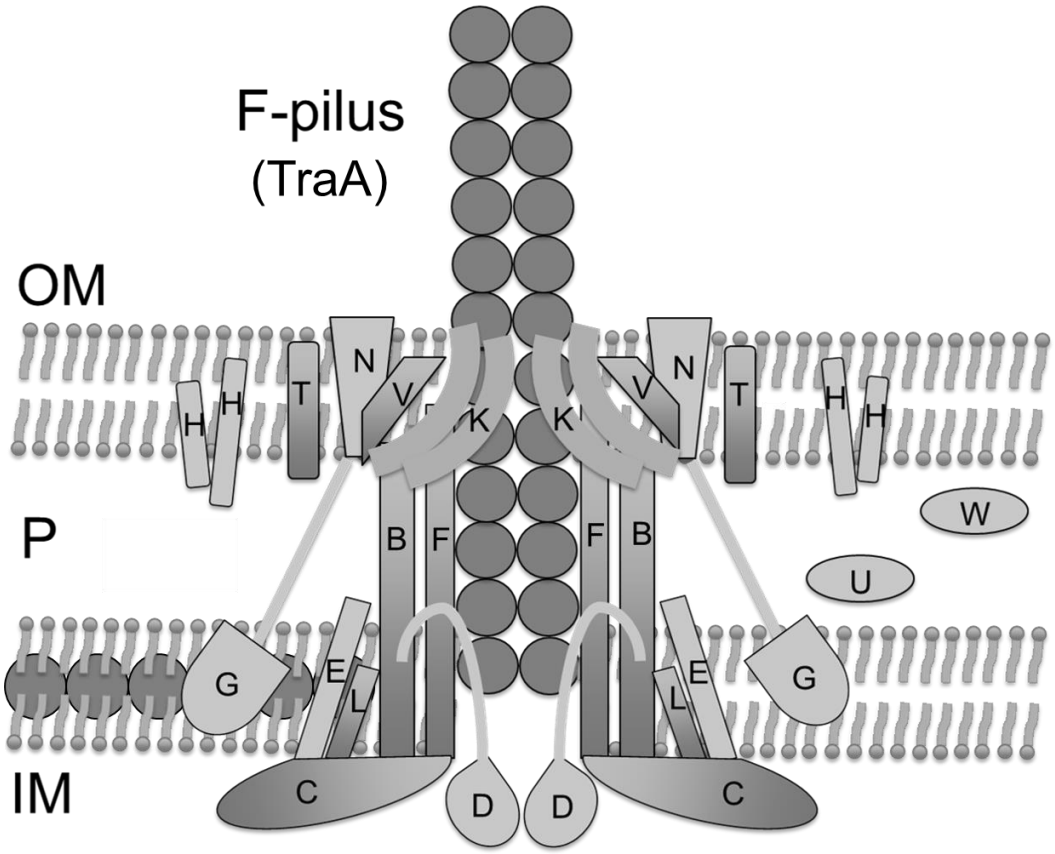

Figure 1.7 Schematic of the F-T4SS.
Known cell envelope localization of genes involved in channel formation and F-pilus secretion are indicated. Protein functions are described in the text. TraN and TraT are outer membrane proteins involved in mating pair stabilization. Adapted from (95).

While proteins and mechanisms involved in pilus extension have been identified, the mechanism describing pilus retraction is still mysterious. Direct evidence for F-pilus retraction was first obtained using fluorescence microscopy techniques to observe pilus retraction occurring in real time (24). Fluorescently labeled R17 phages were used to detect F-pili by proxy of phage binding, and live-cell microscopy was used to assay F-pilus behavior. F-pili were observed to undergo cycles of extension and retraction, with retraction rates of 16 nm/sec and extension rates of 40 nm/sec. F-pili also tended to supercoil when the tips contacted a surface, suggesting that F-pili rotate during extension and/or retraction. Additionally, the finding that cyanide treatment resulted in the sudden loss of surface F-pili suggested that retraction does not require energy (98).

In terms of F-encoded genes, only one gene, *trbI*, has been linked to possibly playing some role in F-pilus retraction. TrbI is a 14.1 kDa inner membrane protein and was shown to have a direct interaction with the assembly protein, TraH (97). Mutants of *trbI* cause cells to produce significantly longer F-pili, which may indicate a retraction deficiency (99). Additionally, a *trbI* deletion grants resistance to contact-dependent inhibition effector proteins, which utilize F-pili to enter and kill target cells (100). However, the same deletion only causes about a 10-fold reduction in conjugation efficiency and titer of phage R17, suggesting that the pili are still capable of retraction, at least in part, to carry out these processes. TrbI is responsible for stabilizing TraH, which is complexed with TraF and TraU (involved in DNA transfer) (97). Since mutations in *traH* affect pilus outgrowth but not tip formation (101), it is possible that if TrbI is lost for any reason, it could lead to the destabilization of TraH which somehow leads to pilus

retraction or disassembly. Still, direct evidence for TrbI promoting pilus retraction has yet to be obtained.

Function of F-pili in Conjugation

The horizontal transfer of genetic material between cells during conjugation involves the secretion of functional F-pili. In gram-negative bacteria, conjugation occurs via direct-cell contact between a conjugative plasmid-bearing donor cell and a recipient cell. In the F-system, the donor cell elaborates dynamic F-pili, which actively probe their surroundings until they encounter a recipient cell. Pilus retraction brings the cells into direct contact, leading to an interaction that results in membrane fusion. This allows the donor cell to directly transfer DNA that contains the *oriT*, a noncoding region of DNA that is recognized by several transport proteins that make up the relaxosome. Traditionally, the F-plasmid is the transferred DNA, however, other plasmids containing the *oriT* site can also be recognized and transferred by conjugation (102). The relaxosome-bound DNA is then nicked by a relaxase at the *nic* site within the *oriT* (103). This nucleoprotein complex is then recruited to the mating channel by an interaction between accessory proteins at the *oriT* and the membrane anchored coupling protein, TraD (104). The relaxase, covalently linked to the 5' end of the DNA, is then passaged through the mating channel. TraD, which functions as a hexameric ATPase, is thought to encircle the DNA and pump it through the mating channel as a single strand with energy from ATP hydrolysis (105). Once the entire DNA strand is passaged to the recipient cell cytoplasm, the original relaxase recircularizes the DNA (106).

Non-conjugative pili in other systems

Beyond conjugative pili, many bacterial species employ other types of pili to mediate important host processes. One of the most common pili are the T4P, which are involved in surface colonization, motility, DNA transformation, and protein secretion (85). Like the conjugative pili, T4P are secreted through a transmembrane channel and undergo cycles of extension and retraction. However, this often occurs through a dedicated motor(s) that controls pilin polymerization and depolymerization. Pilins must still be processed by pre-pilin peptidases before being stored in the inner membrane for use in pilus synthesis. This relies on several assembly proteins which act to stabilize the transmembrane channel. Together, these proteins work to translate the energy given by host ATP into mechanical forces that allow bacteria to survey and interact with their surrounding environment.

Type IV Pili Structure

The T4P filament is composed of pilin monomers (15-20 kDa) arranged with the hydrophobic ends facing inward, adopting a helical structure. They have been reported to be several microns in length with a diameter of 5-8 nm, however, motility pili tend to be shorter, with an average length of 0.8 μm in *P. aeruginosa* (107). Recent advances in cryo-EM studies of T4P structure have revealed impressive detail about the filament structure and how pilin-pilin interactions construct the mature pilus (108). *P. aeruginosa* T4P were shown to have significant variability, with helical rises ranging from 8.9 to 11.9 Å and rotation degrees between 85.3° to 89.3°. Pilin monomers usually contain a globular C-terminal domain which faces outward, with a N-terminal helical spine (α1)

embedded in the inner membrane that helps nucleate pilus extension (108, 109). The filament is lined with these globular domains which protrude outwards, giving rise to a characteristic knobbed texture. Electron density maps revealed electrostatic interactions between Glu5 of the individual pilin monomer and the N-terminal amine of an adjacent monomer which may hold the mature pilus intact.

The T4P transmembrane channel consists of around 10 conserved proteins that make up three major components: the inner membrane motor complex, core alignment structure, and an outer membrane secretin ring that the pilus passes through during extension or retraction (Figure 1.8) (110). In *P. aeruginosa*, the inner membrane motor consists of the rotating platform protein, PilC, and either PilB or PilT, which bind competitively to control extension or retraction, respectively (107). However, in *C. crescentus*, for example, extension and retraction are controlled by a single bifunctional ATPase, CpaF (111). The alignment complex, composed of FimV, PilM, -N, -O, and -P, directly connect the inner membrane motor complex with the outer membrane secretin (PilQ, with assembly chaperone PilF) to ensure the growing pilus is secreted correctly. The channel sequesters both major pilins (PilA), and several naturally adhesive minor pilins that are thought to aid in priming pilus assembly (112). These minor pilins ultimately assemble into the mature pilus tip, granting their adhesive properties to the T4P.

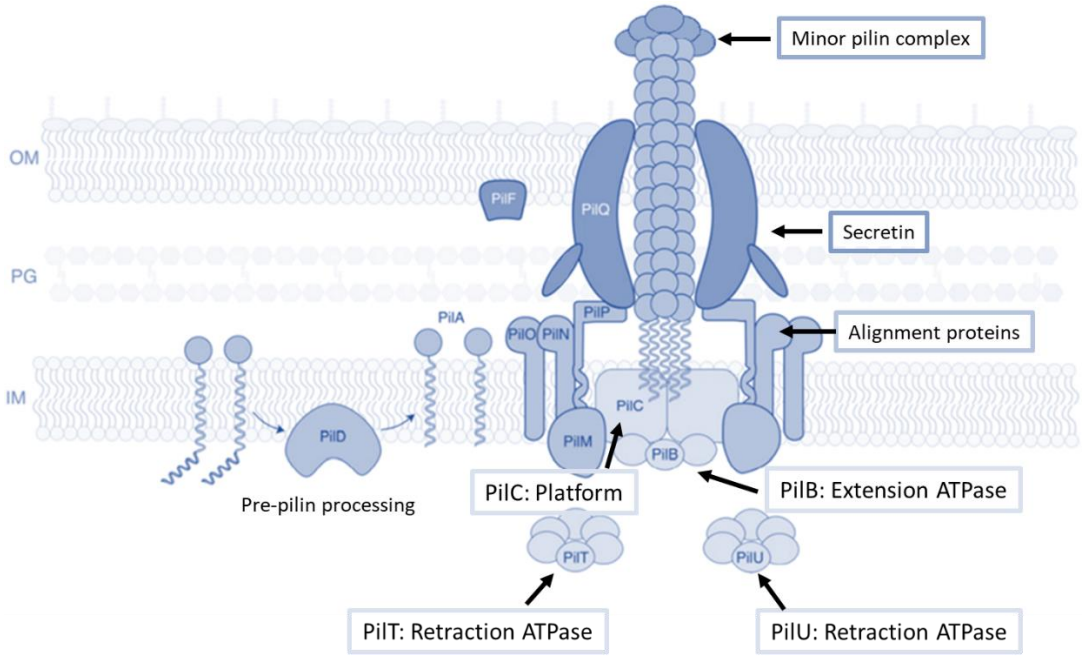

Figure 1.8 Diagram of the T4P transmembrane channel in *P. aeruginosa*. Proteins involved in the formation of the T4P secretion machinery are labeled and grouped based on their function and localization within the cell envelope. PilA monomers are stored in the inner membrane (IM) where they are processed by PilD. The mature PilA monomers are assembled (or disassembled) by the IM platform complex PilC, oriented by the alignment proteins and chaperone, PilF, and the actions of extension/retraction ATPases PilB and PilT. The T4P passes through the envelope by a pore-like channel created by the secretin, oriented by the alignment proteins, with the minor pilin complex forming the T4P tip. Adapted from (113).

Details describing the structure of the T4P transmembrane channel have been revealed in recent cryo-electron tomography studies using *Myxococcus xanthus* cells (114). The channels, termed basal bodies, could be seen spanning the cell envelope with associated T4P attached to the cell surface. Structures for both pilus-loaded and pilus-free basal bodies were built through subtomogram averaging. Generally, the basal body structures comprised of an outer membrane ring that extends into the periplasm, two periplasmic rings, a stem connected to the periplasmic rings and the inner membrane, and several cytoplasmic rings, and a cytoplasmic disc that makes up the platform (not present in the pilus-free structures). The outer membrane ring appeared to be 11.5 nm in diameter. In the pilus-loaded structure, the pilus (6 nm in diameter) displaces the outer membrane ring upwards by about 2 nm compared to the pilus-free structure. The cytoplasmic ring is also ~4 nm wider which could be due to expansion resulting from interactions with the platform.

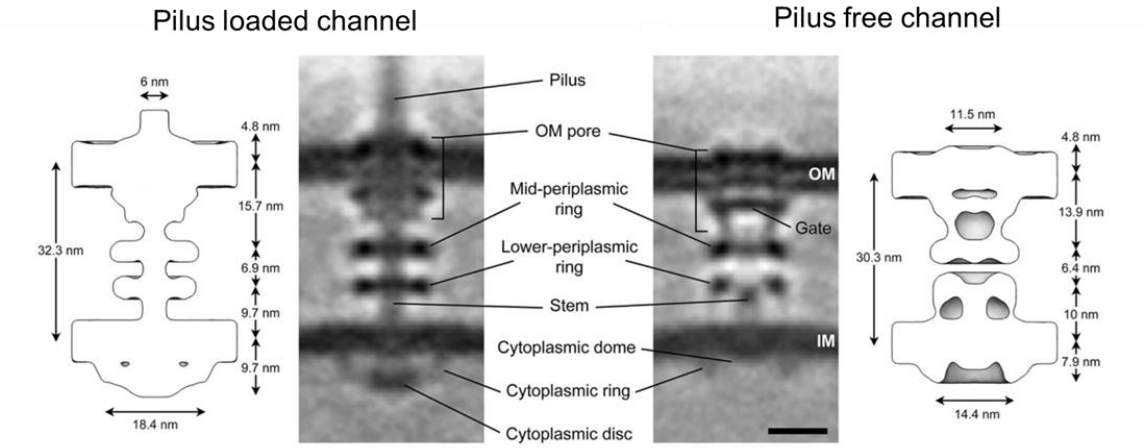

Figure 1.9 The T4P basal body from *M. xanthus*.
Outlines and subtomogram cross sections of the pilus loaded (left, WT) and pilus free (right, Δ*pilB*) channels. Individual structural features are denoted. Adapted from (114).

Synthesis of Type IV Pili

Prior to assembly, the propilin monomers (PilA) are processed by PilD, an inner membrane aspartyl protease that cleaves the N-terminal leader sequence from the PilA peptide, replacing it with a methyl group (115). PilD also performs the same action on minor pilins, allowing both mature major and minor pilins to be stored in the inner membrane prior to use. The minor pilins (FimU, PilV, -W, -X- and E) are thought to complex together within the inner membrane and initiate pilus elongation from below, ultimately manifesting themselves into the T4P tip (116, 117). The minor pilins are in low abundance relative to PilA, which may help limit the formation of extraneous pilus nucleation sites. In fact, misexpression of minor pilins leads to a significant reduction in T4P length, suggesting that regulation of minor pilin expression helps maintain the PilA pool for normal length T4P synthesis (118).

Regulation of PilA expression is controlled by response regulators PilR and PilS. Once autophosphorylated through some unknown signal, PilS phosphorylates PilR, which upregulates *pilA* transcription. It is possible that the PilA concentration plays some autoregulatory role in its own transcription. Mutations in *pilB*, which lead to the intracellular accumulation of PilA, reduces transcription levels of *pilA (119)*. Likewise, *pilT* mutants, which reduce the intracellular pilin pool by favoring T4P assembly and secretion, cause *pilA* transcription levels to increase. Control of minor pilin expression is regulated by a two-component, sensor-kinase system composed of FimS and AlgR. Transcriptional activation of the minor pilin gene cluster requires a phosphorylated AlgR, which binds to two sites that overlap the gene cluster promoter region (120).

While transcriptional regulation of the pilus subunits is relatively simple, the regulatory pathways that control T4P assembly are more complex. The only system known to direct T4P biosynthesis in *P. aeruginosa* is Pil-Chp. Pil-Chp utilizes several proteins that are homologous to proteins of the Che system, which control flagellar rotation in *E. coli* (121). Like the Che system, Pil-Chp utilizes chemotaxis proteins that respond to environmental stimuli to direct the formation of mature T4P. These proteins, called methyl-accepting chemotaxis proteins (MCPs), undergo conformational changes that initiate a signal cascade to direct the synthesis of T4P. The methylation state of MCPs controls the activity of the histidine kinase, CheA, with methylated MCPs leading to greater activation of CheA (122). When activated, CheA becomes autophosphorylated and activates CheY, which directly binds to the flagellar motor protein and induces clockwise rotation of flagella (123). Pil-Chp uses only one MCP, PilJ, which is normally localized at the cell poles (124). PilJ is controlled by the methylation and demethylation activities of PilK and ChpB, respectively (125). PilI is a CheW homolog and helps facilitate the conformational change in PilJ. PilJ acts on the CheA homolog, PilL, which activates two CheY-like regulators, PilG and PilH. Mutational analysis of several regulatory proteins of the Pil-Chp system in *P. aeruginosa* resulted in altered surface T4P levels, with *pilG, -I,* and *-J* reducing surface pili while *pilH* and *pilK* causing hyperpiliated phenotypes (119). This suggests that PilG may stimulate PilB function during extension while PilH stimulates PilT activity during retraction.

In *P. aeruginosa*, dynamic activity of T4P is controlled by PilB and PilT acting on the platform protein, PilC. PilB and PilT act as hexameric, ring-shaped ATPases

which interact directly with PilT through their central pores to elicit their function (114). During extension, ATP hydrolysis by the PilC-bound PilB leads to conformational changes in PilB. Two of the six PilB subunits adopt an open, apo conformation after the release of ADP. The open subunits are pushed up, facing the central pore of PilB, which causes PilC to be forced upwards into the inner membrane. PilC then rotates clockwise to fit back into the pore of PilB. Since PilA is known to interact directly with PilC, this upward and rotational movement of PilC is thought to facilitate incorporation of mature pilins into the T4P filament during extension (126). Similarly, pilus retraction is thought to occur by an equivalent mechanism. PilT also functions through ATP hydrolysis, however, the distribution of the open and closed subunits is opposite that of PilB. Therefore, PilC instead rotates counterclockwise to fit back within the pore of PilT, removing a PilA subunit from the T4P filament in the process (127).

Real-time T4P dynamics have been observed in *P. aeruginosa (107)*, *C. crescentus* (128), and *Vibrio cholerae* (129) using direct labeling of pilin subunits. This approach involves the substitution of a pilin residue with a cysteine residue, which permits thiol-specific labeling of T4P with a fluorescent dye. This technique was used to quantify the synthesis and dynamic activity of T4P in *P. aeruginosa*. Cells were observed to make short, highly dynamic pili, with over 80% of cells producing at least one pilus within the 30 second imaging window. Previously, static images suggested that only ~20% of *P. aeruginosa* cells could produce pili, however, live-cell microscopy suggests that most cells create multiple, short-lived pili (130). The extension velocity was reported to be 361 nm/s while retraction was 644 nm/s with a larger amount of

deviation. Given that the T4P have an average length of 0.8 μm, most pili dynamic events begin and conclude within seconds. Additionally, the frequency of retraction events was unaffected by the presence or absence of a physical surface, suggesting that surface sensing itself does not cause pilus retraction to occur. Instead, a model was proposed wherein the stochastic binding of PilT and PilB motors control extension and retraction events. Stochastic binding was rationalized by observing the frequency of discontinuous retraction events using a mutant of *pilT* that exhibits slow retraction. When retraction was slowed, the frequency of discontinuous retractions increased. The absence of a motor leads to a stalling or dwell event which is characteristic of discontinuous extension or retraction. The increase in discontinuous retractions suggested that the mutant PilT exhibited more binding and unbinding events with the PilC platform, which could mean that motors associate with the PilC platform stochastically to facilitate T4P extension or retraction.

Functions of Type IV Pili in Motility

One trademark function of T4P is their involvement in a widespread form of bacterial surface movement known as twitching motility (Figure 1.9). The term "twitching" refers to the characteristic jerky movements displayed by cells when observed under light microscopy. Only the major subfamily type IVa pili can facilitate twitching motility, as type IVb (often found in enteric bacteria) and Tad pili function in natural transformation and surface colonization, respectively (85). Twitching occurs through the cyclic extension, tethering, and retraction of T4P which work to drag the cell in a direction, analogous to a grappling hook. Despite being thin and short, a single T4P

and PilT motor from *Neisseria gonorrhoeae* can generate retraction forces greater than 100 pN, making them one of the strongest biological machines ever reported (131). The simultaneous tethering and retraction of multiple T4P can generate cooperative forces in the nanonewton range, greatly exceeding forces generated by individual T4P (132). Additionally, cells often exhibit a form of cooperative twitching motility where they group together and move in rafts, but individual cells are still capable of twitching (133). Although this group behavior is common, it is not clear whether all or only some of the cells contribute to group movement.

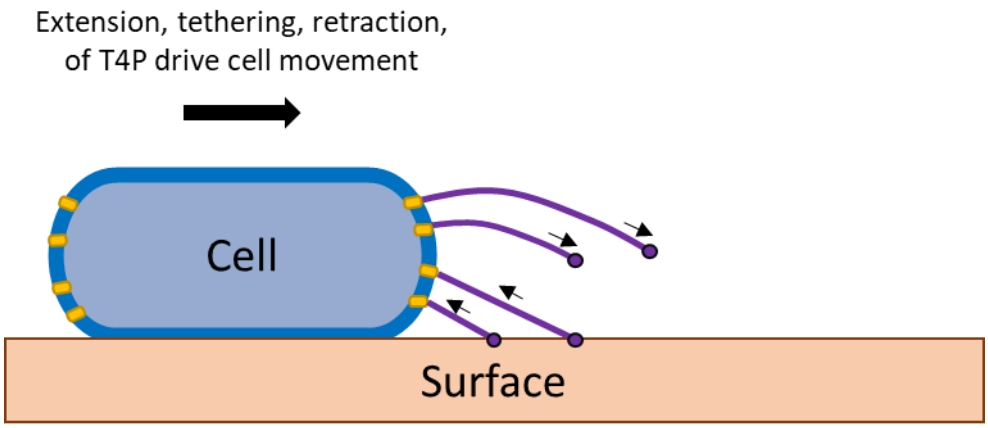

Figure 1.10 Schematic of twitching motility facilitated by T4P.
Cells undergo twitching motility on sufficiently viscous and smooth surfaces. This occurs through the dynamic activity of motor driven T4P. First, T4P extend from the cell surface until they reach a surface. The adhesive tips of the T4P tether to the surface and T4P retraction pulls with enough force to drag the cell towards the T4P tip. This cycle repeats to drive cell movement through twitching motility.

In a traditional twitching motility plate assay, where a colony is picked and stabbed to the bottom of an agar plate and allowed to incubate, a thin expansive colony grows from the original inoculation area. The distance that the colony expands from the inoculation point is indicative of the twitching capabilities of the strain. In *P. aeruginosa*, the rate of colony expansion was determined to be around 0.6 mm/hr after observing colony expansion for 26 hrs. The kinetics of colony expansion follow a near linear trend with brief (~1 hr) pauses every ~4 hrs, possibly due to cell growth and division (133). Cells expanding at the agar-plate interface are considered to be under high-friction which requires additional force generated by the auxiliary retraction ATPase, PilU (134). PilU is thought to interact with PilT and acts as a second gear to permit twitching under high friction. Similarly, PilU is not necessary for pilus retraction in liquid environments, however, PilU alone cannot substitute for PilT to permit retraction in a *pilT* mutant (107).

Several factors can influence the frequency of twitching events and the overall distance traveled by the cell. Environmental factors, such as media composition, play a significant role, as colonies growing in the presence of tryptone or bovine serum albumin have larger diameters (indicative of colony expansion) in twitching motility plate assays (135). However, twitching motility is inhibited in high osmolarity conditions. Additionally, cells have difficulty twitching on dried or rough surfaces, suggesting that the viscosity and smoothness of the surface contribute to successful colony expansion (133). Certain intrinsic factors, such as the production of biosurfactants, help facilitate twitching motility (136). The number of pili produced from

an individual cell also affects the distance travelled, as cells expressing more pili typically migrate farther under light microscopy compared to cells with fewer pili (137). This is possibly due to a combination of cooperative retraction forces as well as an increase in twitching frequency per cell.

Dissertation Overview

The ssRNA phages have served as long-standing model organisms and have provided substantial insight into many ubiquitous biological processes, such as transcription, translation, RNA replication, and complex assembly. However, details describing the biological processes involved in the ssRNA phage lifecycle, especially regarding cell penetration, are still mysterious. The remainder of this work will highlight seminal findings related to early interactions with ssRNA phages and their respective pili, ssRNA phage engagement with the basal body machinery, and genetic determinants involved in cell penetration.

First, new methods to fluorescently label phage and pili will be discussed, as well as the foundational experiments that describe a new phenomenon that results from ssRNA phage infection of *E. coli*: pilus detachment. A detailed quantitative analysis of pilus detachment will be discussed for ssRNA phages MS2, Qβ, and ssDNA phage M13. The work done to characterize TraD as a newfound facilitator of gRNA penetration will be described. Foundational experiments will demonstrate that TraD mutants permit phage binding and ejection of gRNA from the capsid. Quantitative single-molecule fluorescence assays will show that TraD mutants inhibit cell penetration. The use of a

TraD mutant will also provide evidence to show that pilus detachment occurs as a result of an extracellular phage-pilus interaction.

The proposed model to explain the pilus detachment phenomenon will be expanded into an entirely different system: the ssRNA phage PP7 and its interaction with T4P of *P. aeruginosa*. Previously established methods to detect T4P will be used to demonstrate that T4P detachment occurs as a result of infection by PP7. Further, the infection by PP7 was found to inhibit both microscopic twitching motility as well as individual T4P dynamics. Lastly, a mechanism of cell penetration, reliant on additional retraction forces generated by the auxiliary retraction ATPase, PilU, will be described.

The role of TraD in facilitating MS2 gRNA cell penetration will be investigated through an experimental evolution approach and analysis of TraD mutants. A continuous culture of MS2 infecting a background strain producing basal levels of TraD was used as a selection pressure to enrich the MS2 population with variants that can cause visible plaquing on this strain. An evolved population of MS2 emerged, and sequencing revealed that a single point mutation in the Mat protein results in a clear plaque phenotype on the basal TraD strain. Analysis of plaquing phenotypes and gRNA entry of several TraD mutants will demonstrate that the C-terminal region, as well as the nucleotide binding activity of TraD, promote cell penetration of MS2 gRNA.

Additionally, the development of a novel, direct-labeling approach to detect and quantify F-pili dynamics will be described. This method yielded accelerated rates of pilus retraction compared to previously reported values (24). Similarly, an examination of a knockout and misexpression library of the F-pili T4SS genes will be described.

Several key genes for pilus secretion were identified and their effects on pilus number and length will be discussed.

CHAPTER II

SSRNA PHAGE PENETRATION TRIGGERS DETACHMENT OF THE F-PILUS*

Introduction

Single-stranded (ss)RNA phages have been identified for diverse bacterial hosts, including *Escherichia coli* (138, 139), *Pseudomonas aeruginosa* (81, 82), *Caulobacter crescentus* (83), and *Acinetobacter spp.* (54). All known ssRNA phages infect their hosts by initially binding to retractile pili, such as conjugative pili associated with conjugative DNA transfer and the type IV pili (which are not phylogenetically related to conjugative pili) mediating DNA uptake and twitching motility (86). Most of our knowledge regarding RNA phage biology stems from studies of the ssRNA phages that infect enteric bacteria carrying the F sex factor plasmids (95). These plasmids code for type IV secretion systems (T4SSs) and associated F-pili, which are hollow, filamentous, and dynamic appendages that extend and retract to initiate donor - recipient cell contacts during bacterial conjugation (24).

* Reprinted with permission from "ssRNA phage penetration triggers detachment of the F-pilus" by Laith Harb, Karthik Chamakura, Pratick Khara, Peter J. Christie, Ry Young, and Lanying Zeng, *PNAS,* **2020** doi: 10.1073/pnas.2011901117, Copyright 2020 by The Authors.

The infection process has been best studied with the ssRNA phage MS2 and its derivatives. MS2 has a ~3.5 kilobase (kb) genomic RNA (gRNA) that encodes four proteins: the maturation protein (Mat) used for host recognition, the coat protein (Coat) that forms the capsid, the lysis protein (L), and the replicase (Rep), the viral subunit of the RNA-dependent RNA replicase. The virions are ~27 nm in diameter (140) and consist of 178 copies of Coat encapsidating the gRNA, which is bound to a single copy of Mat (141). Infection is initiated when MS2 adsorbs to the side of the F-pilus via the Mat protein. The binding of MS2 to piliated cells at 4°C or free F-pili at 4-37°C is reversible and does not lead to loss of infectivity in the viral particles (60). However, at 37°C, the interaction of MS2 with piliated cells leads to release of the gRNA from the capsid and its penetration into the cell (61), a reduction of cellular nucleoside triphosphates (62), and cleavage of the 44 kDa Mat into two peptides that remain associated with the cell (64).

The role of F-pili in the transfer of gRNA from the virion into the cell is mysterious. Two prevailing models account for the mechanism of transport by F-pili. In the ‘pilus conduction’ model initially proposed by Brinton (1965), the pilus-docked phage delivers its gRNA into the central channel of the F-pilus for conveyance to the cell interior (65). Although there is little direct evidence for this model, the pilus lumen contains basic residues that potentially interact with the negatively charged gRNA (66). In the ‘pilus retraction’ model, the pilus-docked phage gains access to the bacterial cell surface through retraction of the pilus, whereupon the Mat-gRNA complex passes across the cell envelope through the T4SS or another route (142). Although not reported for F-

pili, RNA phage particles have been shown to accumulate at the base of pili elaborated by IncP and IncC plasmids during infection, suggesting that pilus retraction has occurred (60, 143, 144). More support for this model comes from the finding that *P. aeruginosa* cells infected with the ssRNA phage PP7 had a 50% reduction in overall type IV pilus lengths and that phage particles were often seen at the bases of pili, as observed by electron microscopy (67). In the absence of firm experimental support for either model, it remains unknown how the Mat-gRNA complex passes through the bacterial envelope into the cell interior.

In this study, we used fluorescently labeled MS2 phage to characterize F-pilus dynamics during ssRNA phage infection. Strikingly, we discovered that MS2 triggers release of F-pili by a mechanism requiring retraction. Our findings strongly support the 'pilus retraction' model and suggest a novel mechanism for superinfection exclusion resulting from ssRNA phage infection.

Materials and Methods

Bacterial Strains, Phages, Plasmids, and Primers

Strains used in this study are summarized in Table 2.1. All *E. coli* strains were grown in LB media containing appropriate antibiotics at standard concentrations: ampicillin (100 µg/mL), carbenicillin (100 ug/mL), tetracycline (10 µg/mL), rifampicin (50 µg/mL), kanamycin (50 µg/ml), chloramphenicol (10 µg/mL). Cells were grown in baffled flasks at 37°C with shaking (225 rpm) unless otherwise indicated.

Table 2.1 Bacterial strains, phages, plasmids, and primers used in this work.

Bacterial Strain, Phage, or Plasmid	Description	Source
***E. coli* strains**		
RY15177	HfrH *lacI*^{q} *fhuA::*Tn*10*	Ryland Young
LZ1832	MG1655 *lacI*^{q} Δ*lacY*	Laboratory stock
LZ2619	MG1655 F´*proA*$^{+}$*B*$^{+}$ *lacI*^{q} Δ*(lacZ)*$_{M15}$ *zzf::Tn*10(Tet^{R})/ *lacI*^{q} Δ*lacY* [pZE12-Coat-sfGFP]	This work
ER2738	F´*proA*$^{+}$*B*$^{+}$ *lacI*^{q} Δ*(lacZ)M15 zzf::Tn*10(Tet^{R})*/ fhuA2 glnV* Δ*(lac-proAB) thi-1* Δ*(hsdS-mcrB)5*	Ryland Young
MC4100	F- *[araD139]B/r* Δ(*argF-lac*)*169* λ^{-} *e14*$^{-}$ *flhD5301* Δ(*fruK-yeiR*)*725*(*fruA25*) *relA1 rpsL150*(*strR*) *rbsR22* Δ(*fimB-fimE*)*632(::IS1) deoC1*	Peter Christie
HME45*rif*^{r}	W3110 *gal490 pgl*Δ8 λ*cI857* Δ*(cro-bioA) rif*^{r}	Peter Christie
DH5α	F– *endA1 glnV44 thi-1 recA1 relA1 gyrA96 deoR nupG purB20* φ80d*lacZ*ΔM15 Δ(*lacZYA-argF*)U169, hsdR17(*rK*$^{-}$*mK*$^{+}$), λ^{-}	Peter Christie
MC4100*rif*^{r}	F-, *[araD139]*$_{B/r}$, *Δ(argF-lac)169*, *λ*$^{-}$, *e14*, *flhD5301*, *Δ(fruK-yeiR)725(fruA25)*, *relA1*, *rpsL150*(strR), *rbsR22*, *Δ(fimB-fimE)632(::IS1)*, *deoC1*, Δ*yaeH*::Cm^{r,} *rif*^{r}	Anna Konovalova
PC1000	MC4100 pOX38-Tet^{R}	Peter Christie
PC1001	MC4100 pOX38-Tet^{R} Δ*traD*	Peter Christie
X90	F *lacI*^{q} *pro lac /ara* Δ*(pro-lac) nal1 argE(amb) rif*^{R} *thi1*	Christopher Hayes; (100)
CH6939	X90 Δ*traA::cat*	Christopher Hayes; (100)
Phages		
MS2		Laboratory stock
Qβ		Junjie Zhang
M13		Laboratory stock

Table 2.1 Continued

Plasmids		
pBAD24	Crb^r, pBAD cloning vector	Olivier Lichtarge; (145)
pKD13	Kan^r, carries FRT-Kan^R-FRT cassette	Olivier Lichtarge; (146)
pCP20	Crb^r Chl^r, *repA*(Ts); pSC101-based vector expressing the Flp recombinase	Olivier Lichtarge; (146)
pBAD33-coat-sfGFP	sfGFP fusion to MS2 coat protein controlled by pBAD	This work
pZE12-coat-sfGFP	sfGFP fusion to MS2 coat protein controlled by pLac	This work
pOX38-Tet^r	Tet^r derivative of F_{lac}	Laura Frost; (147)
pOX38Δ*traD*::FRT-Km^r-FRT	Tet^r Kan^r, pOX38 with the FRT-Km^r-FRT cassette in place of *traD*	This work
pOX38Δ*traD*	Tet^r, pOX38 deleted for *traD*	This work
pPK31	Crb^r, pBAD24 expressing *traD* from the P_{BAD} promoter	This work
Primers		
KC30	CGGCAGAAAAGTCCACATTG	This work
KC31	CACACTACCATCGGCGCTA	This work
LH1	GATTGGTACCATGGCATCGAACTTCACGCAATT	This work
LH2	GCCGTCTAGATTATTTGTAGAGCTCATCCATGCCG	This work
Del-traD(pOX38)-Frt-Km_F1	AATCAGTCCGACTGACTTTTTTTCTTCGGAATATCATCATGATCCGGGGATCCGTCGACC	This work
Del-traD(pOX38)-Frt-Km_R1	CCTGTTCATCAGAAATCATCTCCCGGCTCAACATCCTCCCCGGCTCCCGTGTAGGCTGGAGCTGCTTCG	This work
Up-traD-pOX38_F	CACTGAGCGGTTGTGCAAATTCTTTGTG	This work
Dn-traD-pOX38_R	GGCCATTTGATCAAATGATCGCAGGTC	This work
traD(pOX38)-NheI_F	CTAGCTAGCAGGAGGAATTCACCATGAGTTTTAACGCAAAGGATATGACCCAGG	This work
traD(pOX38)-HindIII_R	CCCAAGCTTTCAGAAATCATCTCCCGGCTCAACATC	This work

Construction of Coat-sfGFP

Plasmid pBAD33 MS2 Coat-GS_{15}-sfGFP (*cat araC* P_{ara}*::coat-*gs_{15}*-sfGFP*) encoding a Coat-$GlySer_{15}$-linked-super folder Green Florescent Protein was constructed by cloning the synthetic DNA fragment (g-block_MS2Coat_sfGFP from IDT, Inc.) into pBAD33 between the KpnI and HindIII sites. The MS2 *coat* gene was codon optimized to reduce the probability of recombination with the infectious MS2 cDNA clones. To construct the fusion construct, the MS2 Coat (YP_009640125.1) was codon optimized using the codon optimization tool (idtdna.com/CodonOpt) and the final translated product differed by a single amino acid substitution (A125V). A DNA sequence encoding 15 aa "GGGGSGGGGSGGGGS" linker and sfGFP was added in frame with the codon optimized 130 codons of MS2 *coat* to construct the *coat-*gs_{15}*-sfGFP* fusion and finally to facilitate cloning, restriction sites for KpnI and HindIII were added upstream and downstream, respectively. The cloned construct was verified by sanger sequencing (Eton biosciences) with primers KC30 and KC31. The insert from this plasmid was amplified by PCR using primers LH1 and LH2 that introduce KpnI and XbaI sites upstream and downstream of the product, respectively. The product was subcloned into pZE12 for induction with IPTG and confirmed by sequencing.

Preparation of MS2 lysates

A single colony of ER2738 was grown in 5 mL of LB with appropriate antibiotics overnight at 37°C. The overnight culture was diluted 1:100 fold in LB containing 4 mM $CaCl_2$ with antibiotics and grown at 37°C until OD_{600}~0.4 and infected with MS2 at a MOI of 20 and allowed to propagate for 5 hrs. Afterwards, 1%

chloroform was added and the cells were centrifuged at 8000 rpm for 30 mins. The GFP-tagged MS2 was prepared in the same way using LZ2619 cells with 1 mM IPTG treatment 10 mins post-infection. Purification of the phages was achieved using ammonium sulfate precipitation and CsCl gradient centrifugation (148). Briefly, 280g per liter of ammonium sulfate was added to the lysates in small increments before allowing them to chill at 4°C for 4 hrs. The precipitates were sedimented by centrifugation at 8000 rpm for 1 hr and resuspended in MS2 buffer (150 mM NaCl, 5mM EDTA, 50 mM Tris, pH 7.5). The suspensions were dialyzed in 3500-10 kDa MWCO cassettes 3 times at 2 hr intervals with MS2 buffer at 4°C before being treated with DNase at 10 U/mL for another hour at 4°C. A clearing spin was performed, then the phage preparations were mixed with 0.55 g/mL CsCl to produce a final density of 1.38. The suspensions were centrifuged at 45,000 rpm for 24 hours at 4°C. The bands were collected and dialyzed against MS2 buffer and the purified preparations were stored at 4°C.

Pilus detachment assay

Overnight cultures of piliated cells were diluted 1:1000 in LB containing antibiotics and 4 mM $CaCl_2$. The cells were grown to an OD_{600}~0.4 before being diluted into prewarmed LB containing 4 mM $CaCl_2$. Afterwards, purified WT MS2, Qβ, or M13 were added to the culture at an MOI of 5. Infections were performed at 37°C without shaking to minimize pilus agitation. Samples were removed at regular time points using cut pipette tips and dispensed into prechilled tubes and allowed to equilibrate on ice. A small volume equating to MOI=100 of MS2-GFP was added to the samples and left on

ice for 20 mins to allow phage adsorption to the pili. Samples were prepared for microscopy by spotting 1 µL of sample onto a large coverslip (24 × 50 mm, Fisher Scientific) and gently overlaying a small 1 mm-thick 1.5% agarose pad dissolved in PBS on the sample before placing under the microscope. Z stacks of 300 nm were used in the GFP channel to precisely measure pili. Cells and pili were imaged on multiple stage positions (between 10 and 20 per sample) in phase (100 ms exposure to detect cells) and GFP channels (100 ms to detect pili). The images were analyzed using NIS elements software for cell and pili counts and length measurements.

*Construction of pOX38 Δ*traD*

E. coli strain HME45 carrying pOX38 was used to generate a complete deletion of *traD* by recombineering (149). Briefly, a FRT-Kan^R-FRT cassette from pKD13 (146) was PCR amplified with primers to carry flanking 5' and 3' sequences of 41 and 50 bases with homology to the upstream and downstream regions of *traD*. HME45 (pOX38) was induced for expression of the λ *red-gam* genes by growth at 42°C for 15 min, the FRT-Kan^R-FRT amplicon was introduced by electroporation, and transformants were selected by plating on LB agar plates with kanamycin. Plasmid pPK31 expressing *traD* from the P_{BAD} promoter was constructed by PCR amplification of *traD* using primers described in Table 2.1 and pOX38 as a template, digestion of the PCR product with NheI and HindIII, and introduction of the resulting restriction fragment into similarly digested plasmid pBAD24. pPK31 was then introduced by transformation into HME45 carrying pOX38Δ*traD*::FRT-Kan^R-FRT for conjugative transfer of the pOX38 variant into MC4100 carrying pCP20 (146) expressing the Flp recombinase.

Transconjugants were streaked on LB agar and grown at 42°C overnight to induce recombinase expression for excision of the FRT-Kan^R-FRT cassette; the temperature shift also cured temperature-sensitive pCP20. Individual colonies were screened for Tet^r, Chl^s and Kan^s to identify a strain harboring pOX38Δ*traD*. The Δ*traD* mutation was confirmed by PCR amplification across the deletion junction and sequencing of the PCR fragment.

Conjugation assay

Donor and recipient strains were grown overnight in LB broth with appropriate antibiotics. Strains were then diluted 1:50 in fresh antibiotic-free LB broth and incubated with shaking for 3 hr at 37ºC. For induction of *traD*, the overnight donor strain was subcultured 1:50 in LB broth for 1.5 hr, induced with arabinose (0.2% final concentration), and grown for another 1.5 hr at 37ºC. Donor and recipient cultures were mixed in a 1:1 ratio and incubated at 37ºC for 1.5 hr. without shaking. The mating mixtures were then serially diluted and plated onto LB agar containing antibiotics selective for transconjugants (TCs) and donors (D). The frequency of DNA transfer was calculated as the number of TCs per donor (TCs/D). Experiments were repeated 3 times in triplicate and results of a representative experiment are presented.

Phage sensitivity assay

50 µL of overnight grown cells were spread on LB agar plates containing appropriate antibiotics and 0.2% arabinose if necessary for induction of *traD*. After drying, 2 µL of MS2 (10^9 pfu/mL) and M13 (10^{11} pfu/mL) phages were spotted at

different locations on the plate and incubated overnight at 37°C. Plates were then examined for plaque formation indicative of phage sensitivity.

RNA ejection assay

MS2 ejection was measured essentially as described previously (150). Briefly, piliated cells were diluted 1:100 from overnight cultures into LB containing 4 mM $CaCl_2$. Once OD_{600} reached 0.4, cells were diluted to OD_{600} 0.1 in prechilled LB containing 4 mM $CaCl_2$ and 100 µg/mL RNAse A. Purified MS2 was added to this culture at MOI=0.01 and was incubated on ice for 20 mins. Afterwards, the cultures were moved to a 37°C shaking waterbath to initiate infection. At regular timepoints after phage addition, samples were removed and diluted 100-fold into prechilled SM buffer. The titer was then determined for these samples following standard protocol.

RNA smFISH

A set of 48 probes of ~20 nucleotides in length targeting the 5' half of the MS2 genome with at least 2 nucleotide spacing between each probe was designed and synthesized using the Stellaris® Probe Designer from Biosearch Technologies (the sequences can be found in Table 2.2).The probes were designed with a 3' mdC(TEG-amino) modification to enable labeling with 6-carboxytetramethylrhodamine, succinimidyl ester (6-TAMRA, ThermoFisher Scientific, cat no. C6123) following protocols described (151). Briefly, we pooled 7.5 µL of each of the oligo solutions (48 oligo in total, 100 µM each) and added 40 µL of 1 M sodium bicarbonate, pH 8.5. We then added dye solution (1 mg of 6-TAMRA dissolved in 2.5 µL of DMSO and 25 µL of 0.1 M sodium bicarbonate, pH 9.0) to the probe mixture and incubated it protected from

light overnight at 37°C. The next day, we mixed 47 µL of 3 M sodium acetate, pH 5.2, into the solution, and then added 1180 µL of 100% ethanol and incubated the sample -80°C for 3 hr to precipitate the oligos. The oligos were then centrifuged and washed twice more by dissolving the pellet in 45 µL of DEPC-treated water, 5 µL of 3 M sodium acetate, pH 5.2, and 125 µL of 100% ethanol. After the washing steps, the probes were resuspended in 250 µL of 1× TE resulting in a 10× probe stock solution. The probe solution was diluted with 1× TE to make the 1× probe solution upon usage, and the labelling efficiency of the probes was determined using the NanoDrop to be 86%.

The probes were then used to detect MS2 RNA during infection using the following protocol. Overnight cultures of piliated cells were diluted 1:1000 in LB containing 4 mM $CaCl_2$ and appropriate antibiotics. The cells were grown at 37°C with shaking to OD_{600}=0.4 before being diluted into prechilled LB containing 4 mM $CaCl_2$. MS2 at a MOI of 0.5 was added and incubated on ice for 20 mins to allow for adsorption to pili. As a negative control, we added the same volume of SM buffer (100 mM NaCl, 10 mM MgSO4, 50 mM Tris-Cl, pH 7.5) to the culture. The cultures were moved to a 37°C shaking waterbath to initiate infection. At regular time points, an aliquot of the cells was centrifuged at 4500xG for 5 mins and resuspended in 1X PBS containing 3.7% formaldehyde. At this point, the samples were further processed following the established protocol (151). The cells were fixed for 30 mins on a nutator at RT before being washed 3 times in 1X PBS to remove excess formaldehyde. The cells were then treated with 70% ethanol and nutated for 1 hr to permeabilize the cells for probe penetration. The cells were centrifuged and resuspended in wash solution (40% (wt/vol)

formamide, 2× SSC) and incubated at room temperature for 5 min and centrifuged again. For hybridization, the cells were resuspended in 25 μL of hybridization solution (40% (wt/vol) formamide, 2× SSC, 1 mg/mL *E. coli* tRNA, 2 mM ribonucleoside-vanadyl complex and 0.2 mg/ml BSA) containing the probe mixture at a final concentration of 1 μM. The samples were then incubated at 30°C protected from light for overnight. Afterwards, samples were washed three times by incubating the cells in wash solution for 30 min at 30°C. After the third repeat of washing,10 μg/mL DAPI was added to the wash solution and used to stain the *E. coli* DNA. Cells were resuspended in 2× SSC and prepared for imaging. Cells were imaged in phase (100 ms exposure) and in the Cy3 channel to detect 6-TAMRA signals (50 ms exposure). Z-stacks were taken at 300 nm intervals.

Table 2.2 Sequences of smFISH probes used to detect MS2 RNA, oriented 5' to 3'.

MS2 5'_1	AGCGTCTCGCTAAAGACATT	MS2 5'_25	AGCATGTTACCTACAGGTAG
MS2 5'_2	ACCTCCTAGGAATGGAATTC	MS2 5'_26	TTACGTCAGTAACTGTTCCT
MS2 5'_3	ACTAAAAGCTCGCACAGGTC	MS2 5'_27	GAGCGTCAACGCTTATGATG
MS2 5'_4	GAGTTATCTTCAGTCTCACC	MS2 5'_28	CGATGCATGGCTGAGATTTG
MS2 5'_5	GAGTCCAGTTCGAACGATAT	MS2 5'_29	AAGGAGACTTTACGTACGCG
MS2 5'_6	CCCAGTCGAGTTAAAACGAC	MS2 5'_30	TCTAAGGTATGGACCATCGA
MS2 5'_7	TCGATGTGACACTTAACGCC	MS2 5'_31	CGTTGCCTGATTAATGCTAA
MS2 5'_8	TTTGGCTTACAGGGAAGAGG	MS2 5'_32	TTGAGGGCTCTATCTAGAGA
MS2 5'_9	GGCACTTCGATGTAAGTCAA	MS2 5'_33	AGTTAGAAGCCATGCTTCAA
MS2 5'_10	TAAAATTACCCTGGGTGACC	MS2 5'_34	CCATTGTCGACGAGAACGAA
MS2 5'_11	CTCTGCTAAAGCAACACCAA	MS2 5'_35	GAGTTAGAGCTGATCCATTC
MS2 5'_12	TTCACGAGCGCAATGGTTTG	MS2 5'_36	GTTACTTTGTAAGCCTGTGA
MS2 5'_13	CGATCTTCGTTTAGGGCAAG	MS2 5'_37	GATGGTGTATTTGCGATTCT
MS2 5'_14	GCCACGTGTTTTGATCGAAA	MS2 5'_38	TACAGGAAGCTCTACACCAC
MS2 5'_15	AACCAACCGAACTGCAACTC	MS2 5'_39	TTAAGTACGAACGCCATGCG
MS2 5'_16	CCTGGATATCACTCATTAGT	MS2 5'_40	AGTCGGAATTCGTGGCGAAA
MS2 5'_17	CCTTCGTAAGCATCTCATAT	MS2 5'_41	CCTTGCATTGCCTTAACAAT
MS2 5'_18	GTACGGCTCTCATAGGAAGA	MS2 5'_42	ATTAGTAGATGCCGGAGTTT
MS2 5'_19	GGCCATCTAACTTGATGTTA	MS2 5'_43	GGGTAATCCTCATGTTTGAA
MS2 5'_20	AAGTTTGCAGCTGGATACGA	MS2 5'_44	ACTTCTTTGTTGTCTTCGAC
MS2 5'_21	ACGATACGTCGCGATATGTT	MS2 5'_45	CCAGTAGCGACAGAAGCAAT
MS2 5'_22	CCAAACGTGCATCGTTTATG	MS2 5'_46	TGTAAAGTCGTCACTGTGCG
MS2 5'_23	ATACCTAGAGACGACAACCA	MS2 5'_47	TTCGTCCCTTAAGTAAGCAA
MS2 5'_24	ACACTATACCTAGTGGGTTC	MS2 5'_48	TAAGGTCGGATGCTTTGTGA

Fluorescence microscopy imaging

Imaging was performed primarily on a Nikon Eclipse Ti2 inverted epifluorescence microscope using a 100× objective (Plan Apochromat, NA 1.45, oil immersion) at room temperature and acquired using a cooled EMCCD camera with mask (Princeton Instruments). Occasionally, imaging was performed on a Nikon Eclipse Ti inverted epifluorescence microscope using a 100× objective (Plan Fluo, NA 1.40, oil immersion) with a 2.5x TV relay lens, and acquired using a cooled EMCCD camera (IXON 897, Andor, Belfast, UK). Cells were imaged under the phase-contrast and with standard fluorescent filter cubes: GFP filter (Nikon 96363), Cy3 filter (Nikon 96323). When presenting microscopy images in figures, uniform contrast settings are applied for each separate channel throughout the entire figure.

Results

Detection of F-pili by fluorescent labeling of MS2 particles

Previously, ssRNA phage particles labeled with residue-specific fluorescent dyes have been used to identify F-pili by fluorescence microscopy (152, 153). Although this method produces labeled virions, we noted a significant titer loss of 50% after labeling, possibly due to the labeling of Mat by the dye (153). To avoid perturbing the binding interface of the phage particles, we tagged MS2 virions with fluorescent proteins to illuminate F-pili, as previously carried out for labeling of phage lambda and P1 (154, 155). Cells harboring a plasmid encoding the MS2 Coat fused to sfGFP (Fig. 2.1A) were infected with MS2 and subsequently induced for production of the Coat-sfGFP fusion protein. During assembly, the phage incorporates fluorescent Coat proteins, resulting in

mosaic particles containing both native and GFP-tagged Coat (Fig. 2.1B). We typically obtain titers of ~$5x10^{13}$ pfu/mL for both the GFP-tagged and WT purifications. Purified fluorescent phages (here designated MS2-GFP) are easily detected under the fluorescence microscope (Fig. 2.1C). Analysis of the fluorescence intensity of the MS2-GFP foci resulted in a uniform distribution of GFP signal, suggesting that the majority of the foci represent one population of MS2-GFP (Fig. 2.1D). When mixed with cells harboring the F-plasmid, MS2-GFP specifically bind to and illuminate F-pili (Fig. 2.1E). MS2 does not bind to cells that lack F-pili (156) and, accordingly, cells carrying a deletion of the F-pilin gene *traA* were not fluorescent **(**Fig. 2.2).

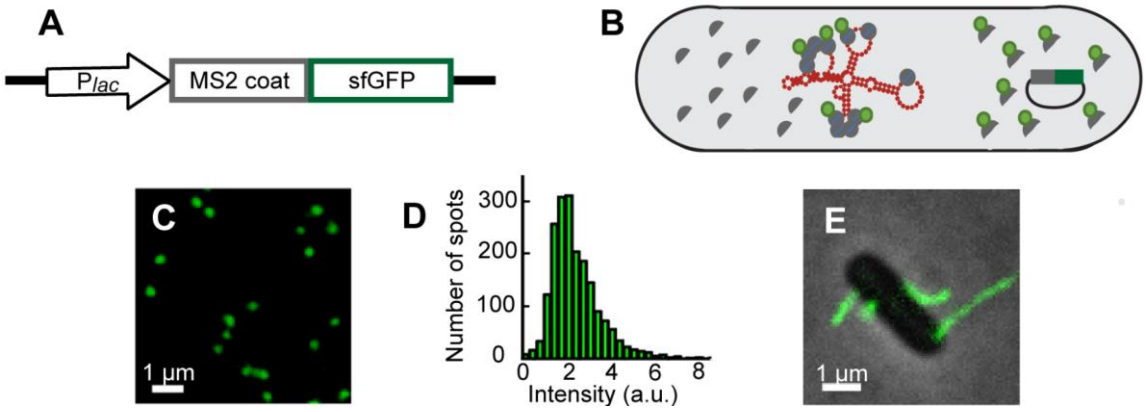

Figure 2.1 Fluorescent capsid labeling of MS2 virions to detect F-pili.
(A) The MS2 coat protein was fused to sfGFP and cloned downstream of P*lac* on the pZE12 vector. (B) Schematic of MS2-GFP assembly. Cells carrying the coat-sfGFP plasmid are infected with WT MS2 (RNA in red, not drawn to scale), then induced with IPTG to produce fluorescent coat proteins. Coat-sfGFP is incorporated along with WT coat proteins to form the mosaic capsid. (C) Purified MS2-GFP particles imaged under the fluorescence microscope. (D) Intensity distribution of MS2-GFP signal (1,826 spots). (E) Strain HfrH incubated with MS2-GFP. The fluorescent virions bind along the F-pili and enable their detection by proxy.

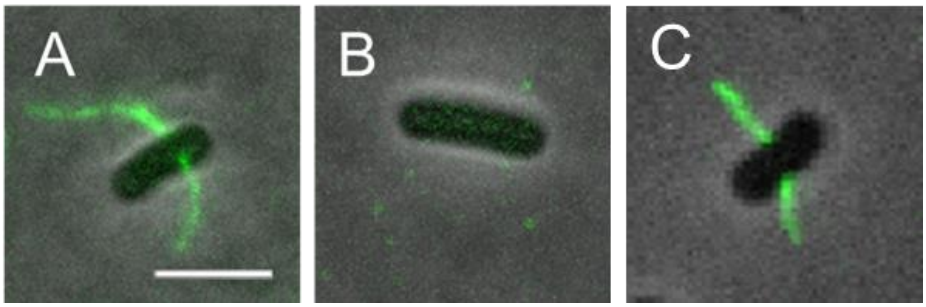

Figure 2.2 MS2-GFP interacting with *tra* mutants.
Cells incubated with MS2-GFP, as described in Methods. (A) Strain X90, carries WT F plasmid; (B) CH6939, F plasmid deleted of *traA* (Δ*traA*); (C) PC1001, F plasmid deleted of Δ*traD*. Scale bar is 2 μm.

Early infection by ssRNA phages leads to F-pilus detachment

Observing pili directly after phage infection has been difficult and traditionally has required the use of electron microscopy (62, 67). Here, we used the fluorescent phage to quantitatively evaluate the effect of MS2 binding on F-pilus behavior in liquid culture (Fig. 2.3). Separate cultures of *E. coli* HfrH were treated with MS2 at a multiplicity of infection (MOI) of 5, or buffer only, and incubated at 37^{o}C. Infections were performed without shaking to prevent pilus shearing. Aliquots were removed at different timepoints, dispensed into prechilled tubes, and allowed to equilibrate on ice prior to the addition of excess MS2-GFP at MOI=100 to visualize the F-pili. Since F-pilus outgrowth and retraction are inhibited on ice (98, 157), the addition of MS2-GFP to quantify pili does not promote further infection.

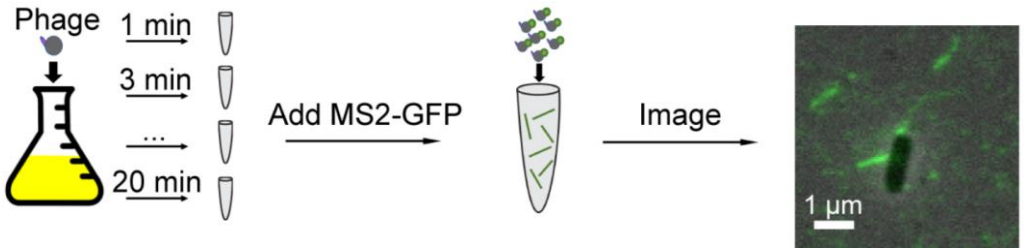

Figure 2.3 Schematic of pilus enumeration assay.
A phage suspension or equivalent buffer is added to a static culture of HfrH. Small aliquots are removed at different timepoints and dispensed into prechilled tubes. A surplus of MS2-GFP is then added to the chilled aliquots and then the samples are imaged by fluorescence microscopy. The representative image depicts detached pili and cell-associated pili.

Remarkably, the MS2-infected culture had a marked increase in the amount of free F-pili in the media, i.e., F-pili not attached to a cell, compared to the buffer-only control culture. As shown in Fig. 2.4A, the frequency of detached pili increases with time and reaches a plateau after ~10 min (~45%), which is when gRNA penetration is essentially complete (158). This suggests that F-pilus detachment is related to MS2 gRNA entry into the cell. Notably, we do not see any increase in detached pili in the uninfected culture, suggesting that the binding of high numbers of MS2-GFP to the pili does not lead to shearing or breakage during imaging.

To determine whether F-pilus detachment is MS2-specific, we tested whether other F-specific phages induce detachment. Like MS2, the ssRNA phage Qβ (an *allolevivirus)* binds to the side of the F-pilus. By contrast, ssDNA phage M13 binds exclusively to the pilus tip. Similar to MS2, we observed an increase in detached pili when cells are infected with Qβ, although ultimately only ~30% of the total pili are detached (Fig. 2.4A). In contrast to MS2 and Qβ, infection by M13 yielded a similar

basal level of pilus detachment as the uninfected control. These results suggest that phage-triggered F-pilus detachment is a phenomenon associated only with infection by ssRNA phages, or at least phages that bind to the sides of the F-pilus.

F-pilus retraction is required for phage-triggered detachment

We next examined how phage MOI affects the frequency and characteristics of F-pilus detachment. Cells were infected with MS2 at MOIs of 0, 0.5, 5, and 10, and the numbers of detached pili were quantitated at 10 min post-infection, which is when pilus detachment reaches a plateau. Notably, the frequency of detached pili increased from ~5% without infection (i.e., MOI = 0) to ~25% at an MOI of 0.5, and further increased and plateaued at ~50% at MOIs of 5 and 10 (Fig. 2.4B). The observed correlation between phage MOI and level of pilus detachment provides further evidence that phage entry triggers F-pilus detachment.

We next exploited differences in MOIs to test whether F-pilus retraction is required for phage-triggered detachment. Because MS2 can bind along the length of the pilus (59), at low MOIs, only a few phages will bind sparsely. By contrast, at high MOIs, phages will saturate the length of the pilus and, importantly, have a greater probability of binding near the base of the pilus. We reasoned that if F-pilus retraction is required for phage-triggered detachment, infection at higher MOIs should enrich for longer species of detached pili than infection at lower MOIs. Indeed, we observed a shift in the distribution towards longer lengths of detached pili with increasing MOI (Fig. 2.4C). The average detached pilus length increases from 1.64 μm at MOI = 0.5 to 2.16 μm and 2.19 μm at MOI = 5 and 10 respectively. The detached pili resulting from MS2 infection

are generally shorter than the cell-associated pili in the uninfected culture, which had an average of 2.66 μm (Fig. 2.5). These findings strongly indicate that MS2 causes detachment of F-pili in the process of retraction.

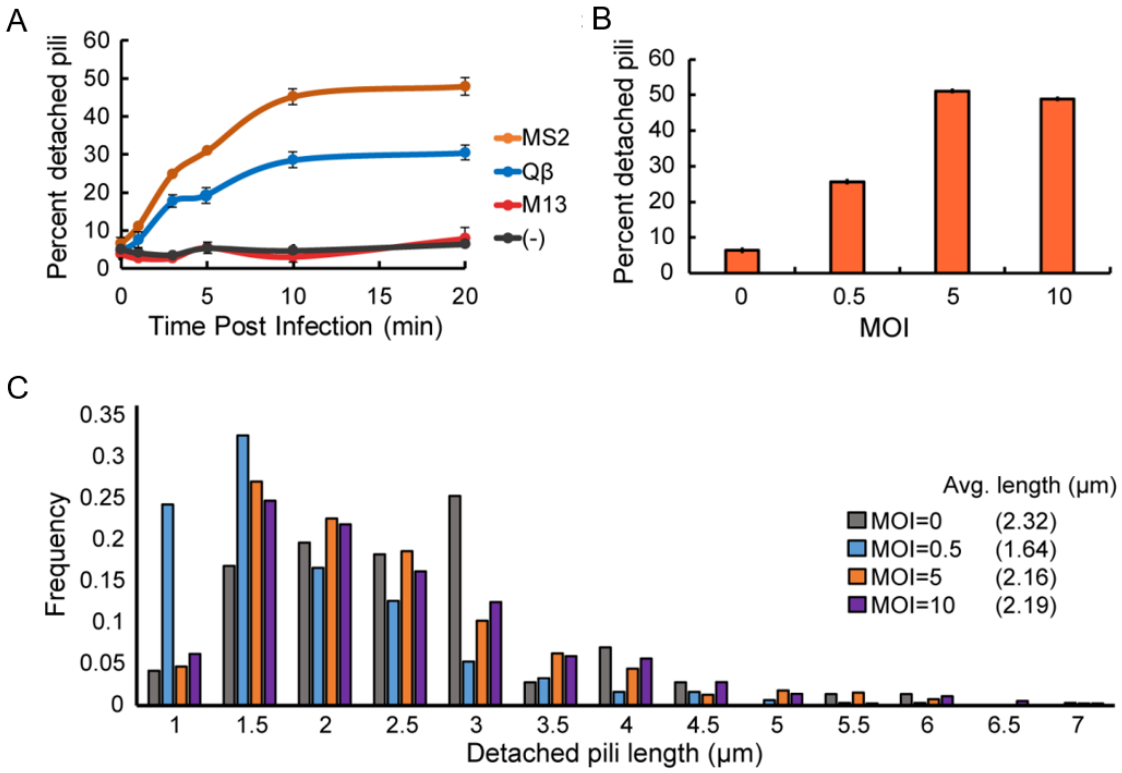

Figure 2.4 Infection by ssRNA phages leads to pilus detachment.
(A) Frequency of pili detachment over time (No. of pili: MS2 (4,701), Qβ (3,070), M13 (3,730), HfrH control (2,814)). The percentage of detached pili is the number of detached pili divided by the number of total pili (detached and cell-associated). (B) MOI effect on pilus detachment (No. of pili per MOI: 0 (1,072), 0.5 (1,170), 5 (1,130), 10 (1,123)). HfrH cells were infected with different MOIs of MS2 and samples were collected at 10 min. Note that MOI = 0 means uninfected. (C) Length distribution of detached pili at different MOIs (No. of detached pili per MOI: 0 (71), 0.5 (300), 5 (380), 10 (351)). Detached pili from MS2 infected cultures at 10 min post-infection were measured for length (average lengths of detached pili per MOI: 0 (2.32 μm), 0.5 (1.64 μm), 5 (2.16 μm), 10 (2.19 μm). Error bars denote standard deviation (SD). For (A), on points where error bars are not visible, SD is less than 1%. Each experiment was repeated at least twice.

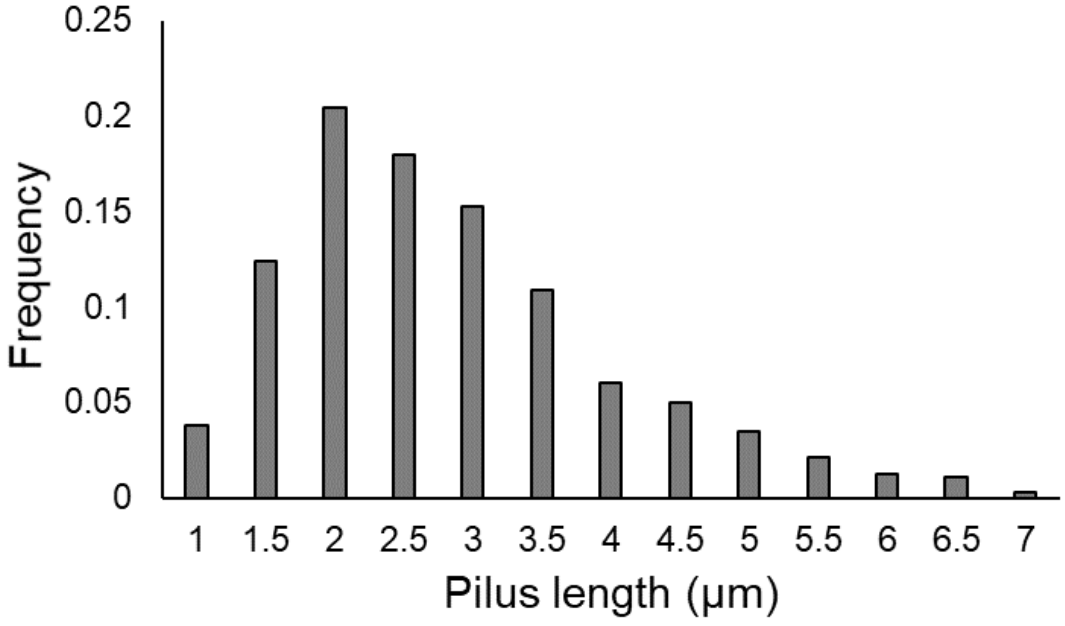

Figure 2.5 Length distribution of F-pili associated with HfrH cells in the absence of phage infection.
Pili were measured at the 10 min time point (No. of pili: 661, average length: 2.66 μm).

MS2-resistant mutant ΔtraD inhibits gRNA entry

Having gathered evidence suggesting that F-pilus retraction is required for MS2-triggered detachment, we next asked whether subsequent steps of phage infection are also required. Studies of MS2 and related phages, e.g., R17, have shown that the F-plasmid-encoded T4SS is required for phage entry, implying that the phage crosses the cell envelope via the T4SS channel (159). However, discriminating between the requirements of the F-pilus receptor and elaboration of the T4SS channel for phage infection and pilus detachment is challenging because mutations of T4SS components almost invariably abolish pilus production (160). One prominent exception is that mutation of TraD, an ATPase situated at the channel entrance that couples the F-plasmid substrate to the T4SS for conjugative transfer, blocks infection by the MS2-related phage f2 without effects on F-pilus biogenesis or phage adsorption (161). We thus explored the contribution of TraD to MS2 infection and MS2-triggered detachment of F-pili. First, we asked whether MS2 is capable of ejecting its gRNA upon binding to F-pili elaborated by Δ*traD* mutant cells. When ssRNA phages bind to F-pilus receptors, they undergo a process termed ‘‘eclipse’’, which involves release of the capsid from the phage particle, leaving the RNA susceptible to exogeneous RNase (61). Therefore, phage eclipse can be assessed through the addition of exogenous RNase to a culture prior to infection and then use of a plaque assay to determine if there is a reduction in plaque-forming units (pfu) of phage recovered from the culture supernatant (150).

We assayed for MS2 gRNA ejection upon binding of strains harboring pOX38, a fully functional variant of the F-plasmid F_{lac}, and an isogenic strain in which *traD* was

cleanly deleted from pOX38 (162). Our studies confirmed that the strain harboring pOX38 Δ*traD* elaborates WT levels of F-pili as monitored by MS2-GFP phage binding (Fig. 2.6) but failed to conjugatively transfer the F-plasmid through the F-encoded T4SS in mating assays (Table 2.3). By use of the phage eclipse assay, we determined that MS2 infection of the Δ*traD* mutant in the presence of RNase resulted in a decrease in viable phage particles recovered from the culture supernatant over time, becoming undetectable by 10 min (Fig. 2.7A). It is important to note that no loss of phage viability was reported when intact phage particles were incubated with RNase, indicating that the loss of infectivity requires phage eclipse (150). This decrease in pfu counts closely resembled that observed with MS2 infection of the RNase-treated parental strain harboring native pOX38 (Fig. 2.7A). MS2 thus commits to infection by releasing its gRNA upon binding to F-pili elaborated by both pOX38-carrying WT and Δ*traD* mutant cells.

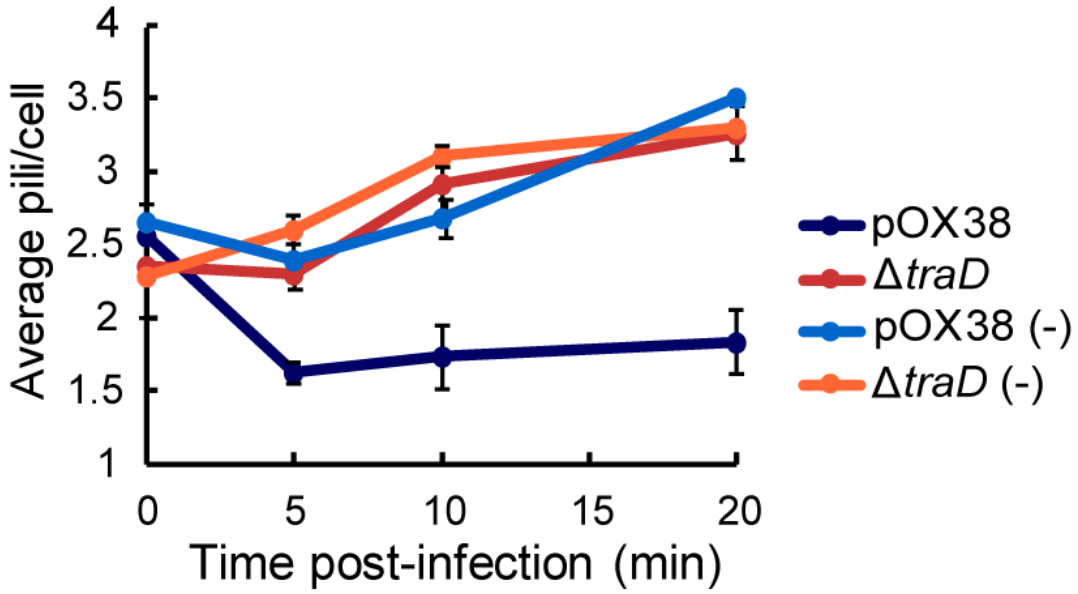

Figure 2.6 The change in the average number of cell-associated pili over time in uninfected (-) and infected samples from pOX38 and Δ*traD* cells.
Error bars denote SD. Where error bars are not visible, the SD is below 0.1.

Table 2.3 Phenotypic characterization of the Δ*traD* mutation.

Strains	**TCs/D**	**MS2 sensitivity**	**Qβ sensitivity**	**M13 sensitivity**
MC4100 (pOX38)	0.27	Sensitive	Sensitive	Sensitive
MC4100 (pOX38Δ*traD*)	0	Resistant	Sensitive	Sensitive
MC4100 (pOX38Δ*traD*, pPK31)	0.24	Sensitive	Sensitive	Sensitive

Conjugation efficiency was expressed as a ratio of transconjugants (TCs) per donor cell (D). For MS2 infection, sensitive is defined as forming clear plaques on the indicated strain. Resistant means the phage was unable to form plaques on the indicated strain.

The phage eclipse assay monitors release of gRNA from its capsid, but does not provide an indication of whether gRNA enters the bacterial cytoplasm. To determine if the Δ*traD* mutation affects gRNA entry into the cell, we used single molecule fluorescent *in situ* hybridization (smFISH) to directly detect MS2 RNA in the cell. As shown in Fig. 2.7B with probes designed to bind to the first half of the MS2 genome, we visualized MS2 RNA in pOX38-carrying cells. Single fluorescent foci corresponding to MS2 RNA were observed within 5 min of infection, larger clusters of fluorescence at 10 min post-infection, and at 20 min post-infection the signal filled the cell indicative of phage RNA replication. In striking contrast, no signal was detected upon MS2 infection of Δ*traD* cells, even after 10 min post-infection. By quantifying the percentage of infected pOX38-carrying cells, i.e., cells containing a detectable MS2 RNA signal over time, we found that the MS2 entry period is concluded by 10 min (Fig. 2.7C). Thus, despite the capacity of MS2 to undergo phage eclipse upon binding F-pili elaborated by strains harboring either pOX38 or the Δ*traD* variant, the phage RNA enters the cytoplasm only of pOX38-carrying cells. We conclude that TraD is required for passage of the MS2 gRNA across the cell envelope or entry into the cytoplasm.

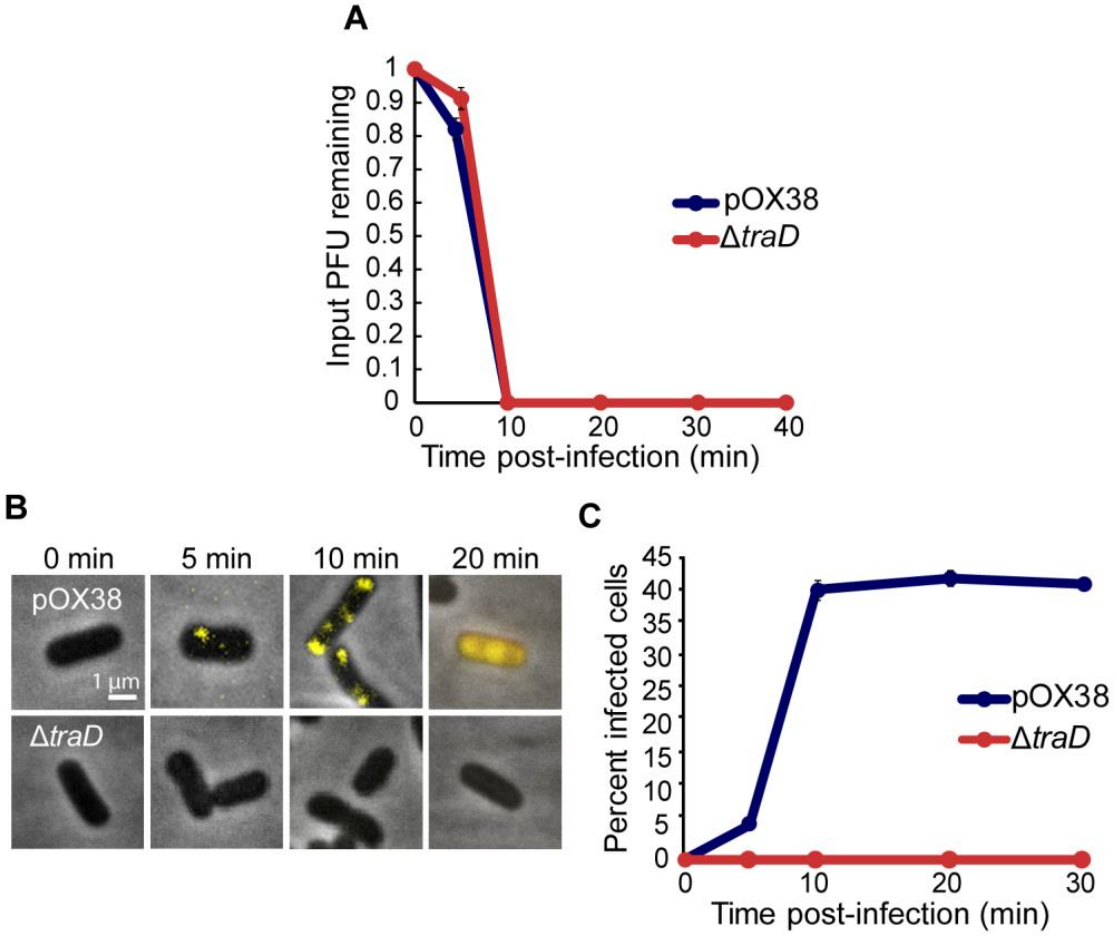

Figure 2.7 MS2 resistant mutant Δ*traD* inhibits MS2 gRNA entry.
(A) Loss of MS2 titer over time during infection of pOX38 or Δ*traD* cells in the presence of RNase. (B) Representative images of MS2 RNA in infected cells as detected by smFISH (MOI=0.5). The yellow signal (6-TAMRA) is indicative of MS2 RNA. The top row is pOX38 cells at different time points post-infection, while the bottom row is Δ*traD* cells. (C) The percentage of infected cells (i.e. cells containing MS2 RNA compared to the total cells) at different time points post-infection (No. of cells: pOX38 (4,515), Δ*traD* (3,511)).

MS2 triggers detachment of F-pili elaborated by ΔtraD mutant cells

We showed above that MS2-triggered detachment of F-pili requires pilus retraction (Fig. 2.4). We next asked if pilus detachment also requires phage entry. In view of our evidence the Δ*traD* mutation permits extracellular stages of infection, e.g., phage binding and eclipse, but blocks phage entry, we tested whether phage infection triggers release of F-pili from Δ*traD* mutant cells. Interestingly, reminiscent of our findings with HfrH cells, infection of the Δ*traD* mutant also induced pilus detachment. At 10 min post-infection, MS2 triggered F-pilus detachment from the Δ*traD* mutant, albeit at a lower frequency of ~20% compared with ~40% for infection of pOX38-carrying cells **(**Fig. 2.8A**).** We also measured the lengths of the detached pili found in supernatants of strains harboring pOX38 and the Δ*traD* mutant plasmid (Fig. 2.8B). The distribution of pili from the MS2-infected Δ*traD* mutant was similar to that from the infected pOX38-carrying strain, with average lengths of 2.31 μm and 1.99 μm, respectively. The difference in length could be attributed to the increased length of F-pili elaborated by Δ*traD* cells, as we determined that the average length of pili bound to Δ*traD* cells is 2.65 μm compared to 2.40 μm for pili bound to pOX38-carrying cells (Fig. 2.9). Together, these findings indicate that, first, F-pili elaborated by the Δ*traD* mutant retract and, second, F-pilus retraction is necessary for MS2-triggered pilus detachment. Finally, MS2 triggers F-pilus detachment prior to entry of the gRNA into the cytoplasm.

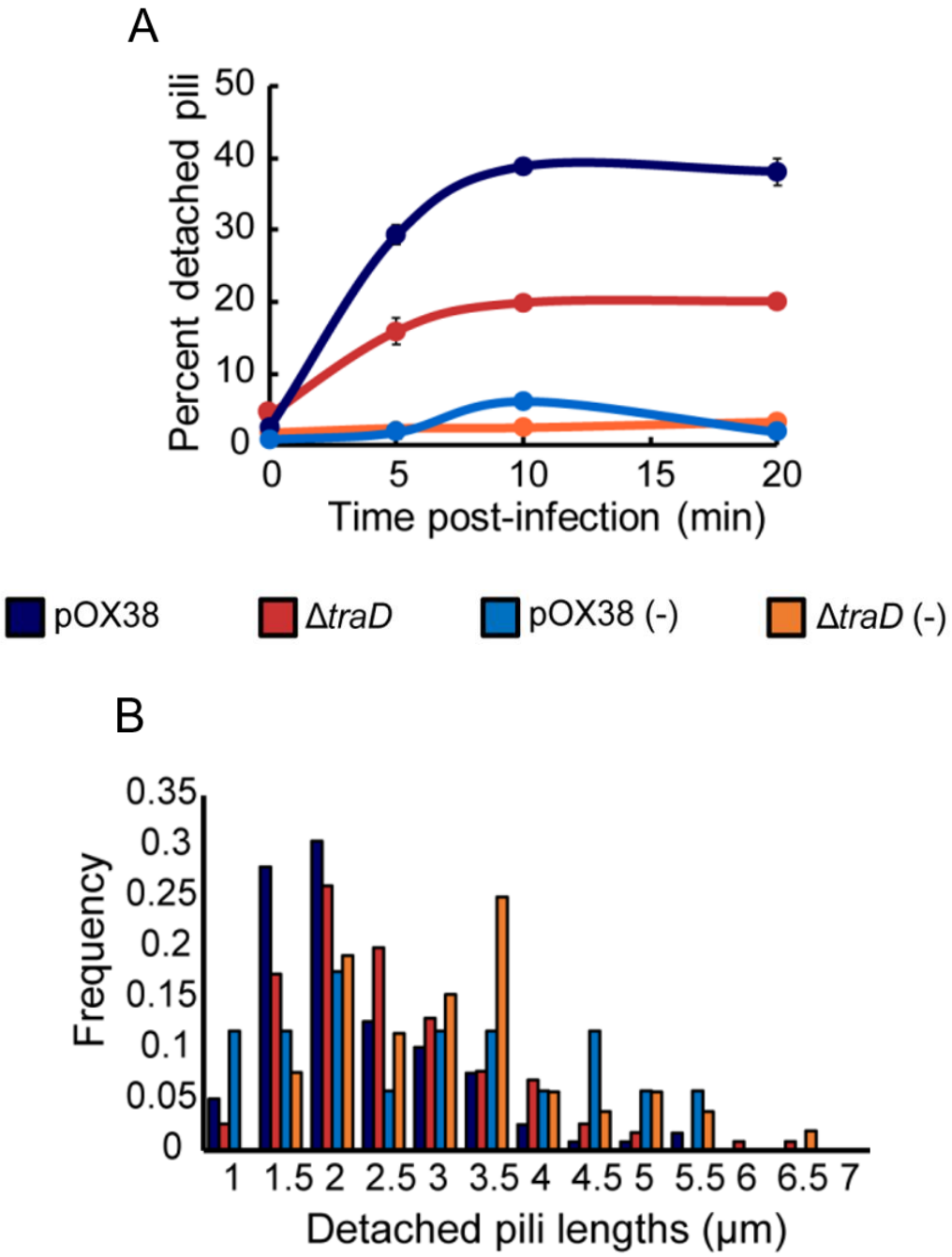

Figure 2.8 MS2 resistant mutant Δ*traD* releases pili after infection with MS2.
(A) Frequency of pili detachment over time when MS2 interacts with Δ*traD* cells and pOX38. The experiment was performed as in Fig. 2 (No. of pili: pOX38 (1,424), Δ*traD*

Figure 2.8 cont.
(1,669), Δ*traD* (-) (2,450), pOX38 (-) (2,088)). Minus symbols indicate the uninfected controls. (B) Length distribution of detached pili from samples in (A) at 10 min post-infection. (No. of detached pili per sample and average lengths: pOX38 (118, 1.99 µm), Δ*traD* (115, 2.31 µm), Δ*traD* (-) (17, 2.68 µm), pOX38 (-) (52, 2.92 µm). Error bars denote SD. Where error bars are not visible, SD is less than 2%. Each experiment was repeated at least twice.

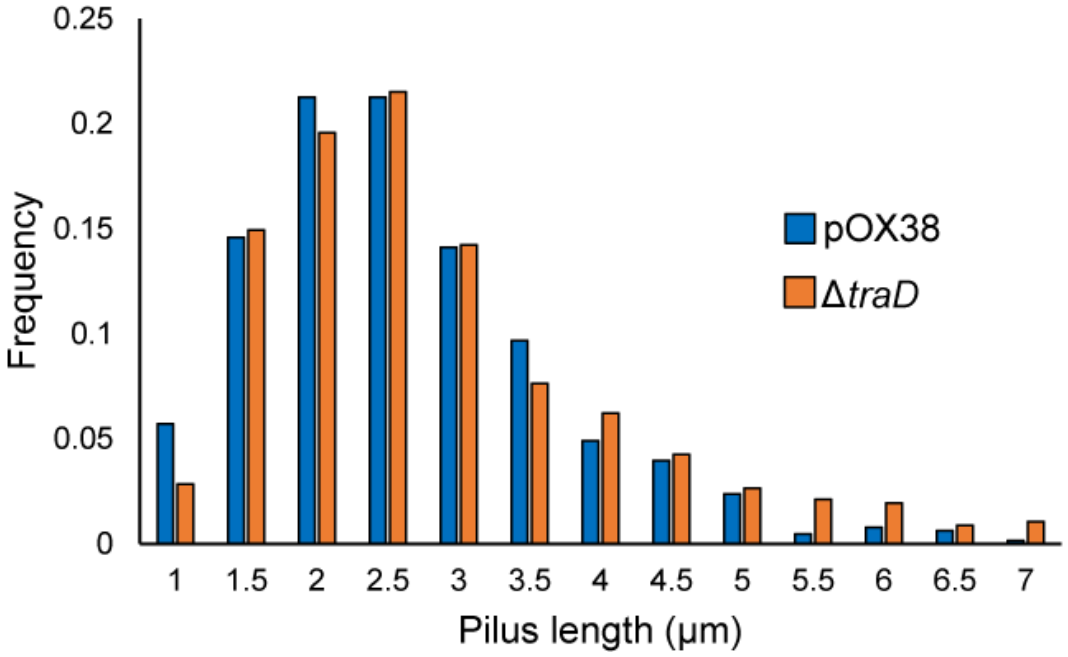

Figure 2.9 Length distribution of cell associated F-pili from pOX38 and Δ*traD*.
The pili were measured at the 10 min timepoint. No. of pili per sample and average length: pOX38 (630, 2.40 µm); Δ*traD* (562, 2.65 µm).

Discussion

In this study, we explored the fate of F-pili after infection with pilus-specific phages. We discovered that the ssRNA phages MS2 and Qβ trigger detachment of F-pili from the bacterial cell surface early during the infection process. Both the degree of detachment and the length of detached pili were correlated with the MOI, supporting the notion that pilus retraction is required for phage-triggered detachment. We also found that deletion of the TraD coupling protein blocks entry of MS2 gRNA into the host cell cytoplasm but does not affect the initiating steps of phage binding or 'eclipse', or phage-triggered pilus detachment. Our findings support a conclusion that MS2 and, likely other ssRNA phages such as Qβ, induce detachment of the F-pilus at a step of the infection process subsequent to the 'eclipse' phase but prior to entry of gRNA into the cell. We propose the following model (Fig. 2.10) to account for our findings, and further suggest that ssRNA phage-triggered detachment of F-pilus receptors represents a previously undescribed mechanism of superinfection exclusion.

ssRNA phages initiate infection by binding to the sides of the F-pilus **(**Fig. 2.10A**),** which has been shown to dynamically extend and retract (24). During retraction, bound phages are drawn close to the surface of the cell (Fig. 2.10B). To explain how phages might trigger F-pilus detachment during the retraction phase, it is first important to summarize recent structural findings for the F-encoded T4SS and associated F-pilus obtained by *in situ* cryoelectron tomography (cryoET). Importantly, these studies established that the diameter of the T4SS channel is only ~3.5 nm, considerably less than the width of the mature F-pilus (~8.5 nm). To reconcile this finding with early evidence

that F-pili assemble and retract by reiterative rounds of extraction and reincorporation of TraA pilin monomers from and into an inner membrane pilin pool, it was proposed that F-pili nucleate in two stages. First, TraA pilins are extracted from the inner membrane to build a thin protofilament, which extends through the central channel of the T4SS. Second, as the protofilament reaches the cell surface, it packs into the helical array visualized for the mature pilus. This two-stage assembly reaction proceeds until receipt of a signal for retraction, whereupon the process reverses and ultimately shunts pilin monomers back into the inner membrane. Interestingly, it was also observed that the walls of the F-pilus at the junction with the T4SS channel were thinner than in the mature helical fiber. The protofilament – mature pilus structural transition thus might represent a point of weakness that could account for the observed susceptibility of F-pili to breakage by shear forces (90).

In the context of this new model for F-pilus biogenesis, we propose one of two outcomes for pilus-bound phage upon encountering the pilus - T4SS channel junction during pilus retraction. Further retraction might generate a force that causes disruption of the Mat-pilin contacts and thus release of the virions. Alternatively, contact of the comparatively bulky phage with the pilus - protofilament junction might cause a torsional stress that breaks the mature pilus form the protofilament. In the latter pathway, after detachment of the mature pilus, further retraction of the protofilament would effectively pull Mat and associated gRNA from the virion and into the T4SS channel (Fig. 2.10C). The empty capsid, lacking any ability to bind to the cell, is released (Fig. 2.10D).

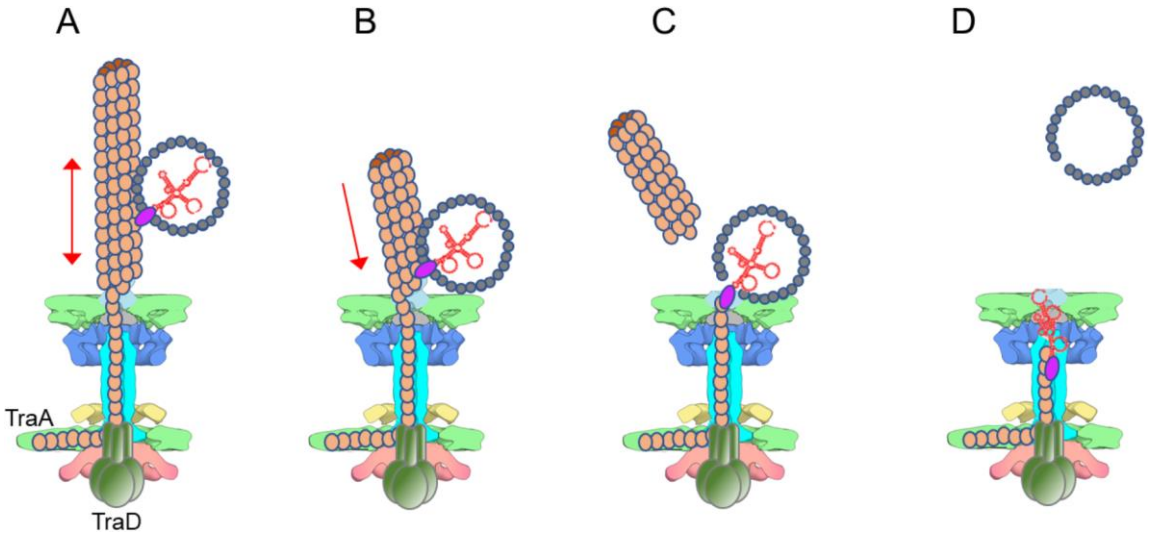

Figure 2.10 Model for pilus-detachment facilitated gRNA entry of ssRNA phage MS2.
(A) The ssRNA phage (not to scale) binds to the side of the pilus (orange) using the Mat (magenta). (B) Pilus retraction brings the ssRNA phage to the cell surface and in proximity to the basal body. (C) Continued retraction forces the Mat-gRNA (red) complex into the distal end of the basal body, causing breakage of the pilus at the point of entry. (D) Passage through the basal occurs and entry is faciliated by TraD (green). This figure was adapted with permission from (90).

Even relieved of the distal pilus and the viral capsid, the pilin-Mat-gRNA complex still represents a formidable cargo to traverse the T4SS channel, given the megadalton size of the gRNA. Unless the channel expands during this process, its diameter is too small to accommodate the numerous secondary structures that occupy most of the gRNA. It is also possible that the energy driving pilus retraction, e.g., ATP hydrolysis or the proton motive force, suffices to extract the Mat-gRNA complex from the virion and denature the secondary and tertiary structure of the gRNA. Other than the requisite Mat - pilin contacts for gRNA entry, we do not know if Mat or the capsid exterior also form specific contacts with the external surface of the channel. Even if so, these additional interactions are not required for phage infection, because the Mat-gRNA complex itself is infectious (163). Consequently, the strength of the Mat - pilin interaction is the driving factor, for successful infection, and it may also specifically underlie the dependence of MS2, but not Qβ, on the TraD T4CP for infection. Previous work has shown that MS2 adsorbs much more readily to F+ cells than Qβ (59), presumably reflecting differences in binding interactions between the two Mat proteins with F-pilin. TraD may thus be needed to detach the Mat_{MS2} from the pilin at the cytoplasmic interface of channel, but not for the comparatively weaker $Mat_{Q\beta}$ - pilin interaction.

We also visualized gRNA entry into the bacterial cytoplasm over time by use of smFISH. At early post-infection times, we detected one or a few foci, possibly reflecting sites of phage penetration across the cell envelope and entry of the gRNA into the cytoplasm. Between 10 and 20 min post-infection, phage replication ensues,

resulting in a proliferation of phage nucleic acid throughout the cell. Interestingly, in pOX38-carrying cells, we did not observe a significant increase in the cell-associated pili per cell following the 10 min entry period. By contrast, cells harboring the pOX38 Δ*traD* variant, or cells not exposed to phage, continue to elaborate F-pili over time, well beyond the 10 min time-frame required for phage entry into pOX38-carrying cells (Fig. 2.6**)**. Coupled with our finding that Δ*traD* cells are protected from infection by MS2, these findings suggest that phage infection blocks synthesis of F-pili, possibly due to the energy burden exacted on the host cells as evidenced by a reduction in cellular nucleotide triphosphatases that accompanies infection.

In summary, we have identified two mechanisms by which ssRNA phages can infect F-plasmid-carrying cells, but in the process render their hosts less susceptible to superinfection by other phages that are dependent on F-pili for attachment. First, infection triggers detachment of the F-pilus receptors. This effectively prevents other male-specific phages from infecting the same host cell, and it coincidentally generates a pool of F-pilus 'decoys' in the milieu to which phage bind non-productively, thus reducing the numbers of phage particles available for infection. Second, entry of phage into host cells imposes a block on further F-pilus assembly, again rendering host cells less susceptible to superinfection. In view of the selective advantage accompanying superinfection exclusion, we propose that one or both mechanisms may be prevalent in ssRNA phage systems that are dependent on retractile conjugative or type IV pili for infection.

CHAPTER III

SSRNA PHAGE PENETRATION CAUSES DETACHMENT OF TYPE IV MOTILITY PILI

Introduction

The single-stranded (ss) RNA phages infect a wide variety of hosts such as *Escherichia coli* (138, 139), *Caulobacter crescentus* (83), *Acinetobacter spp.* (54), and *Pseudomonas aeruginosa* (81, 82). All ssRNA phages are thought to exploit the mechanics of host-encoded surface pili to promote infection. These pili are dynamic, extracellular structures that facilitate several diverse host processes, such as conjugation (142), motility, and surface colonization (85). Bacteria encode large, multicomponent transmembrane complexes to control pilus assembly, secretion, and activity. For example, the paradigm ssRNA coliphages MS2 and Qβ utilize the conjugative F-pili (encoded by the fertility factor, or F-plasmid) to recognize the host, which are produced through type IV secretion systems (T4SSs) (95). Alternatively, the ssRNA *Pseudomonas* phage PP7 uses type-IV pili (T4P) which facilitate twitching motility (85). These are secreted through polar T4P machine complexes (114). Although most of our understanding of ssRNA phage biology comes from studies utilizing phages that infect *E. coli*, many commonalities exist between ssRNA phages that infect a diverse range of hosts.

The ssRNA phages make up the family *Leviviridae* and are among the smallest and simplest non-tailed phages. They carry linear, positive-sense ssRNA genomes about

4 kB in size (11). Generally, they encode 4 proteins: a maturation protein (Mat) used to recognize the host pili, a coat protein(s) which makes up the capsid, an RNA-dependent RNA polymerase, and a lysis protein. They form icosahedral, T=3 particles around 25 nm in diameter which contain 178 copies (89 dimers) of the coat protein and an exterior Mat protein.

The ssRNA phages bind to the side of their respective pili via an interaction between Mat and the pilus subunits (58). Infection leads to the release of the genomic RNA (gRNA) from the capsid which then penetrates the cell envelope through a lesser-known mechanism. A generally accepted model describing ssRNA phage cell penetration is the pilus retraction model, whereby the pilus-bound phage is brought to the cell surface by pilus retraction. Support for this model comes from the observation that *P. aeruginosa* T4P appeared to be around 50% shorter in length after infection with ssRNA phage PP7, and that phages were often seen at the bases of pili on the cell surface (67).

However, passage through the cell envelope may not be entirely explained by pilus retraction. Our recent work has described a phenomenon associated with ssRNA cell penetration: initial penetration of the MS2 or Qβ gRNA leads to the detachment of F-pili (164). We also found that MS2 gRNA entry into the host cytoplasm is reliant on the host-encoded coupling protein, TraD. The release of F-pili resulting from ssRNA coliphage infection causes the host to be less susceptible to superinfection, which may provide fitness advantages to the infecting phage population. This prompted us to further

investigate the pilus detachment phenomenon by expanding into other pilus-phage systems.

In this work, we utilized direct fluorescent labeling of pili to study the behavior of *P. aeruginosa* T4P during infection by PP7. Remarkably, we found that infection by PP7 results in the rapid release of T4P and that this release (and consequently, PP7 gRNA cell penetration) relies on extraneous forces generated by an auxiliary retraction ATPase. Our findings suggest that pilus detachment is likely a widespread phenomenon among pilus-specific ssRNA phages.

Materials and Methods

Bacterial Strains and Phages

Strains used in this study are summarized in (Table 3.1). Cells were grown in LB media at 37 °C with shaking (265 rpm) unless otherwise indicated.

Table 3.1 Bacterial strains and phages used in this work.

Strains	Description	Source
P. aeruginosa PAO1	Wild-type	Laboratory stock
ZG 1586	PAO1 *pilA*-A86C	Zemer Gitai
ZG 1593	PAO1 Δ*flic*	Zemer Gitai
ZG 1587	PAO1 Δ*flic pilA*-A86C	Zemer Gitai
ZG 1589	PAO1 *pilT*::[*Tn5*] *pilA*-A86C	Zemer Gitai
ZG 1592	PAO1 *pilU*::[*Tn5*] *pilA*-A86C	Zemer Gitai
Phages		
PP7		Laboratory Stock

Preparation of PP7 Lysates

A single colony of PAO1 was grown in 5 mL of LB overnight at 37 °C. The overnight culture was diluted 1:100-fold in LB and grown at 37 °C until OD_{600} ~0.4 and infected with PP7 at an MOI of 20 and allowed to propagate for 5 h with shaking. Then 1% chloroform was added, and the cells were centrifuged at 8,000 rpm for 30 min at 4 °C. Purification of the phages was achieved using ammonium sulfate precipitation and CsCl gradient centrifugation (38). In brief, 280 g per liter of ammonium sulfate was added to the lysates in small increments, followed by chilling at 4 °C for 4 h. The precipitates were sedimented by centrifugation at 8,000 rpm for 1 h at 4 °C and resuspended in 10 mL PP7 buffer (150 mM NaCl, 5 mM EDTA, and 50 mM Tris pH 7.5). The suspensions were dialyzed in 3.5–10 kDa molecular weight cutoff cassettes three times at 2-h intervals with 1L PP7 buffer exchanges at 4 °C, followed by treatment with DNase I at 10 U/mL for 1 h at 4 °C. A clearing spin was performed at 10,000 x g for 40 minutes, after which the phage preparations were mixed with 0.55 g CsCl per gram of phage solution to produce a final density of 1.38 g/mL. The suspensions were added to 13.5 mL Quick-Seal tubes (Beckman Coulter), placed into a Type 70.1 Ti fixed angle rotor (Beckman Coulter) and centrifuged at 45,000 rpm for 24 h at 4 °C. The bands (~2 mL) were collected and dialyzed against PP7 buffer as described, and the purified preparations were stored at 4 °C.

Sample Preparation for Labeling T4P

A single colony of a *pilA*-A86C containing strain was used to inoculate overnight cultures grown in LB media at 37 °C. The overnight culture was diluted 1:100 in fresh

LB and allowed to grow until the OD_{600}=0.4. Prior to this, working stocks of Alexafluor-488 C5-maleimide were prepared as follows. A 1 mg tube of Alexafluor-488 C5-maleimide was dissolved in dimethyl sulfoxide to a final concentration of 5 mg/mL, aliquoted, and stored in -20 °C. The dye was diluted 1:100 into a 100 µL aliquot of cells which were then incubated in the dark at 37 °C for 45 min. Cells were washed twice with LB by centrifugation at 6,000 rpm for 30 seconds in a tabletop centrifuge prior to use.

Pilus Detachment Assay

Labeled cells were placed into prewarmed tubes at 37 °C before a small aliquot of purified PP7 or equivalent buffer was added to the culture at different MOIs. Infections were performed without shaking to minimize pilus agitation. Samples were removed at indicated time points and dispensed into prechilled tubes and allowed to equilibrate on ice. Samples were prepared for microscopy by spotting 1 µL of sample onto a large coverslip (24 x 50 mm, Fisher Scientific) and gently overlaying a small, 1 mm-thick 1.5% agarose pad dissolved in PBS onto the sample before placing under the microscope. A series of 5-9 Z stacks of 300 nm were used to precisely measure pili. Samples were imaged on multiple stage positions (between 8 and 20 per sample) in phase (100 ms to detect cells) and green channels (100 ms to detect pili). The images were analyzed using NIS elements software for cell and pili counts.

Live-cell Observation of Motility and T4P Dynamics

Overnight cultures grown in LB were diluted 1:100 into fresh LB and incubated at 37 °C with shaking until the OD_{600} reached 0.4. For observation of twitching motility

without fluorescence, 50 µL of the log-phase cells were dispensed into prewarmed glass tubes at 37 °C and treated with either 5 µL of PP7 at MOI=5, or equivalent buffer, and allowed to incubate for 20 minutes without shaking. Afterwards, the sample was collected and pelleted by centrifugation at 6000 x g for 30 seconds. The supernatant was discarded and the pellet was resuspended in ~1 µL of LB. The suspension was spotted onto a large coverslip (24 x 50 mm, Fisher Scientific) and overlaid with a 0.5% agarose pad dissolved in LB. Another small coverslip (18 x 18 mm, Fisher Scientific) was placed on top of the pad. The samples were placed into a custom heat chamber set to 30 °C and placed under the microscope and imaged under phase contrast every 5 sec for 10 minutes. To observe T4P dynamics, cells were labeled and treated with PP7 at MOI=5 or equivalent buffer as previously described for 20 minutes without shaking. The sample was then pelleted by centrifugation at 6000 x g for 30 seconds. The supernatant was discarded and the pellet was resuspended in 1 µL of LB. Samples were prepared for microscopy by spotting the 1 µL sample onto a large coverslip (24 x 50 mm, Fisher Scientific) and gently overlaying a small, 1 mm-thick 0.5% agarose pad dissolved in LB onto the sample, placing an 18 x 18 mm coverslip on top of the pad, then placing under the microscope. Cells were imaged at 2 s intervals for 2 minutes at 30 °C unless otherwise indicated.

RNA smFISH

A set of 48 probes each ~20 nt long targeting the full length PP7 genome with at least a 2-nt spacing between each probe was designed and synthesized using the Stellaris

Probe Designer (Biosearch Technologies); the sequences are listed in Table 3.2. The probes were designed with a 3′mdC(TEG-amino) modification to enable labeling with Alexa Fluor 568 NHS Ester (succinimidyl ester; Thermo Fisher Scientific, catalog no. A20003) following previously described protocols (151). In brief, we pooled 7.5 μL of each of the oligo solutions (48 oligo in total, 100 μM each) and added 40 μL of 1 M sodium bicarbonate, pH 8.5. We then added dye solution (1 mg of dye dissolved in 2.5 μL of DMSO and 25 μL of 0.1 M sodium bicarbonate, pH 9.0) to the probe mixture and incubated the mixture protected from light overnight at 37 °C.

The next day, we mixed 47 μL of 3 M sodium acetate (pH 5.2) into the solution, added 1,180 μL of 100% ethanol, and incubated the sample at −80 °C for 3 h to precipitate the oligos. The oligos were then centrifuged and washed twice more by dissolving the pellet in 45 μL of DEPC-treated water, 5 μL of 3 M sodium acetate, pH 5.2, and 125 μL of 100% ethanol. After the washing steps, the probes were resuspended in 250 μL of 1 ×TE, resulting in a 10×probe stock solution. The probe solution was diluted with 1×TE to make the 1×probe solution on use, and the labeling efficiency of the probes was measured at >90% using a NanoDrop One UV-Vis Spectro-photometer (Thermo Fisher Scientific).

The probes were then used to detect PP7 RNA during infection using the following protocol. Overnight cultures of piliated cells were diluted 1:100 in LB. The cells were grown at 37 °C with shaking to an OD_{600} of 0.4 prior to the addition of PP7 at an MOI of 0.5. As a negative control, the same volume of buffer was added to another culture. At regular time points, an aliquot of the cells was centrifuged at 4500 ×

g for 5 min and resuspended in 1×PBS containing 3.7% formaldehyde. At this point, the samples were further processed following the established protocol. The cells were fixed for 30 min on a nutator at room temperature before being washed three times in 1×PBS to remove excess formaldehyde. The cells were then treated with 70% ethanol and nutated for 1 h to permeabilize the cells for probe penetration. The cells were centrifuged and resuspended in wash solution (40% [wt/vol] formamide, 2×SSC), incubated at room temperature for 5 min, and then centrifuged again. For hybridization, the cells were resuspended in 25 μL of hybridization solution (40% [wt/vol] formamide, 2×SSC, 1 mg/mL *E. coli* tRNA, 2 mM ribonucleoside-vanadyl complex, and 0.2 mg/mL BSA) containing the probe mixture at a final concentration of 1 μM. The samples were incubated overnight at 30 °C, protected from light. Afterward, samples were washed three times by incubating the cells in wash solution for 30 min at 30 °C. After the third washing, 10 μg/mL DAPI was added to the wash solution and used to stain the P. aeruginosa DNA. Cells were resuspended in 2 ×SSC and prepared for imaging. Cells were imaged in phase (100 ms exposure) and in the mCherry channel to detect Alexa Fluor 568 signals (50-ms exposure). Z-stacks were taken at 300-nm intervals.

Fluorescence Microscopy Imaging

Imaging was performed on a Nikon Eclipse Ti2 inverted epifluorescence microscope using a 100×objective (Plan Apochromat, NA 1.45, oil immersion) at room temperature and acquired using a cooled EMCCD camera with mask (Princeton Instruments). Cells were imaged under the phase-contrast and with the following fluorescent filter cubes: ET Gm #2 FISH (Chroma 49308, green) and mCherry filter

(Nikon 96365). When presenting microscopy images in figures, uniform contrast settings were applied for each separate channel throughout the entire figure.

Table 3.2 Sequences of smFISH probes used to detect PP7 RNA, oriented 5' to 3'.

PP7 1	GGCTGTAATAGTGTTCTTCG	PP7 25	CTTCCGCAAAAGGTTGTACA
PP7 2	AAAAACGGGGGGGTCAGTTT	PP7 26	GAAAGCTATAAGGCTTGCGC
PP7 3	TACACTCGAGCGTTATCTTC	PP7 27	GGTTCATAACGCGACAGTTG
PP7 4	CGAAGTTACCTTCGGATCAG	PP7 28	AATAAGGATCTTCGCGAGGC
PP7 5	TCGCGTCTCTCCTTATAAAG	PP7 29	GCCAAAAGTCGGAAAGCCAA
PP7 6	ATTACCGACCATCTTAAGGG	PP7 30	CTTTAAAGCTGGGAGCGAGA
PP7 7	CCGAAGATGAGCTCGAGATG	PP7 31	ATCACTCGCAGTAATACCTT
PP7 8	GGGCAATTCAGCATACTCAA	PP7 32	TCATCGACGATTGTGTATCC
PP7 9	GTACATCTACGGAGTTATCC	PP7 33	AGCGACAAAATCGAACCGGC
PP7 10	GTGCGAACGGAACCTGTAAT	PP7 34	CATAGCGATGAAGCGAACCG
PP7 11	AAGCGCTGTTCGAACACTTG	PP7 35	AGCAGCATGTTAAGTTCTGG
PP7 12	CTGTTTCAAAGGTAACGCCG	PP7 36	TTTAGTCGCTGGGTATTGAG
PP7 13	TTCTGGGATAGAACCGTGTA	PP7 37	TATCGGAAGCGCTAGACAGA
PP7 14	TCGGGAAAGTCTTTCCAACG	PP7 38	GGTTCGGAGATCCAATACAT
PP7 15	AACGTCAGCATGGAACCGAA	PP7 39	ATATCATCGCCGTAAATGGC
PP7 16	GTTTGAGATAACGCTGTGCG	PP7 40	CTCTACTACGCATTCACTGA
PP7 17	GTTTTGGACATTATGTCCTC	PP7 41	CCCCAATAACTCTTATCGAG
PP7 18	ACCTTCTCTTCGAAGATCTG	PP7 42	GGAAAAGGGCAGGTAGGTTA
PP7 19	TTAGGTTGACTCGATACGCG	PP7 43	CCGCTTTGGTATGTATGATA
PP7 20	TGGTGGAGCAATCAACGACG	PP7 44	AAGTGTAAGCCGGCAGTAAT
PP7 21	CGAGGGACTTGGTCAAATCG	PP7 45	AATGGTACGCGGGAAGACAC
PP7 22	GCTACTAAGGGTTTCCATAT	PP7 46	CGACGTATCGAACTTCGTCA
PP7 23	AGGAAGACCGAGCTCAGAAG	PP7 47	AACGATATCTCTTCCTCTCA
PP7 24	AGTACTCTTTTGCGAACTGC	PP7 48	CGGACTACGAGGTCAGAAGA

Results

PP7 Binds and Cleaves PAO1 T4P during Pilus Retraction

To detect and quantify T4P in *P. aeruginosa* PAO1, we employed a previously established method that permits direct fluorescent labeling of the T4P filament (107). A single cysteine substitution (A86C) in the *pilA* gene, encoding the major subunit of the T4P filament, permits labeling using thiol-specific fluorescent dyes. Cysteine modifications to detect various pili have been used in several cases and typically maintain their function (111, 128, 129). To ensure that the cysteine-modified pili still permit PP7 infection, we performed a standard titer assay to confirm. We found that PP7 is still able to infect the A86C mutant at a similar efficiency as the WT strain (Table 3.3), suggesting that adsorption to the pili and productive infection is unaffected by this mutation.

Table 3.3 Efficiency of Plating of different PAO1 mutants used in this study.

Strain	Efficiency of Plating (EOP)
PAO1 Δ*fliC*	1
PAO1 Δ*flic pilA*-A86C	0.86 ± 0.09
PAO1 *pilT*::[*Tn5*] *pilA*-A86C	$<10^{-9}$
PAO1 *pilU*::[*Tn5*] *pilA*-A86C	$<10^{-9}$

EOP and standard deviations of PP7 titer on different PAO1 mutants. EOP is determined by dividing the titer of a PP7 preparation on a test strain by the titer of the same preparation on the indicator strain (PAO1 Δ*fliC*). Experiments were performed at least twice.

We next used this technique to quantitatively assess the behavior of T4P directly after the addition of infectious PP7 particles. Separate cultures of cysteine-modified PAO1 were labeled and treated with either purified PP7 at an MOI of 5, or an equivalent buffer, and placed at 37 °C without agitation to reduce possible shearing of the T4P. Aliquots were removed at certain time points, dispensed into prechilled tubes, and were allowed to equilibrate prior to imaging. Remarkably, we observed a marked increase in the frequency of free T4P present in the surrounding media (Figure 3.1). This detachment is rapid, as most of the detachment occurs within 3 minutes post-infection before plateauing around 20 minutes post-infection (Figure 3.1B). Notably, the uninfected cells exhibit only minimal levels of pilus detachment, suggesting that some early stage of PP7 infection leads to the release of T4P.

We next examined how MOI influences the frequency of T4P detachment. Cells were infected with increasing MOIs and T4P detachment was quantified at 20 minutes post-infection, which is when the pilus detachment frequency plateaus. We found that MOI modulates the level of T4P detachment, with higher MOIs leading to greater levels of T4P detachment (Figure 3.1C). We observed that the frequency of detachment reaches a plateau at MOIs of 50 or above. The greater frequency of pilus detachment with increasing MOIs provides further evidence that detachment of T4P results from PP7 infection.

The retraction model for ssRNA phage infection suggests that pilus retraction brings the pilus-bound phage to the cell surface where it is internalized (164). In *P. aeruginosa*, retraction is primarily controlled by the ATPase activity of PilT (107). We

used a retraction deficient *pilT* mutant to investigate how disruptions in T4P retraction affects the frequency of T4P detachment post-infection with PP7 over time. The infections were performed as previously described using the cysteine-modified PAO1 strain inactivated for *pilT* through a transposon insertion (107). The *pilT* T4P could be easily detected after fluorescent labeling, but retraction was not observed in this mutant (107). Additionally, PP7 was unable to form plaques on this *pilT* strain when challenged with 10^9 pfu/mL in a standard agar assay (Table 3.3), suggesting that T4P retraction promotes productive PP7 infection. During infection, we did not observe an increase in detached T4P compared to the uninfected control at any time point (Figure 3.1D). This suggests that T4P retraction is required for T4P detachment to occur.

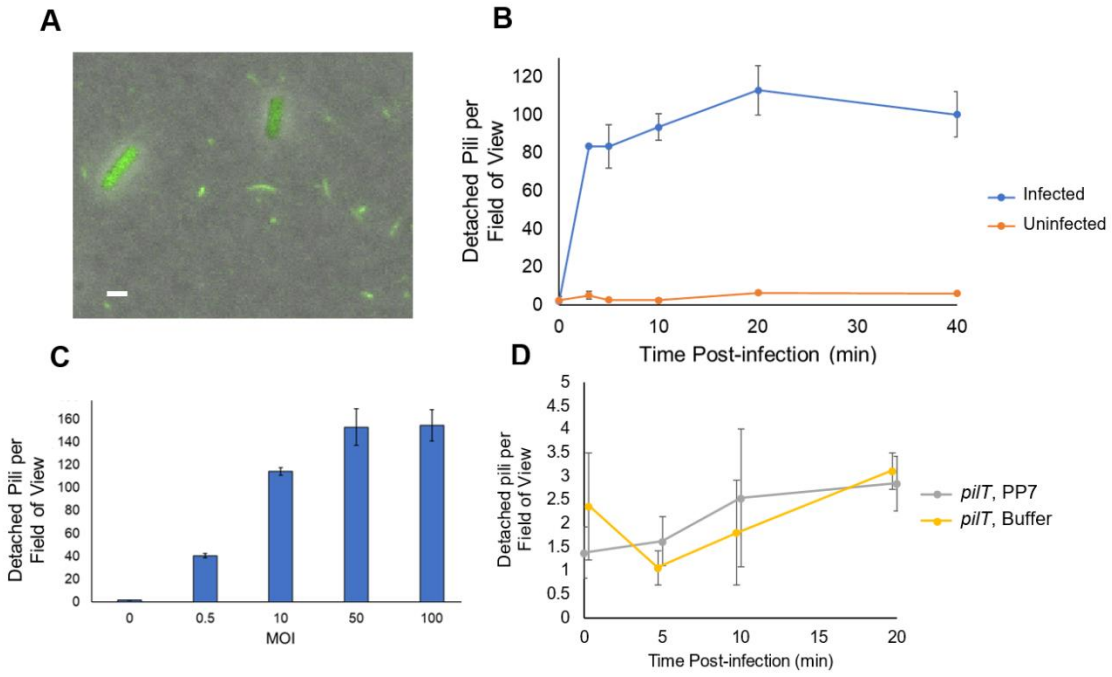

Figure 3.1 PP7 cleaves PAO1 T4P through pilus retraction.
(A) Representative image of detached T4P resulting from PP7 infection. (B) Frequency of detached T4P over time after infecting labeled cells with MOI=5 or equivalent buffer. Frequencies are presented as the detached T4P counts per imaging field of view at each time point. (C) MOI effect on T4P detachment. Samples were infected with the indicated MOI and collected 20 mins post-infection for analysis. (D) Frequency of T4P detachment over time in a retraction deficient *pilT* background. Cells were infected with MOI=5 or equivalent buffer and analyzed for T4P detachment. Points are slightly offset to avoid overlap. Scale bar is 1 µm. Error bars represent standard deviation. At least 200 cells were analyzed per time point or MOI. Experiments were performed at least twice.

PP7 Infection causes a Reduction in T4P Dynamics and Motility

The observation that PP7 infection results in the detachment of T4P prompted an investigation into how PP7 infection affects the function of these T4P. In *P. aeruginosa*, T4P mediate twitching motility through extension, tethering, and retraction to drive cell movement (85). While individual cells are capable of twitching, cells typically exhibit social motility by moving together in rafts (133, 165). Both extrinsic and intrinsic factors, such as media composition (135) and production of biosurfactants affect twitching motility differently (136). Factors that affect T4P production influence twitching motility, as cells that express more pili usually migrate farther distances when observed under light microscopy (137). Therefore, we explored how T4P detachment affects the frequency of twitching motility.

First, we observed how cells respond to PP7 infection under microscopy conditions that permit twitching motility (Figure 3.2). Cells were infected with PP7, placed onto a glass coverslip, and overlaid with a 0.5% agarose pad dissolved in LB prior to observation under light microscopy. Healthy, uninfected cells undergoing twitching motility typically display bursts of linear movement, direction reversals, and snapping to parallel alignment with neighboring cells. When cells collide with a surface, they typically reverse their movement direction, thus, cells at high density can appear to "jiggle" as they undergo frequent reversals (166). However, cells infected with PP7 displayed infrequent twitching events, with most cells appearing nonmotile (Figure 3.2). This suggests that PP7 infection and subsequent T4P detachment inhibits microscopic twitching motility in *P. aeruginosa*.

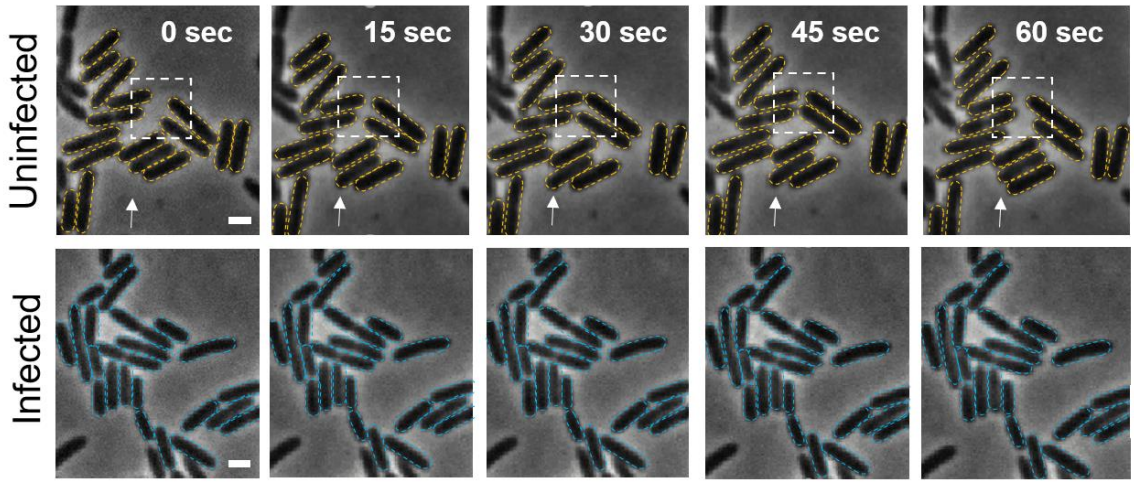

Figure 3.2 Microscopic Twitching Motility is largely Inhibited by PP7 Infection. Phase contrast image sequences illustrating twitching activities of buffer treated (top row) and PP7 infected (bottom row) ZG1587 cells. Cells were treated with PP7 or buffer for 20 minutes prior to preparation for live-cell microscopy. Cells were observed for up to 10 minutes and representative cell populations are presented. Individual cells are outlined to highlight motility between image sequences. White box and arrow indicate examples of twitching motility. Scale bar is 1 µm. Experiments were performed at least three times.

We next sought to determine how PP7 infection affects the dynamic activity of T4P. Cells labeled with Alexafluor-488 C5 maleimide were infected with PP7 for 20 minutes and T4P dynamics were observed under fluorescence microscopy (Figure 3.3A). As expected, the uninfected cells display typical, frequent T4P dynamic activity, with around 80% of cells producing at least one dynamic T4P within a 1 min observation window (Figure 3.3B). In contrast, only about 7% of the cells exhibited normal T4P dynamics after infection by PP7. In the infected population, most cells either did not produce T4P or maintained static T4P at the cell surface. Together, these observations suggest that PP7 infection causes both T4P detachment and prevents further elaboration of T4P from infected cells. The presence of static T4P among the infected cell population also suggests that infection may disrupt motor function and lead to T4P stalling on the cell surface. Additionally, the loss and subsequent inhibition of T4P biosynthesis resulting from PP7 infection supports our finding that infected cells are largely nonmotile under twitching conditions.

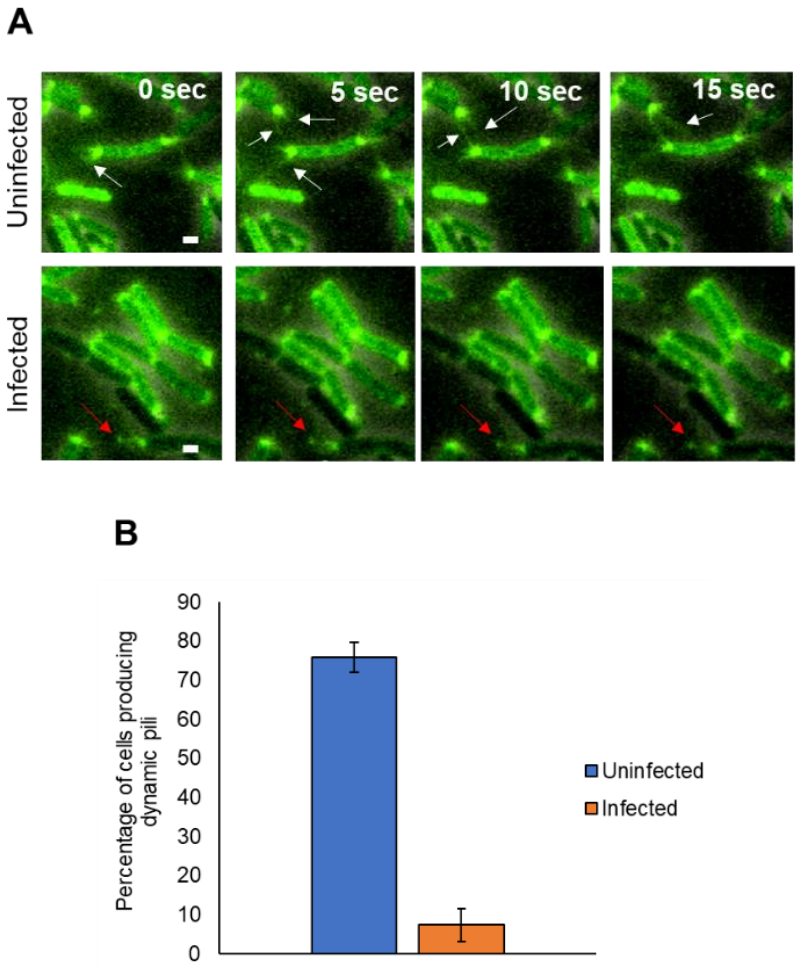

Figure 3.3 T4P Dynamic Activity is Inhibited by PP7 Infection.
(A) Representative live-cell fluorescent imaging sequences for buffer treated (top row) and PP7 infected (bottom row) Alexafluor-488 C5 maleimide labeled ZG1587 cells. Cells were treated for 20 minutes prior to observation. In the top row, extension and retraction of several T4P can be observed between frames (indicated by white arrows). Static T4P appear more frequently in the infected cells (bottom row, red arrow). Scale bar is 1 µm. (B) Quantitative analysis of T4P dynamic activity in buffer treated (uninfected) and PP7 infected cells. Error bars represent standard deviation. At least 80 cells were analyzed per experiment. Experiments were performed three times.

The Auxiliary Retraction ATPase, PilU, is required for Pilus Detachment

After identifying T4P retraction as a requirement for T4P detachment, we sought out other potential genes that could affect T4P detachment and subsequent infection by PP7. *P. aeruginosa* encodes a second retraction ATPase, PilU, which is thought to promote T4P retraction in high friction environments (134). Evidence for this stems from experiments which show that *pilU* mutants exhibit normal T4P dynamics in free solution yet are unable to mobilize in standard twitching agar assays (107, 134). Cells demonstrate twitching motility by moving across the surface-agar interface away from the initial point of inoculation, which may impose higher friction forces compared to free solution. Interestingly, we observed that a PAO1 strain inactivated for *pilU* does not permit plaquing by PP7 in a standard agar assay (Table 3.2). Since PilU likely works to generate additional retraction forces, we investigated how a *pilU* mutant affects the frequency of pilus detachment. We used the same T4P labeling approach to quantify pilus detachment after the addition of PP7 in a *pilU* inactivated mutant (107). In the PP7 treated sample, the frequency of detached pili closely resembled the basal levels found in the negative control at each time point (Figure 3.4). This suggests that *pilU* plays a role in eliciting pilus detachment.

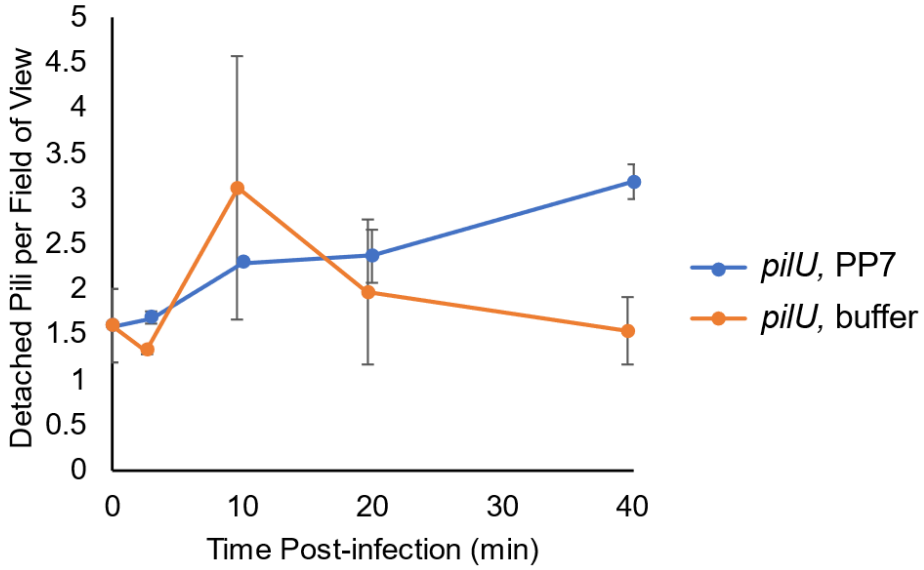

Figure 3.4 PilU promotes T4P detachment during PP7 infection.
Frequency of T4P detachment over time after treating labeled, *pilU* deficient cells with PP7 at MOI=5 or equivalent buffer. Frequencies are presented as the detached T4P counts per imaging field of view at each time point. Error bars represent standard deviation. Points are slightly offset to avoid overlap. At least 200 cells were analyzed per time point. The experiments were performed at least twice.

PilU is required for the cytosolic penetration of PP7 gRNA

After observing that T4P detachment occurs through pilus retraction and is contingent upon additional retraction forces generated by PilU, we next investigated how the *pilU* mutant affects the subsequent cytosolic penetration of PP7 gRNA during infection. We used a single molecule fluorescent in-situ hybridization (smFISH) approach to detect PP7 RNA in the cell (151). Using a fluorescent probe set targeting the full-length PP7 genome, we first visualized PP7 RNA in the WT background strain at several time points post-infection. Single fluorescent foci corresponding to the intracellular PP7 RNA were observed at 3 min post-infection (Figure 3.5A). At 10 minutes post-infection, more foci and larger clusters of fluorescent signal could be seen. Cells accumulated more diffuse fluorescent signal at 20 minutes post-infection, which is indicative of RNA replication. Over time, more cells became infected, indicated by a greater percentage of cells containing fluorescent signal. We quantified the percentage of cells containing fluorescent signal over time and observed that the PP7 entry period is largely concluded by 20 minutes (Figure 3.5B). Interestingly, this entry period closely resembles the timeline of pilus detachment, where we observed that the frequency of detached T4P plateaus around 20 minutes post-infection. In contrast, PP7 RNA penetration was inhibited in the *pilU*-inactivated background strain (Figure 3.5). As a control, we performed the same experiment in the retraction motor *pilT*-inactivated strain and did not observe any signal corresponding to PP7 RNA (Figure 3.6). Overall, this suggests that PilU is required for efficient RNA penetration during infection,

possibly by generating sufficient forces to facilitate detachment of T4P, and subsequent cytosolic penetration of the gRNA.

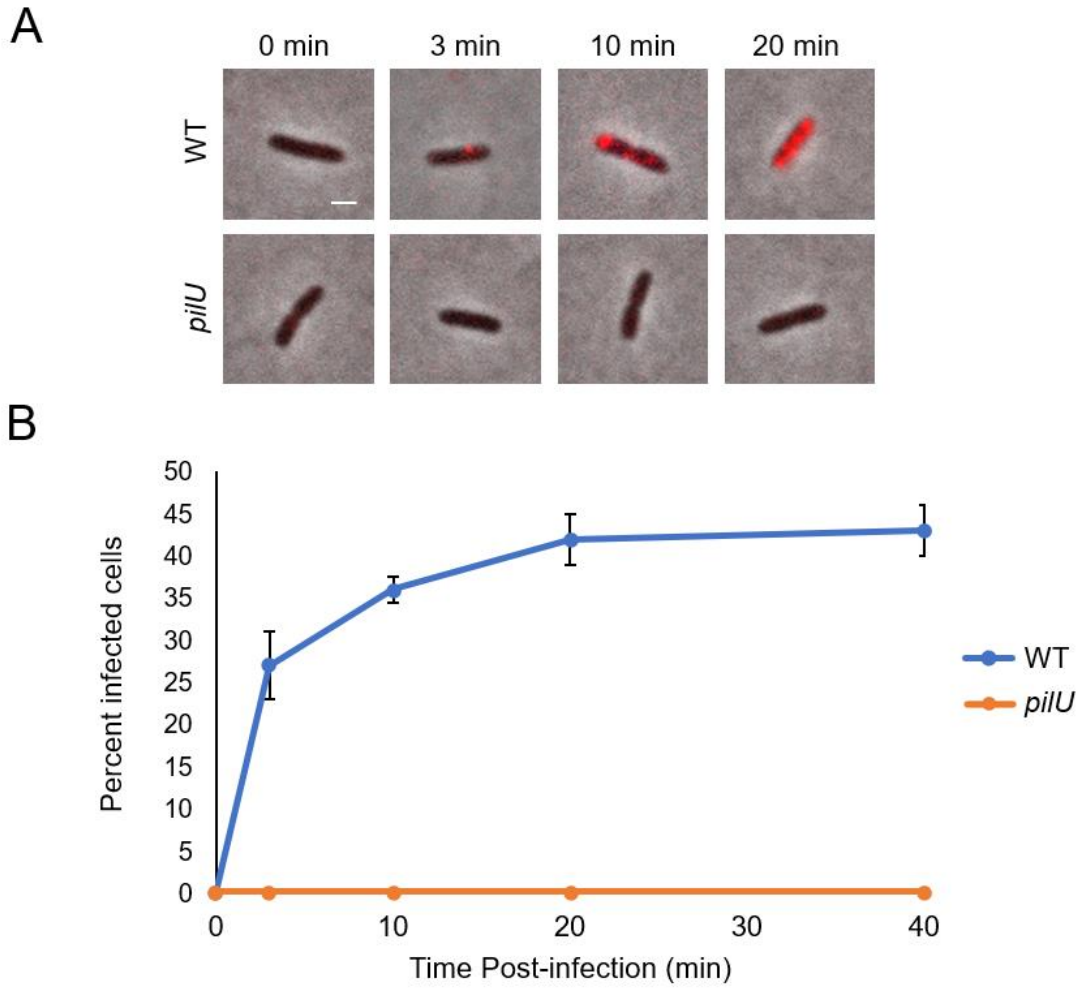

Figure 3.5 PilU is required for cell penetration of PP7 RNA.
(A) Representative images of PP7 RNA in infected cells as detected by smFISH (MOI=0.5). The red signal (Alexafluor 568) indicates PP7 RNA. (Top) ZG1587 cells at different time points post-infection. (Bottom) ZG1592 cells. (B) Percentage of infected cells (i.e., cells containing PP7 RNA compared to the total cells) at different time points post-infection. Error bars denote standard deviation. Scale bar = 1 μm. At least 300 cells were analyzed per time point. The experiment was performed twice.

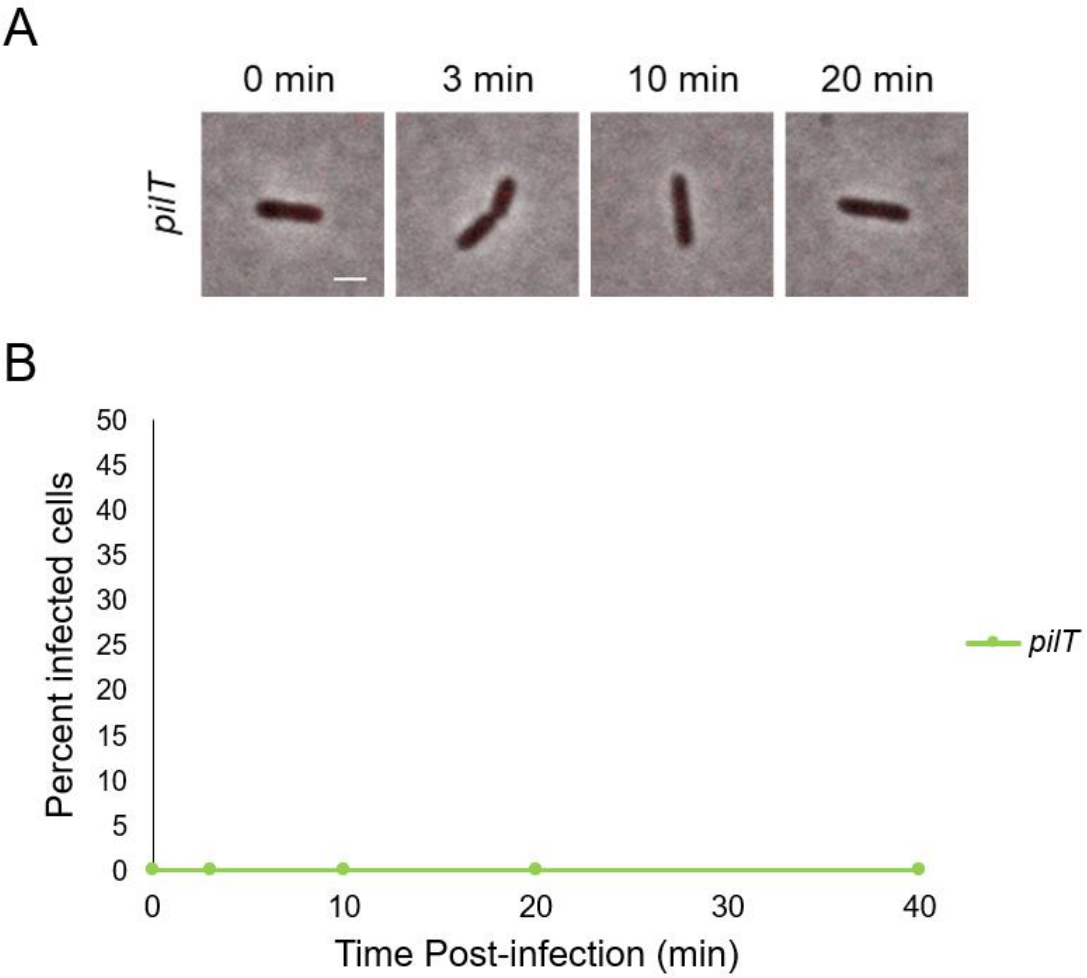

Figure 3.6 Pilus retraction is required for cell penetration of PP7 RNA.
(A) Representative smFISH images of *pilT* deficient cells after the addition of PP7 to detect cell penetration of PP7 RNA (MOI=0.5). Different time points post-addition of PP7 are shown. (B) Quantification of the percentage of infected cells (i.e., cells containing PP7 RNA compared to the total cells) at different time points post-addition of PP7. Scale bar = 1 μm. At least 300 cells were analyzed per time point. The experiment was performed twice.

Discussion

In our previous work, we discovered that the ssRNA coliphages MS2 and Qβ cause detachment of F-pili at the cell surface during initial penetration of the viral payload (164). Additional findings showing that F-pilus biosynthesis is inhibited through ssRNA infection suggested that several mechanisms exist that cause the host to be less susceptible to superinfection through pilus disruption (164). The possible fitness advantages therein prompted our investigation into T4P detachment during PP7 infection of *P. aeruginosa*.

Remarkably, we discovered that PP7 infection causes T4P detachment from the cell surface and that the degree of T4P detachment scaled with MOI. The use of a T4P retraction deficient *pilT* mutant showed only basal levels of T4P detachment, suggesting that detachment occurs through a mechanism involving pilus retraction. Using smFISH with the *pilT* mutant to visualize gRNA entry into the host cytoplasm, we found that cell penetration is also contingent on pilus retraction. These findings provide strong support for the pilus-retraction model to describe pilus detachment and subsequent gRNA penetration. This model, in brief, proposes that ssRNA phages, bound to the side of their respective pili via the Mat protein, are brought to the cell surface through pilus retraction. Like the F-T4SS, the channel of the T4P machine from *Myxococcus xanthus* cells was reported to be quite narrow, with a diameter of 11.5 nm (114). The mature T4P from *M. xanthus* had a diameter of 6 nm and density corresponding to the T4P spanned the entire channel, suggesting that there may be limited free space within the pilus-docked channel. Engagement of the relatively bulky pilus-bound phage with the distal

end of the pilus channel may cause stress on the pilus during continued retraction. In order to accommodate the Mat-gRNA complex into the channel, the T4P may become severed and released at the point of entry. After detachment, continued pilus retraction likely pulls the Mat-gRNA complex further through the cell envelope followed by entry of the gRNA into the host cytoplasm to initiate infection.

After observing T4P detachment resulting from PP7 infection, we determined how this phenomenon affects twitching motility. Twitching motility relies directly on the extension, tethering, and retraction of T4P to drag the cell forward. Interestingly, we discovered that PP7 infection largely inhibits twitching motility due to effects on T4P activity and biosynthesis. The loss of T4P through detachment and inhibition of new T4P secretion caused most cells to lack twitching motility when observed under light microscopy. These findings are supported by previous work demonstrating that T4P number correlates with the frequency of twitching events (137). Therefore, alterations to T4P number, such as those associated with ssRNA phage infection, can affect the ability of host cells to undergo twitching motility.

In addition to pilus retraction, we also discovered that the auxiliary retraction ATPase, PilU, is required for both T4P detachment and subsequent cytosolic penetration of the gRNA. PilU acts as a second retraction motor and appears to be engaged only when T4P are under relatively large loads, such as high friction while twitching under agar surfaces or biofilm matrices (134, 167). The separate but cooperative functions of PilT and PilU suggests that *P. aeruginosa* possesses sensing mechanisms to determine when the T4P is under high load to engage PilU efficiently. This could manifest as

physical compression forces instilled on the cell from an agar matrix that trigger high load retraction. Alternatively, disruptions in T4P dynamic activity could signal to the cell that it is within a high friction environment and therefore needs PilU to facilitate twitching motility. For the *P. aeruginosa* cell, the pilus-bound PP7 virion may be considerable cargo, given the mode of binding and the megadalton sized gRNA. It is possible that once retraction brings the pilus-bound phage to the cell surface, it causes the T4P to stall temporarily, effectively mimicking a high friction environment. PilU may then be engaged to promote stronger pilus retraction, resulting in T4P detachment and internalization of the PP7 gRNA. Our live-cell observations of T4P dynamics after the addition of PP7 showed instances of stalled T4P, which may provide support for this process. Additionally, we quantified the number of T4P associated with the cell after the addition of PP7 from our pilus detachment assays. We observed that cells have more surface T4P in the presence of PP7 (Figure 3.7). This observation is not necessarily a result of PP7 infection, however, since *pilT* mutant cells also appeared to have more surface pili compared to their basal levels without PP7. This suggests that the interaction between PP7 and T4P can lead to the enrichment of surface pili, possibly by slowing or stalling T4P retraction.

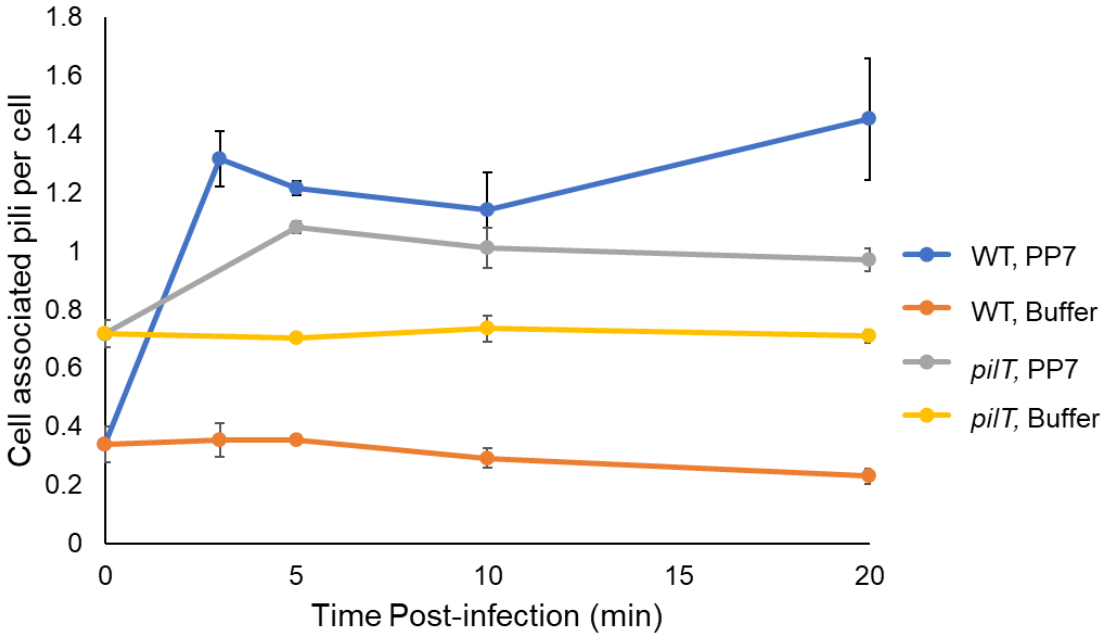

Figure 3.7 Addition of PP7 Increases Number of Cell Associated Pili.
The change in average number of cell associated T4P after the addition of PP7 or equivalent buffer to Alexafluor-488 C5 maleimide labeled cells. Cells were treated and incubated at 37 °C without shaking and aliquots were collected and imaged at the indicated time points. Cells were not washed (i.e., centrifuged) after treatment with PP7 or buffer. At least 200 cells were analyzed per time point. The experiment was performed at least twice.

In summary, exploring the behavior of T4P in *P. aeruginosa* after the addition of ssRNA phage PP7 revealed that the pilus detachment phenomenon is also present in this entirely separate pilus-phage system. Similar to our findings in the F-T4SS, several mechanisms were identified that work to prevent superinfection by other phages. First, T4P detachment occurs during infection, which directly removes surface pili. These pili become present in the surrounding media and can act as decoys for free phage to bind nonproductively, but reversibly, to further deter superinfection. Second, infection also inhibited the secretion of new T4P post-detachment, further discouraging superinfection by preventing receptor biosynthesis. Given that superinfection exclusion mechanisms provide fitness advantages, these mechanisms may be widespread among other diverse ssRNA phages that rely on the mechanics of retractile pili for cell penetration.

CHAPTER IV

GENETIC ANALYSIS OF DETERMINANTS OF SSRNA BACTERIOPHAGE CELL PENETRATION BY EXPERIMENTAL EVOLUTION

Introduction

Phages and their hosts are locked in an evolutionary arms-race: a predator-prey dichotomy where each entity must evolve to match the fitness changes of the other or face extinction (168). This conflict has high ecological relevance and is thought to influence global nutrient cycling and climate (169-171), evolution and diversity of the biosphere (1), and evolution of pathogenic bacteria (2). As bacteria evolve their phage defense mechanisms, such as restriction-modification systems, phages must evolve to counter these defenses.

Phage evolution is mediated by natural selection, or a bias towards retaining a specific allele(s) that increases reproductive success in a specific environment. The rate of evolution occurring through natural selection depends on the strength of the selection pressure and the mutation rate of the organism involved. Weak selection pressures will cause slow changes in phenotype (172), therefore, studying evolution on a reasonable time scale typically involves increasing the mutation rate, either by utilizing an organism with an already high mutation rate, such as an RNA phage (173), or by using a mutagenic chemical such as nitrosoguanidine (174).

The ssRNA bacteriophages have been favored for use in evolution studies because of their rapid generation times, extremely high mutation rates, and relatively

small genome sizes (175). This makes ssRNA phages particularly susceptible to selection pressures that can quickly spawn new genetic variants of which the full genomes can be sequenced. Evolvability of ssRNA phages has been assayed under different environmental pressures such as temperature (175), premature lysis, and variable host density (176). These selection pressures generally lead to increased fitness under the respective condition. The genomes of these newly evolved populations of phage can then be sequenced to assign a genotype-phenotype relationship to better understand how adaptation occurred.

Our previous work demonstrated that a host-encoded coupling protein, TraD, is required for RNA penetration of the ssRNA coliphage MS2 (164). TraD is responsible for initiating the secretion of the F-plasmid during conjugation in an ATP-dependent manner (177). It forms a hexameric ring on the cytoplasmic side of the type IV secretion system (T4SS) basal body and interacts with constitutive proteins bound to the F-plasmid in preparation for transfer to the recipient cell (178). Coupling proteins possess N-terminal transmembrane domains to associate with the inner membrane and highly conserved nucleotide binding domains (179). They share sequence similarities with the FtsK and SpoIIIE DNA translocases, which act as DNA pumps functioning in cell division and sporulation, respectively (180).

However, the mechanism describing how TraD facilitates RNA entry is still unclear. In this study, a continuous culture approach was used to adapt the ssRNA phage MS2 towards TraD independence to better understand how TraD facilitates RNA penetration. Maintaining a culture of MS2 and *E. coli* cells with tightly regulated, low

levels of TraD lead to a mutant MS2 population overtaking the culture within 15 hrs. Sequencing of this population revealed three single point mutations in the *mat*, *coat*, and *rep* genes. Recapitulating these mutants individually in the MS2 genome revealed that the mutation in the *mat* gene provides MS2 improved infectivity with low levels of TraD. Additionally, plaquing on various TraD mutants revealed that the C-terminal regions of TraD promote infection.

Materials and Methods

Bacterial strains, Phages, Plasmids, Primers

The bacterial strains, phages, plasmids, and primers are summarized in Table 4.1. All *E. coli* strains were grown in LB media containing appropriate antibiotics at standard concentrations: ampicillin (100 μg/mL), carbenicillin (100 μg/mL), tetracycline (10 μg/mL), chloramphenicol (10 μg/mL), and kanamycin (50 μg/mL). Cells were grown in baffled flasks at 37 °C with shaking (265 rpm) unless otherwise indicated.

Table 4.1 Bacterial Strains, Phages, Plasmids, and Primers used in this work.

Strains	Description	Source
PC1000	MC4100 pOX38-Tet^R	Peter Christie
PC1001	MC4100 pOX38-Tet^R Δ*traD*	Pratick Khara
PC1002	MC4100 pOX38-Tet^R Δ*traD* [pBAD24]	Peter Christie
PC1003	MC4100 pOX38-Tet^R Δ*traD* [pBAD24-*traD*$_{pOX38}$]	Abu Amar M. Al Mamun
RY34378	NEB5α [pT7MS2K] [pBAD33-MS2coatA2V-CI857]	Ryland Young
RY34462	DH5α [pBAD33-MS2coatA2V-CI857]	Ryland Young
LZ2646	DH5α [pT7MS2K (G1192T)] [pBAD33-MS2coatA2V-CI857]	This work
LZ2647	DH5α [pT7MS2K (A1543T)] [pBAD33-MS2coatA2V-CI857]	This work

Table 4.1 cont.

PC1004	MC4100 pOX38-Tet^R Δ*traD* [pBAD24-*traD*$_{pOX38}$ (K198Q)]	Yang Grace Li
PC1005	MC4100 pOX38-Tet^R Δ*traD* [pBAD24-*traD*$_{pOX38}$ ΔCT15]	Abu Amar M. Al Mamun
PC1005	MC4100 pOX38-Tet^R Δ*traD* [pBAD24-*traD*$_{pED208}$]	Abu Amar M. Al Mamun
PC1006	MC4100 pOX38-Tet^R Δ*traD* [pBAD24-*traD*$_{pOX38}$ CT15$_{pED208}$]	Yang Grace Li
PC1007	MC4100 pOX38-Tet^R Δ*traD* [pBAD24-*traD*$_{pED208}$ CT15$_{pOX238}$]	Yang Grace Li
PC1008	MC4100 pOX38-Tet^R Δ*traD* [pBAD24-*traD*$_{pOX38}$ CT166$_{pED208}$]	Yang Grace Li
PC1009	MC4100 pOX38-Tet^R Δ*traD* [pBAD24-*traD*$_{pED208}$ CT148$_{pOX38}$]	Yang Grace Li
Phages		
MS2		Laboratory stock
MS2 (G1192T)		This work
MS2 (A1543T)		This work
Qβ		Laboratory stock
Plasmids		
pT7MS2K	MS2 cDNA plasmid under control of T7 promoter	Ryland Young
[pBAD33-MS2coatA2V-CI857]	MS2 *coat*/ *CI857* transcriptional fusion under control of pBAD promoter	Ryland Young
pBAD24	Crb^R pBAD cloning vector	Peter Christie
[pBAD24-*traD*$_{pOX38}$]	*traD* from pOX38 pBAD expression vector	Peter Christie
[pT7MS2K (G1192T)]	MS2 cDNA plasmid containing single substitution in *mat*	This work
[pT7MS2K (A1543T)]	MS2 cDNA plasmid containing single substitution in *coat*	This work
[pBAD24-*traD*$_{pOX38}$ (K198Q)]	*traD* from pOX38 expression vector containing Walker A motif K198Q mutation	Peter Christie
[pBAD24-*traD*$_{pOX38}$ ΔCT15]	*traD* from pOX38 with 15 residue C-terminal deletion	Peter Christie
[pBAD24-*traD*$_{pED208}$]	*traD* from pED208 pBAD expression vector	Peter Christie

Table 4.1 cont.

[pBAD24-*traD*$_{pOX38}$ CT15$_{pED208}$]	*traD* from pOX38 with last 15 c-terminal residues from TraD$_{pED208}$	Peter Christie
[pBAD24-*traD*$_{pED208}$ CT15$_{pOX238}$]	*traD* from pED208 with last 15 c-terminal residues from TraD$_{pOX38}$	Peter Christie
[pBAD24-*traD*$_{pOX38}$ CT166$_{pED208}$]	*traD* from pOX38 with last 166 residues from TraD$_{pED208}$	Peter Christie
[pBAD24-*traD*$_{pED208}$ CT148$_{pOX38}$]	*traD* from pED208 with last 148 residues from TraD$_{pOX38}$	Peter Christie
Primers		
KC182-Seq	TCGTTATAGCGGACCGCGTGTCTG	Ryland Young
KC183-Seq	AAAGTGGCAACCCAGACTGTTGGTGG	Ryland Young
KC449-Seq	TTGCGTCGCGAGTTGTGAGGC	Ryland Young
KC450-Seq	GAGACCTTCGTCCCCTCCGTTC	Ryland Young
KC466-Seq	CGGTAATTGGCGCCAGGCG	Ryland Young
KC467-Seq	GGCTGCCTGTAAGGAGCCTG	Ryland Young
KC468-Seq	GAAACCTGTTGACAATCTCTTCGCCC	Ryland Young
KC469-Seq	TAGCCAAGCAGCTAGTTACCAAATCGG	Ryland Young
KC721-Seq	GGGTGGGACCCCTTTCGGGGTCCTGCTC	Ryland Young
KC722-Seq	TGGGTGGTAACTAGCCAAGCAGCTAGTTAC	Ryland Young
1192_gibsonINS_FWD	CTGTGGAGAGACAGGGCACTGCTAAGGCCCAAATCTCATCCA TGCATCGAGGGGTACAAT	This work
1192_gibsonINS_REV	CGAACTTCTTGTAAGGCGCTGCATCCTGCA	This work
1543_gibsonINS_FWD	ATCGCAAATACACCATCAAAGTCGAGGTGCCTAAAGTGGCAA TCCAGACTGTTGGTGGTG	This work
1543_gibsonINS_REV	TGGGAGAAAACTCCACACCAGGCGATCGGA	This work
1192_gibsonVEC_FWD	TGCAGGATGCAGCGCCTTACAAGAAGTTCG	This work
1192_gibsonVEC_REV	GGGCCTTAGCAGTGCCCTGTCTCTCCACAG	This work

Table 4.1 cont.

1543_gibsonVEC_FWD	TCCGATCGCCTGGTGTGGAGTTTTCTCCCA	This work
1543_gibsonVEC_REV	GCACCTCGACTTTGATGGTGTATTTGCGAT	This work

Evolution Experiment

The experiment was performed in a turbidostat placed in a 37 °C incubator. The turbidostat media reservoir was prepared with fresh LB containing antibiotics. All tubing was wrapped in foil and autoclaved prior to use. An overnight culture of PC1003 was grown in 2 mL LB with appropriate antibiotics. The overnight culture was diluted 1:200 into the 30 mL vessel containing the growth media and incubated at 37 °C. Once the OD_{650} reached 0.1, purified MS2 was added to the vessel at MOI=0.00001. The dilution rate was adjusted to maintain the culture density at OD_{650}=0.4. The culture was maintained for 18 hrs using about 2 L of media. Afterwards, the effluent chamber containing the lysate was collected and filter sterilized.

Purification of Evolved MS2 lysate

The lysate from the turbidostat experiment was plaque purified three times by streaking a 5 µL spot of the lysate onto a lawn of PC1003 and incubating at 37 °C overnight. The resulting plaques were picked with a pipette tip and dispensed into 100 µL of LB and the process was repeated two additional times. The resulting purified plaque was mixed with liquid top agar containing PC1003 cells and poured onto plates for full plate infections. These were incubated overnight which produced confluently lysed plates. 4 mL of LB were added to the tops of the plates and the top agar layer was

collected and filter sterilized. These produced a lysate of ~10^{10} pfu/mL. RNAse A and DNAse I at 10 U/mL were added to the lysates and treated for 45 minutes at room temperature (RT). Afterwards, 0.5 M NaCl and 10% PEG were added to the lysate and nutated to dissolve. The lysate was stored at 4 °C overnight. The lysate was then centrifuged at 10,000 x g for 1 hr at 4 °C. The supernatant was removed and resuspended with 2 mL of SM buffer. An equal volume of chloroform was added to get rid of excess PEG. The lysate was centrifuged again and the supernatant was collected.

RNA Extraction

RNA extraction was performed using 300 µL of the purified lysate following the QIAamp Viral RNA Mini protocol with the provided reagents. Briefly, a 1120 µL volume of a 1:1 mix of AVL and EtOH was added to the lysate and incubated at RT for 1 hr. The volume was added to the spin column and centrifuged at 10,000 x g for 1 min at RT. The column was washed with 500 µL once with buffer AW1 and then once with AW2. A drying spin was performed before the column was eluted with 35 µL of TE buffer pH 7.5. Next, poly(A) tail synthesis was performed using 15 µL of the MS2 RNA, 2 µL of 10X *E. coli* poly(A) polymerase reaction buffer, 2 µL 10mM ATP, 1 µL *E. coli* poly(A) polymerase. The reaction was mixed and incubated at 37 °C for 30 min. Afterwards, 0.4 µL of 0.5M EDTA containing RNA secure was added.

First-strand cDNA synthesis was performed using 11 µL of MS2 poly(A) RNA, 1 µL 50 µM primer KC450 containing RNA secure, and 1 µL 10mM dNTP. The reaction was mixed and heated to 65 °C for 5 minutes, then placed on ice for 1 minute. This reaction mixture was added to 7 µL of RT reaction mixture containing 38 µL of 5x

SSIV buffer, 9.5 µL 100 mM DTT, 9.5 µL ribonuclease inhibitor, 9.5 µL SSIV RT. The mixture was placed into a thermocycler and incubated at 23 °C for 10 minutes, 53 °C for 10 minutes, and 80 °C for 10 minutes. This was done for 10 cycles. The resulting mixture was PCR purified using the QIAquick PCR Purification kit and this was used as a template to amplify regions of the genome for sanger sequencing (Eton Biosciences) using the sequencing primers (-Seq) in Table 4.1.

Recapitulation of Identified Mutants

Resulting mutants were recapitulated using a Gibson assembly kit with the primers in Table 4.1 and the pT7MS2K plasmid as a template. Gibson assembly reactions for each mutant were electroporated into RY34462 cells grown in the presence of 0.4% L-arabinose. Colonies were recovered and mutations were confirmed by sequencing. To generate lysates of MS2 mutants, single colonies of the respective strain containing the mutated cDNA plasmid was grown in 5 mL glass tubes containing LB, chloramphenicol, kanamycin, and 0.4% L-arabinose at 30 °C in a rotary drum overnight. The next day, the cultures were treated with 1% chloroform for 10 minutes, then centrifuged at 4,500 x g for 10 minutes at 4 °C and the supernatants were collected. Plaquing phenotypes were tested on the PC1003 strain using standard protocol.

RNA smFISH

A set of 48 probes of ~20 nucleotides in length targeting the 5’ half of the MS2 genome with at least 2 nucleotide spacing between each probe was designed and synthesized using the Stellaris® Probe Designer from Biosearch Technologies (the sequences can be found in Table 4.2). The probes were designed with a 3’ mdC(TEG-

amino) modification to enable labeling with 6-carboxytetramethylrhodamine, succinimidyl ester (6-TAMRA, ThermoFisher Scientific, cat no. C6123) following protocols described (151). Briefly, we pooled 7.5 μL of each of the oligo solutions (48 oligo in total, 100 μM each) and added 40 μL of 1 M sodium bicarbonate, pH 8.5. We then added dye solution (1 mg of 6-TAMRA dissolved in 2.5 μL of DMSO and 25 μL of 0.1 M sodium bicarbonate, pH 9.0) to the probe mixture and incubated it protected from light overnight at 37 °C. The next day, we mixed 47 μL of 3 M sodium acetate, pH 5.2, into the solution, and then added 1180 μL of 100% ethanol and incubated the sample -80°C for 3 hr to precipitate the oligos. The oligos were then centrifuged and washed twice more by dissolving the pellet in 45 μL of DEPC-treated water, 5 μL of 3 M sodium acetate, pH 5.2, and 125 μL of 100% ethanol. After the washing steps, the probes were resuspended in 250 μL of 1× TE resulting in a 10× probe stock solution. The probe solution was diluted with 1× TE to make the 1× probe solution upon usage, and the labelling efficiency of the probes was determined using the NanoDrop to be 86%.

The probes were then used to detect MS2 RNA during infection using the following protocol. Overnight cultures of cells were diluted 1:1000 in LB containing 4 mM $CaCl_2$ and appropriate antibiotics. The cells were grown at 37 °C with shaking to OD_{600}=0.4 before being diluted into prechilled LB containing 4 mM $CaCl_2$. MS2 at an MOI of 0.5 was added and incubated on ice for 20 mins to allow for adsorption to pili. As a negative control, we added the same volume of SM buffer (100 mM NaCl, 10 mM MgSO4, 50 mM Tris-Cl, pH 7.5) to the culture. The cultures were moved to a 37 °C shaking waterbath to initiate infection. At regular time points, an aliquot of the cells was

centrifuged at 4500 x g for 5 mins and resuspended in 1X PBS containing 3.7% formaldehyde. At this point, the samples were further processed following the established protocol (151). The cells were fixed for 30 mins on a nutator at RT before being washed 3 times in 1X PBS to remove excess formaldehyde. The cells were then treated with 70% ethanol and nutated for 1 hr to permeabilize the cells for probe penetration. The cells were centrifuged and resuspended in wash solution (40% (wt/vol) formamide, 2× SSC) and incubated at room temperature for 5 min and centrifuged again. For hybridization, the cells were resuspended in 25 μL of hybridization solution (40% (wt/vol) formamide, 2× SSC, 1 mg/mL *E. coli* tRNA, 2 mM ribonucleoside-vanadyl complex and 0.2 mg/ml BSA) containing the probe mixture at a final concentration of 1 μM. The samples were then incubated at 30 °C protected from light for overnight. Afterwards, samples were washed three times by incubating the cells in wash solution for 30 min at 30 °C. After the third repeat of washing,10 μg/mL DAPI was added to the wash solution and used to stain the *E. coli* DNA. Cells were resuspended in 2× SSC and prepared for imaging. Cells were imaged in phase (100 ms exposure) and in the Cy3 channel to detect 6-TAMRA signals (50 ms exposure). Z-stacks were taken at 300 nm intervals.

Table 4.2 Sequences of smFISH probes used to detect MS2 RNA, oriented 5' to 3'.

MS2 5'_1	AGCGTCTCGCTAAAGACATT	MS2 5'_25	AGCATGTTACCTACAGGTAG
MS2 5'_2	ACCTCCTAGGAATGGAATTC	MS2 5'_26	TTACGTCAGTAACTGTTCCT
MS2 5'_3	ACTAAAAGCTCGCACAGGTC	MS2 5'_27	GAGCGTCAACGCTTATGATG
MS2 5'_4	GAGTTATCTTCAGTCTCACC	MS2 5'_28	CGATGCATGGCTGAGATTTG
MS2 5'_5	GAGTCCAGTTCGAACGATAT	MS2 5'_29	AAGGAGACTTTACGTACGCG
MS2 5'_6	CCCAGTCGAGTTAAAACGAC	MS2 5'_30	TCTAAGGTATGGACCATCGA
MS2 5'_7	TCGATGTGACACTTAACGCC	MS2 5'_31	CGTTGCCTGATTAATGCTAA
MS2 5'_8	TTTGGCTTACAGGGAAGAGG	MS2 5'_32	TTGAGGGCTCTATCTAGAGA
MS2 5'_9	GGCACTTCGATGTAAGTCAA	MS2 5'_33	AGTTAGAAGCCATGCTTCAA
MS2 5'_10	TAAAATTACCCTGGGTGACC	MS2 5'_34	CCATTGTCGACGAGAACGAA
MS2 5'_11	CTCTGCTAAAGCAACACCAA	MS2 5'_35	GAGTTAGAGCTGATCCATTC
MS2 5'_12	TTCACGAGCGCAATGGTTTG	MS2 5'_36	GTTACTTTGTAAGCCTGTGA
MS2 5'_13	CGATCTTCGTTTAGGGCAAG	MS2 5'_37	GATGGTGTATTTGCGATTCT
MS2 5'_14	GCCACGTGTTTTGATCGAAA	MS2 5'_38	TACAGGAAGCTCTACACCAC
MS2 5'_15	AACCAACCGAACTGCAACTC	MS2 5'_39	TTAAGTACGAACGCCATGCG
MS2 5'_16	CCTGGATATCACTCATTAGT	MS2 5'_40	AGTCGGAATTCGTGGCGAAA
MS2 5'_17	CCTTCGTAAGCATCTCATAT	MS2 5'_41	CCTTGCATTGCCTTAACAAT
MS2 5'_18	GTACGGCTCTCATAGGAAGA	MS2 5'_42	ATTAGTAGATGCCGGAGTTT
MS2 5'_19	GGCCATCTAACTTGATGTTA	MS2 5'_43	GGGTAATCCTCATGTTTGAA
MS2 5'_20	AAGTTTGCAGCTGGATACGA	MS2 5'_44	ACTTCTTTGTTGTCTTCGAC
MS2 5'_21	ACGATACGTCGCGATATGTT	MS2 5'_45	CCAGTAGCGACAGAAGCAAT
MS2 5'_22	CCAAACGTGCATCGTTTATG	MS2 5'_46	TGTAAAGTCGTCACTGTGCG
MS2 5'_23	ATACCTAGAGACGACAACCA	MS2 5'_47	TTCGTCCCTTAAGTAAGCAA
MS2 5'_24	ACACTATACCTAGTGGGTTC	MS2 5'_48	TAAGGTCGGATGCTTTGTGA

Results

Experimental adaptation of MS2 towards TraD independence

To better understand the relationship between MS2 and TraD, we took an experimental evolution approach to select for MS2 mutants with reduced dependence on TraD. Taking advantage of the hypermutability of ssRNA phages to accelerate evolution, we utilized a continuous culture device (turbidostat) to maintain MS2 infection of cells with restricted TraD levels (Figure 4.1A). We utilized a pOX38 Δ*traD* strain containing a medium copy plasmid encoding for *traD* under control of the pBAD promoter (PC1003). The cells were grown in media without arabinose so that only the basal level of TraD would be expressed, acting as the selection pressure. Cells were grown to OD_{650}=0.1 before being infected with MOI=0.00001 purified WT MS2. The experiment was performed for 18 hrs, sampling the OD_{650} every minute (Figure 4.1B). After ~15 hrs (~900 minutes), the OD_{650} showed a sharp decline that continued to lower until the end of the experiment. This is presumably when an evolved population of MS2, capable of infecting PC1003 cells efficiently, took over the population. The WT MS2 forms extremely faint plaques on this strain (Figure 4.2A), however, the turbidostat lysate formed clear plaques (Figure 4.2B). Therefore, we were able to evolve a population of MS2 to infect cells with only basal levels of TraD.

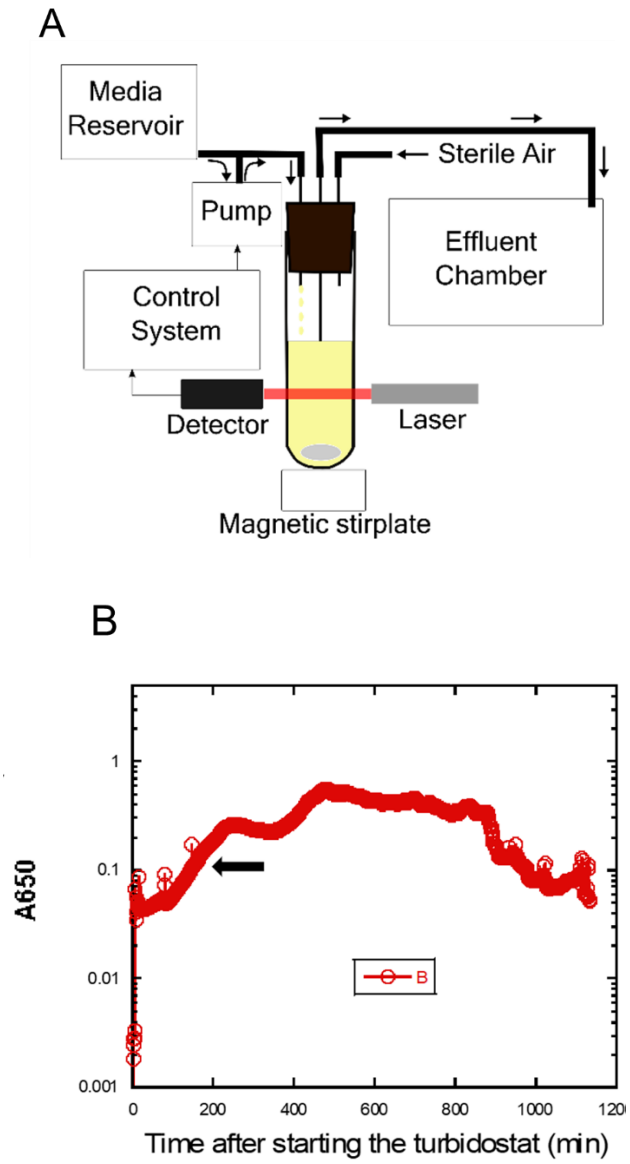

Figure 4.1 Experimental adaptation of MS2 using turbidostat setup.
(A) Schematic of turbidostat components. Fresh media is pumped into the chamber at a rate controlled by the OD_{650} as measured by the detector. Media overflow, cells, and phage are pumped out of the vessel into the effluent chamber to be collected. (B) OD_{650} readings of PC1003 during the turbidostat experiment. Black arrow indicates when WT MS2 was added to the culture.

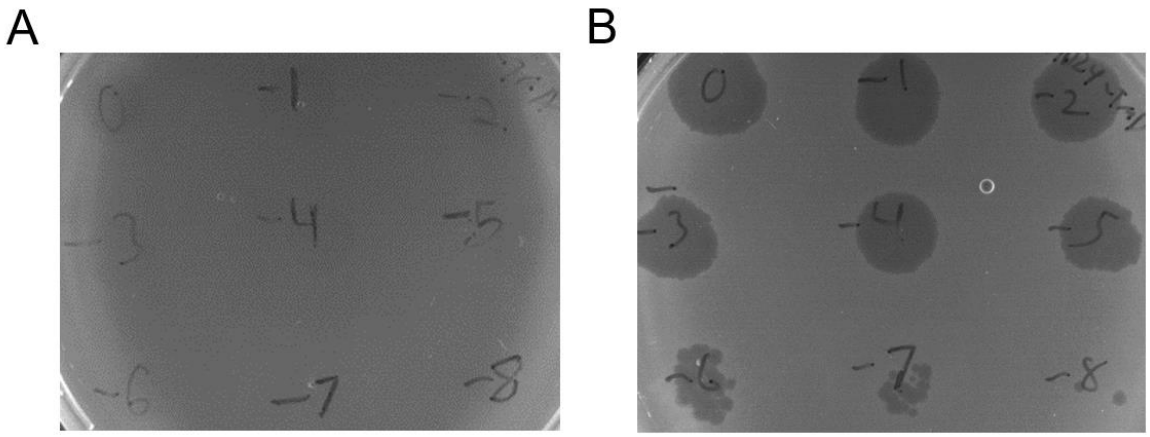

Figure 4.2 Evolved MS2 has improved plaquing with basal TraD.
(A) WT MS2 spot dilutions on PC1003 cells without induction (basal levels). (B) Evolved MS2 lysate on the same strain showing clear plaques. The experiment was performed at least twice.

Mutation in mat is sufficient for plaquing on basal levels of TraD

To better understand the rationale for the new clear plaque phenotype on basal TraD levels, we sequenced an isolate of MS2 from the evolved lysate resulting from the turbidostat experiment. Two plaques were purified from the lysate and amplified to ~$5x10^{10}$ pfu/mL. The lysates were precipitated with PEG and the RNA was extracted. The RNA from one lysate was degraded and could not be analyzed further. The intact RNA from one lysate was converted to cDNA and sequenced. The sequence returned 3 individual point mutations located in different genes in the genome (Figure 4.3). The first is a G->T base change causing an alanine to serine substitution at amino acid 355 in the Mat protein. The second is a A->T base change resulting in a threonine to isoleucine substitution at position 70 in the Coat protein. The third is a T->C base change at position 98 of *rep*, leading to a serine to proline substitution.

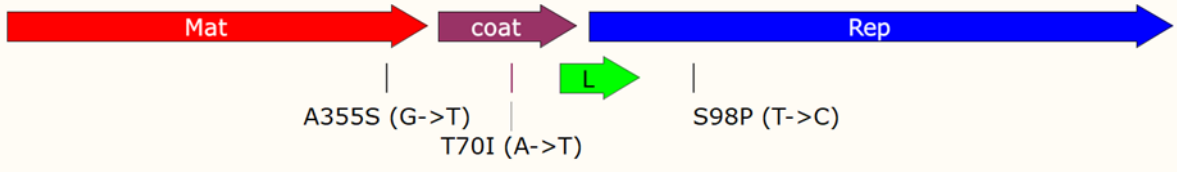

Figure 4.3 Mutations found in the evolved MS2 genome.
Base changes and resulting amino acid changes are shown below the respective affected gene. Illustration generated through SnapGene.

Any of these mutations could result in the clear plaque phenotype, either by a change in the protein, RNA structure, or both. To determine which mutation was responsible for the clear plaque phenotype, each point mutation was reconstituted separately in the MS2 genome and the resulting virions were assayed for their plaque phenotype. Currently, we were only able to reconstitute the Mat and Coat protein mutations, as the attempt for the replicase mutation returned as wildtype after sequencing. The mutant lysates were spotted on the basal TraD strain with and without arabinose induction to determine the plaquing phenotypes (Figure 4.4). It appears that only the Mat mutant was able to plaque efficiently on the basal TraD strain. The change in the gRNA in the *mat* gene (position 1192) is in a region of the gRNA away from the 3'-UTR, which interacts with the Mat, making it unlikely to play a role in cell penetration (75).

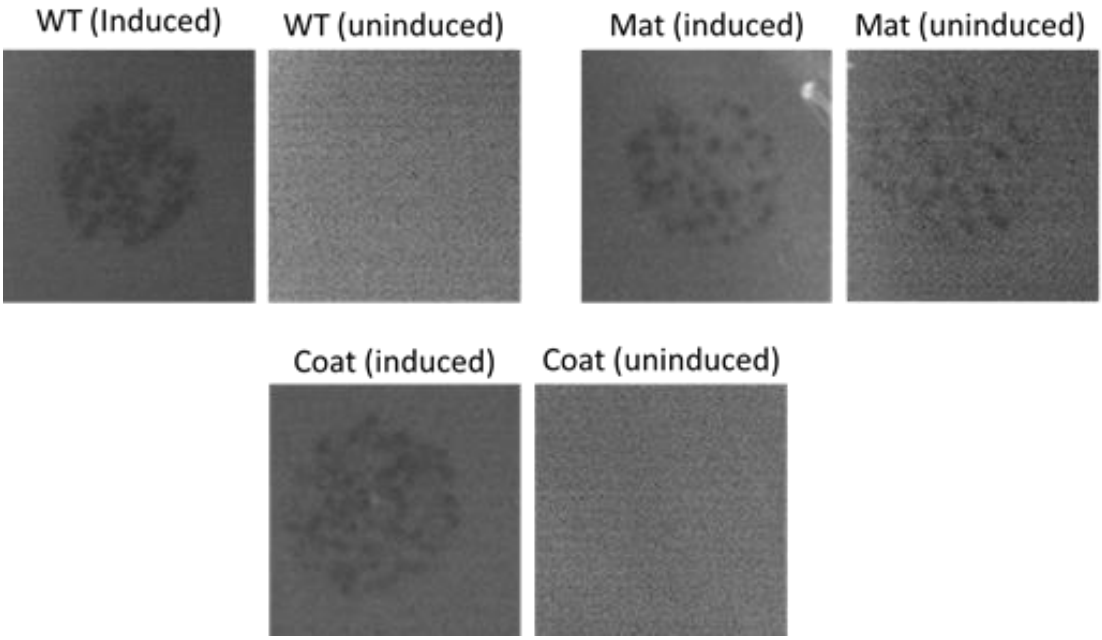

Figure 4.4 Plaquing phenotypes of individual evolved MS2 mutant lysates. Lysates generated from the recapitulated evolved MS2 mutants were spotted on PC1003 cells with or without induction by 0.2% L-arabinose. Mat corresponds to the G1192T mutant and Coat corresponds to the A1543T mutant lysates. The experiment was performed at least twice.

The A355S mutation is located on the pilus contacting β-region of the Mat protein. Although this residue is not one that normally contacts the pilus, it is adjacent to two arginine residues (Arg36 and Arg99) and one histidine residue (His357) that are known to interact with pilin subunits (Figure 4.5) (58). Therefore, it is possible that this mutation alters the Mat-pilus interaction in some way that allows the Mat-gRNA complex to pass through the basal body more efficiently. This could result from a lowered affinity for the pilus, allowing the Mat-gRNA complex more flexibility to pass through the basal body. Alternatively, the mutation could improve the interaction with TraD, possibly by acting as an improved scaffold for TraD oligomerization.

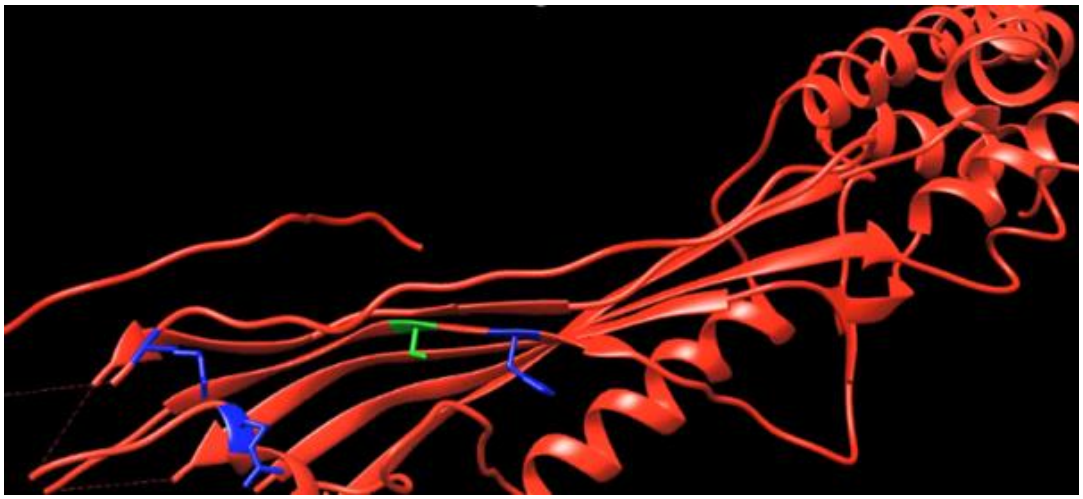

Figure 4.5 Structure of MS2 Mat protein with A355S mutation highlighted. Mat protein structure as determined by Cryo-electron microscopy. The β-region is focused on and contains the A355S mutation shown in green. Two arginine (left) and one histidine (right) residues known to contact the pilus shown in blue. Structure visualized through PyMol. PDB: 6NM5.

TraD C-terminal domains and ATPase activity promote efficient infection

Our previous work established that the TraD coupling protein is responsible for facilitating cell penetration of MS2 gRNA into the host cytoplasm during infection. TraD normally functions in conjugation by interacting directly with host relaxosome components to associate the conjugative DNA with the mating channel. The large, cytoplasmic facing C-terminal domains determine the specificity of DNA mobilization, as C-terminal truncations reduce both mating efficiency and specificity of DNA mobilization (181). Specific interactions were detected between the last 15 residues of TraD and TraM, a DNA binding protein that helps associate TraD with the DNA to be transferred (182). Given the dual-function of TraD in mobilizing both DNA and RNA, we sought to determine how the native function of TraD influences the efficiency of infection by MS2.

We utilized several TraD mutants encoded on pBAD24 vectors to complement the pOX38 Δ*traD* background strain and determined the plaquing efficiency of MS2 on these strains (Figure 4.6). A deletion of the CT15 residues reduced the plaquing efficiency of MS2 by about 10-fold (Table 4.3), suggesting that this region contributes in some way to efficient plaquing. Additionally, we tested a substitution in the walker A nucleotide binding motif of TraD (K198Q). Mutations in this motif inhibit translocation of conjugative DNA, presumably by blocking ATP-binding and subsequent hydrolysis (183). This strain yielded no plaques when challenged with 10^9 pfu of MS2. To determine if this mutation blocks cell penetration of the MS2 genomic RNA (gRNA), we utilized single molecule fluorescent *in situ* hybridization (smFISH) to directly visualize

cytosolic MS2 gRNA in infected cells (Figure 4.7). Using a probe set targeting the first half of the MS2 genome, we detected cytosolic MS2 gRNA in Δ*traD* cells expressing either WT TraD or TraD (K198Q) from pBAD24 vectors. The cells expressing WT TraD showed single fluorescent foci corresponding to MS2 RNA at 5 mins post-infection. Large clusters and more frequent foci could be seen in cells infected at the 10 and 20 min timepoints. However, in the TraD (K198Q) expressing cells, fluorescence microscopy images from several timepoints post-infection showed no smFISH signal, suggesting that ATP binding and hydrolysis by TraD is required for MS2 cell penetration (Figure 4.7).

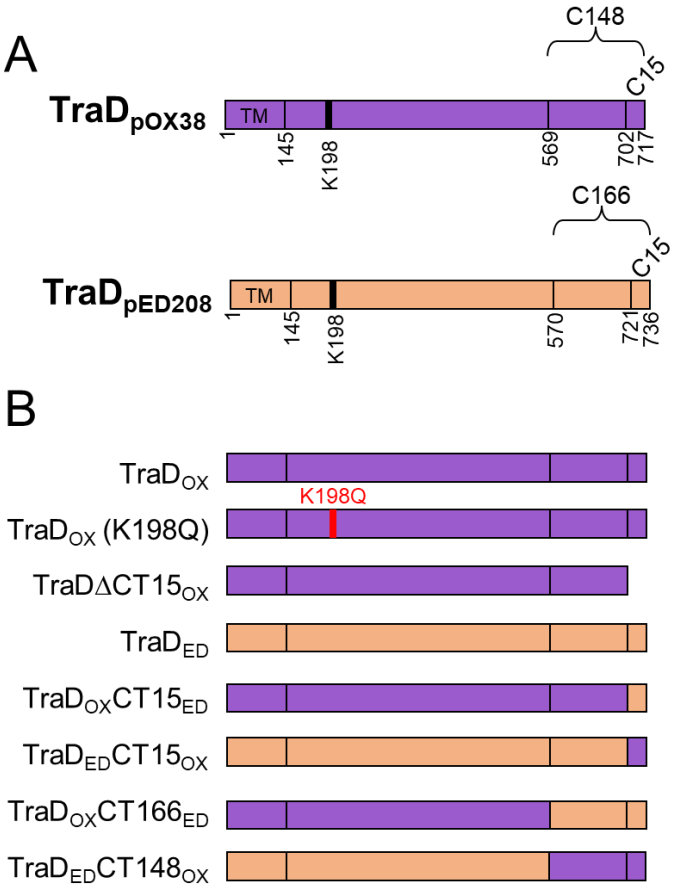

Figure 4.6 Organization of TraD Mutants for Complementation Studies.
(A) Organization of the full-length TraD WT constructs from the pOX38 and pED208 systems. Transmembrane (TM) regions and locations of domain swaps or mutations are indicated. (B) List of mutant TraD constructs used in complementation assays.

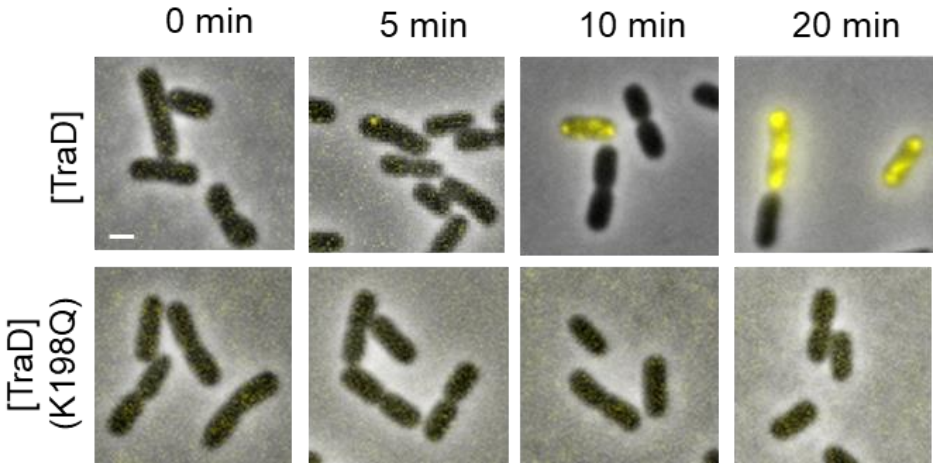

Figure 4.7 TraD Nucleotide Binding is Required for MS2 Cell Penetration. Representative images of MS2 RNA within cells detected by smFISH (MOI=0.5). The yellow signal (6-TAMRA) indicates cytosolic MS2 RNA. The top row is the pOX38 Δ*traD* background strain containing pBAD24-*traD*. The bottom row is the same strain containing pBAD24-*traD* (K198Q). Scale bar = 1 µm. At least 200 cells were imaged per sample. The experiment was performed at least twice.

Some TraD mutants were created by swapping the C-terminal domains with those of TraD from the F-family conjugative plasmid, pED208. The F-plasmid variant pED208 shares sequence similarity among the *tra*/*trb* genes of the pOX38 (184). However, it encodes a pilus system that is resistant to MS2. The full-length *traD* genes from the pOX38 and pED208 systems share 49% sequence identity (67% sequence similarity). However, the C-terminal 148 and 166 regions of $TraD_{pOX38}$ and $TraD_{pED208}$, as well as the last 15 residues of both genes, are highly dissimilar, only sharing 30% and 13% sequence identity, respectively (Figure 4.8). A chimeric $TraD_{pOX38}$ containing a substitution of the last 8 residues from $TraD_{pED208}$ fails to mobilize plasmids in conjugation assays (185). Additionally, mutant derivatives that are unable to mobilize conjugative plasmids in the F-like conjugative system, R1, also inhibit plaquing by the MS2-related ssRNA phage, R17 (186). Therefore, we investigated how several chimeric TraD constructs affected the plaquing efficiency of MS2. Plaque assays revealed that all the chimeric TraD constructs reduced the efficiency of plating (EOP) to some degree (Table 4.3). Notably, the large C-terminal domain swaps ($TraD_{pOX38}$ $CT166_{pED208}$ and $TraD_{pED208}$ $CT148_{pOX38}$) yielded very turbid plaques that were uncountable at higher dilution series (Figure 4.9). As a control, the ssRNA coliphage Qβ, which does not require TraD at all to facilitate infection, was able to form clear plaques on all the complementation strains.

Figure 4.8 Pairwise Alignment of TraD gene products from pOX38 and pED208. Comparison of protein sequences show 49.1% sequence identity and 66.9% sequence similarity with 4.7% gaps. Solid lines connecting residues indicate exact matches. Two

Figure 4.8 cont.
dot matches are similar residues. Single dot matches are dissimilar residues. Dashes between residues in the sequence indicate gaps in the alignment. Alignment and output was generated using EMBOSS Needle (187).

Table 4.3 EOP of MS2 by Complementation of TraD Mutants

Strain [Plasmid]	EOP
WT pOX38 [pBAD24]	1
Δ*traD* [$traD_{pOX}$]	0.94
Δ*traD* [$traD_{pOX}$ ΔCT15]	0.08
Δ*traD* [$traD_{pED}$/$CT15_{pOX}$]	0.12
Δ*traD* [$traD_{pOX}$/$CT166_{pED}$]	$<10^{-4}$ (turbid plaques)
Δ*traD* [$traD_{pED}$/$CT148_{pOX}$]	$<10^{-4}$ (turbid plaques)
Δ*traD* [$traD_{pOX}$/$CT15_{pED}$]	0.57
Δ*traD* [$traD_{pED}$]	0.06
Δ*traD* [$traD_{pED}$ ΔCT15]	0.04
Δ*traD* [$traD_{pOX}$ (K198Q)]	$<10^{-9}$
Δ*traD* [$traD_{pOX}$ (K198Q) ΔCT15]	$<10^{-9}$

Efficiency of plating (EOP) was determined by dividing the titer of a MS2 preparation on a test strain by the titer of the same preparation on the indicator strain. Strains were induced by addition of 0.2% L-arabinose to the plate media. The experiment was performed at least twice.

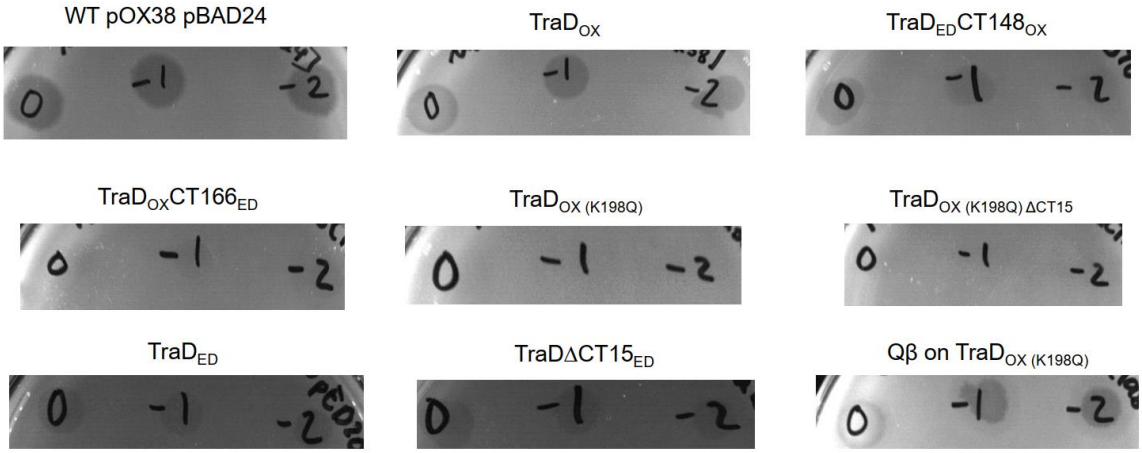

Figure 4.9 Plaquing phenotypes of MS2 on different TraD mutants.
Spot titers of WT MS2 or Qβ on cells expressing various TraD mutants from pBAD24 vectors. Unless indicated, each plasmid is in a Δ*traD* background and being expressed with 0.2% L-arabinose in the plate media. Depicted strains had differing plaque phenotypes compared to the induced PC1003 strain. Qβ infection is not dependent on TraD and was therefore used as a control to ensure functional pili production. The experiment was performed at least twice.

Discussion

The “male-specific” ssRNA phages have evolved to use conjugative pili as receptors to recognize the host. They bind exclusively to the sides of the pilus and exploit the mechanics of the T4SS machinery to facilitate penetration of their gRNA through the cell envelope. Some ssRNA phages only require a functional pilus associated with T4SS subunits to permit infection. However, the group I ssRNA phages (MS2, R17, f2) also require the conjugative coupling protein, TraD, to permit infection in F-like plasmid systems (188). TraD normally functions in the unidirectional transfer of conjugative DNA in its single-stranded form from donor to recipient cell. Interestingly, only group I ssRNA phages have evolved to require pilus systems competent for conjugative transfer to permit cell penetration, although the exact rationale is unknown.

Previous studies involving the F-like R1 conjugative plasmid demonstrated that the perturbations to the NTP-binding site of the coupling protein inhibit plaquing of R17 (159). Interestingly, the relaxase, TraI, responsible for nicking the conjugative plasmid and piloting it through the mating channel, was also shown to be required for R17 infection, although this was not true for the pOX38 system. Specific domains involved in the interaction between the conjugative DNA and the relaxase, the catalytic tyrosine, and the TSA region (which interacts with TraD), were all required for R17 infection. A model was proposed where TraD, associated with the cytoplasmic end of the T4SS and relaxosome components, awaits a signal transmitted through the pilus to initiate activity. The signal can originate through mating pair formation, or possibly R17 binding. Processing of this signal activates the ATPase activity of TraD which facilitates

transport of the ssRNA phage gRNA into the cytoplasm, essentially hijacking the machinery to facilitate import, rather than export, of a nucleoprotein complex.

In this study, we used experimental adaptation to evolve a population of MS2 using a strain expressing low levels of TraD as a selection pressure. A new population of MS2 that could cause a clear plaque phenotype under these conditions arose. Sequencing and recapitulation of mutants revealed that a single mutation in the *mat* gene was responsible for the clear plaque phenotype. The nucleotide substitution (G1192T) created a missense mutation, converting the alanine at position 355 to a serine residue. The A355S mutation was located in the β-region of Mat which contains residues that are known to contact the pilus during host recognition. In the infectious particle, the nucleotide at position 1192 is located within a region of the gRNA away from the Mat. Therefore, while we cannot rule out the possibility that the single base change may contribute in some way to this phenotype, the A355S mutation may play a more significant role. TraD is known to interact directly with protein constituents (TraM) bound to the ssDNA form of the conjugative plasmid in preparation for transfer. Therefore, it is possible that import of the MS2 gRNA bound to the Mat protein could mimic substrate translocation during conjugation, and that this mutation benefits this process in some way. TraD, unlike many other T4SS subunits, associates with the mating channel only transiently (90). If the TraD pool is restricted, for example, through basal expression from a plasmid source, the reduced availability could limit the frequency of cell penetration of incoming phage gRNA, since TraD exists functionally as a hexamer (177). The mutation could improve

the recruitment of TraD to the correct T4SS basal body to facilitate oligomerization of the TraD hexamer and subsequent cell penetration.

Alternatively, since the evolved mutation is located within the β-region, it is possible that it could alter the adsorption kinetics or affinity for the pilin subunits. This would draw parallels to the ssRNA phage Qβ, which binds less efficiently to pili than MS2 (59) and is also not dependent on TraD for infection. The differences in binding interactions between Mat-pilin complexes of MS2 and Qβ could rationalize the TraD requirement. The ATPase activity of TraD may be necessary to pull the Mat-gRNA complex of MS2 away from pilin at the cytoplasmic end of the basal body, but may be dispensable for the weaker interactions between the Qβ Mat and pilin subunits.

We also investigated how various TraD mutants affected entry and productive infection of MS2. A substitution in the NTP-binding domain of $TraD_{pOX38}$ inhibited plaquing by MS2 by preventing cytosolic penetration of the gRNA. This finding supports previous work in the R1 plasmid system and demonstrates that the ATPase activity of $TraD_{pOX38}$ is required for MS2 cell penetration. Additionally, the use of $TraD_{pOX38}$ mutants containing deletions or chimeric regions from $TraD_{pED208}$ demonstrated that perturbations to the C-terminus of TraD affects the plaquing efficiency of MS2. The importance of the C-terminus in recruiting the conjugative plasmid and determining the efficiency of DNA mobilization suggests that MS2 infection may be influenced by conjugative plasmid transfer. These findings corroborate those found in the R1 plasmid, where deletions of the *oriT* or *nic* sites, responsible for TraM and relaxase binding, respectively, abolishes infection by R17 (186).

Overall, our findings stress the importance of functional conjugative coupling proteins in permitting ssRNA phage infection. In broader context, conjugative plasmids are under constant evolutionary pressure to disseminate themselves throughout bacterial populations while also maintaining strategies to protect against male-specific phages. Among F-like plasmids, natural variations in the pilin sequences can attenuate phage sensitivity (59). However, the link between conjugative plasmid coupling and ssRNA phage infection suggests that cells mating at high frequency may also be more susceptible to phage predation. Moreover, the requirement for TraI to permit infection of R1, but not pOX38 carrying cells could suggest that phage resistance is a driving factor for diversification of F-like plasmids.

CHAPTER V

ANALYSIS OF GENETIC DETERMINANTS INVOLVED IN F-PILUS SECRETION

Introduction

Many species of gram-negative bacteria secrete long, filamentous, extracellular appendages called conjugative pili to facilitate horizontal gene transfer through conjugation, or bacterial cell mating. Conjugation contributes to the transfer of antibiotic resistance genes (185), pathogenicity factors implicated in a variety of diseases (186) and has also been shown to facilitate biofilm formation (55), which may protect otherwise susceptible bacteria from antimicrobial treatment (187). The prevalence, rapid rate of transfer, and general promiscuity of conjugative plasmids have encouraged their research to improve our understanding of antibiotic resistance gene transfer and acquisition.

Conjugative pili are dynamic polymers composed of thousands of repeating subunits called pilins that arrange in a helical fashion to form the mature filament. The pili are assembled and controlled by large, multicomponent, transmembrane complexes called type IV secretion systems (T4SSs) usually encoded on transmissible plasmids. The best-studied conjugative pili are the F-pili secreted from the T4SS encoded on the F-plasmid (142). The F-T4SS contains several *tra*/*trb* genes that control the biosynthesis and activity of F-pili. Most of these genes are essential for F-plasmid transfer. Mutational analysis has helped broadly describe the role several *tra/trb* genes play in F-pilus synthesis and conjugation (95).

F-pilus production begins with the processing of the propilin subunits encoded by *traA*. TraA monomers are inserted into the inner membrane and stabilized by TraQ (92). They are processed through acetylation at Ala52 and cleavage of the N-terminus by TraX (189). The mature TraA monomers are stored in the inner membrane prior to extraction during F-pilus assembly. The assembly process is facilitated by several proteins, including TraE, -K, -B, -V, -C, -W, -G, -F, -H, -L, and TrbC (95). Some functions for these proteins have been ascertained through mutational analysis. The F-pilus tip is assembled by the activities of TraE, -K, -C, -G, and -L, while TraB, -V, -W, -F, and -H facilitate pilus elongation. TraB, -V, and -K are part of the transmembrane channel structure (96). The cytoplasmic end of the channel contains both TraL and TraE, which are associated with the inner membrane and help recruit TraC, the ATPase that passages TraA monomers through the channel during pilus extension.

While several genes can be broadly classified based on proposed functions, cellular localization and interacting partners, direct evidence describing the individual contributions of each gene in facilitating F-pilus synthesis and function has yet to be obtained. In this study, we used fluorescent labeling of F-pili to examine a knockout and misexpression library of conserved T4SS genes and determined the effects on F-pilus synthesis. Several key genes for pilus secretion were identified and their effects on pilus number and length were quantified. In addition, we developed a novel, direct-labeling approach to observe and measure F-pili dynamics under live-cell microscopy. This method yielded accelerated rates of pilus retraction compared to previously reported values (24).

Materials and Methods

Bacterial strains, Phages, Plasmids, Primers

Strains used in this study are summarized in Table 5.1. Cells were grown in LB media at 37 °C with shaking (265 rpm) unless otherwise indicated. When appropriate, LB was supplemented with antibiotics at standard concentrations: ampicillin (100 µg/mL), tetracycline (10 µg/mL), streptomycin (50 µg/ml).

Table 5.1 Bacterial strains, plasmids, and primers used in this work.

Strains	Description	Source
PC1000	MC4100 pOX38-Tet^R	Peter Christie
PC1010	MC4100 pOX38-Tet^R [pBAD24]	Peter Christie
PC1011	MC4100 pOX38-Tet^R Δ*trbC*	Peter Christie
PC1012	MC4100 pOX38-Tet^R Δ*traW*	Peter Christie
PC1013	MC4100 pOX38-Tet^R Δ*traN*	Peter Christie
PC1014	MC4100 pOX38-Tet^R Δ*traF*	Peter Christie
PC1015	MC4100 pOX38-Tet^R Δ*traU*	Peter Christie
PC1016	MC4100 pOX38-Tet^R Δ*traH*	Peter Christie
PC1017	MC4100 pOX38-Tet^R Δ*trbI*	Peter Christie
PC1018	MC4100 pOX38-Tet^R Δ*trbB*	Peter Christie
PC1019	MC4100 pOX38-Tet^R Δ*traE*	Peter Christie
PC1020	MC4100 pOX38-Tet^R Δ*traG*	Peter Christie
PC1021	MC4100 pOX38-Tet^R [pBAD24-*traA*]	Peter Christie
PC1022	MC4100 pOX38-Tet^R [pBAD24-*traB*]	Peter Christie
PC1023	MC4100 pOX38-Tet^R [pBAD24-*traC*]	Peter Christie
PC1024	MC4100 pOX38-Tet^R [pBAD24-*traD*]	Peter Christie
PC1025	MC4100 pOX38-Tet^R [pBAD24-*traF*]	Peter Christie
PC1026	MC4100 pOX38-Tet^R [pBAD24-*traG*]	Peter Christie
PC1027	MC4100 pOX38-Tet^R [pBAD24-*traH*]	Peter Christie
PC1028	MC4100 pOX38-Tet^R [pBAD24-*traI*]	Peter Christie
PC1029	MC4100 pOX38-Tet^R [pBAD24-*traK*]	Peter Christie

Table 5.1 Cont.

PC1030	MC4100 pOX38-Tet^R [pBAD24-*traT*]	Peter Christie
PC1031	MC4100 pOX38-Tet^R [pBAD24-*traU*]	Peter Christie
PC1032	MC4100 pOX38-Tet^R [pBAD24-*traV*]	Peter Christie
PC1033	MC4100 pOX38-Tet^R [pBAD24-*traW*]	Peter Christie
PC1034	MC4100 pOX38-Tet^R [pBAD24-*trbB*]	Peter Christie
PC1035	MC4100 pOX38-Tet^R [pBAD24-*trbC*]	Peter Christie
PC1036	MC4100 pOX38-Tet^R [pBAD24-*trbI*]	Peter Christie
PC1037	MC4100 pOX38-Tet^R [pBAD24-*traE*]	Peter Christie
PC1038	MC4100 pOX38-Tet^R [pBAD24-*traG*]	Peter Christie
PC1039	MC4100 pOX38-Tet^R [pBAD24-*traL*]	Peter Christie
PC1040	MC4100 pOX38-Tet^R [pBAD24-*traM*]	Peter Christie
ER2738	F´*proA*$^+$*B*$^+$ *lacI*^{q} Δ*(lacZ)M15 zzf::Tn*10(Tet^R)*/ fhuA2 glnV* Δ*(lac-proAB) thi-1* Δ*(hsdS-mcrB)5*	Ryland Young
PL15	RP437 *fliC*st Δ*motAB*	Pushkar Lele
DH5α	Δ*lacZ ΔM15* Δ*(lacZYA-argF) U169 recA1 endA1 hsdR17(rK-mK+) supE44 thi-1 gyrA96 relA1*	Laboratory stock
LZ2662	PL15 F´*proA*$^+$*B*$^+$ *lacI*^{q} Δ*(lacZ)M15 zzf::Tn*10(Tet^R)*/* [ptrc99a-*traA* (A113C)]	This work
Plasmids		
pBAD24	Amp^R, pBAD cloning vector	Peter Christie
ptrc99a	Amp^R, IPTG-inducible expression vector	Chris Hayes
Primers		
FWD_TraA_A113C	CATCATCTCTGTATTTATTTGTGTGGGTATGGCCGTCG	This work
REV_TraA_A113C	CGACGGCCATACCCACACAAATAAATACAGAGATGATG	This work

Detection and quantification of F-pili using MS2-GFP

F-pili were observed and quantified using fluorescence microscopy following the previously established method (164). Briefly, overnight cultures were diluted 1:100 in LB containing antibiotics. The cells were grown to an OD_{600} ~0.4 and a small aliquot was collected and dispensed into prechilled tubes and allowed to equilibrate on ice. For misexpression of *tra*/*trb* genes, 0.2% L-arabinose was added to the cells at OD_{600} ~0.4 and the culture was allowed to incubate for an additional 1 hr. A small volume equating to MOI=100 of MS2-GFP was added to the samples and left on ice for 20 minutes to allow phage adsorption to pili. Samples were prepared for microscopy by spotting1 µL of sample onto a large coverslip (24 x50 mm, Fisher Scientific) and gently overlaying a small 1 mm-thick 1.5% agarose pad dissolved on PBS on the sample before placing under the microscope. Z stacks of 300 nm were used in the GFP channel to precisely measure pili. Samples were imaged on multiple stage positions (between 10 and 20 per sample) in phase (100 ms exposure to detect cells) and GFP channels (100 ms to detect pili). The images were analyzed using NIS elements software for cell and pili counts and length measurements.

PCR and plasmid construction

The plasmid ptrc99a encoding *traA* was used as a template in PCR to perform site directed mutagenesis (SDM) using the primers in Table 5.1. The SDM reaction causes a single base change leading to the substitution of Ala113 with Cys for thiol-specific labeling. The PCR reactions were treated with DPN-I and transformed into

chemically competent DH5α cells. The single substitution mutation (A113C) was confirmed by sequencing.

Construction of LZ2662

Conjugation between PL15 and ER2738 was performed as follows. Overnight cultures of donor (ER2738) and recipient (PL15) cells were diluted 1:100 and grown in LB until the cells reached OD_{600} ~0.4. The cells were washed once in fresh LB, mixed at a 1:3 donor/recipient ratio in a total volume of 1 mL, and incubated at 37 °C without shaking for 3 hrs. Afterwards, cells were vortexed for 30 seconds, serially diluted and plated on selective media. Transconjugates were collected and transformed with the ptrc99a-*traA* (A113C) plasmid using TSS transformation.

Live-cell observation of F-pili dynamics

An overnight culture of LZ2662 was diluted 1:100 in LB containing antibiotics and grown at 37 °C. Once the OD_{600} ~0.15, the cells were induced with 1 mM IPTG and allowed to incubate for 2 hrs. Prior to use, working stocks of Alexafluor-568 C5-maleimide were prepared as follows. A 1 mg tube of Alexafluor-568 C5-maleimide was dissolved in dimethyl sulfoxide to a final concentration of 5 mg/mL, aliquoted, and stored in -20 °C. The dye was diluted 1:200 into a 100 µL aliquot of cells which were then incubated in the dark at 37 °C for 30 mins. While waiting, a homemade flow cell was constructed by placing two pieces of ~1 cm wide tape onto a large (24 x 50 mm) coverslip, creating a central channel between the tape. After labeling, a 15 µL aliquot of the labeled cells was dispensed and spread within the central channel using a pipette tip. The flow cell was allowed to incubate at room temperature for 7 mins to permit sticking

of the cells to the glass surface. The flow cell was then flushed with 500 µL of LB and then gently dipped 10 times into a 50 mL conical tube containing 20 mL of fresh LB. This was repeated once more with a new tube containing fresh LB. The areas around the central channel were gently dried and 20 µL of LB was added to the channel. A small (18 x 18 mm) coverslip was placed on top of the channel and sealed with nail polish. The flow cell was then placed into a custom heat chamber set to 30 °C and placed under the microscope. The samples were left at 30 °C for 20 mins to allow pili dynamics to initiate. Samples were imaged in phase (100 ms exposure to detect cells) and mCherry (Nikon 96365) channels (20 ms to detect pili) at indicated imaging intervals. The images were analyzed using NIS elements software for retraction rate measurements.

Results

Phenotypic characterization of pOX38 deletion mutants

Many core components that contribute to the assembly of the F-T4SS are highly conserved among other F-plasmid systems (184). These conserved assembly proteins include *trbB*, *trbC*, *trbI*, *traW*, *traN*, *traF*, *traU*, and *traH* (184). We examined these *tra/trb* gene deletions in a model F-plasmid system, pOX38: a fully functional, derepressed variant of the original F-plasmid missing a large, nonessential section of DNA resulting from cleavage by HindIII (162). We examined how each deletion affected F-pilus production and length using our previously established MS2-GFP F-pilus detection method (164). The parental pOX38 strain produced an average of ~2 pili per cell with an average pilus length of ~2.2 µm, which aligns well with previously reported values (Figure 5.1) (164). Most of the F-T4SS deletion strains greatly reduced

the number of pili per cell, with the Δ*traF* and Δ*traH* mutants completely inhibiting F-pilus synthesis (Figure 5.1A). Both the Δ*traN* and Δ*trbB* strains produced about 0.5 pili per cell, suggesting that they contribute less significantly to F-pilus synthesis.

Most of the F-T4SS deletions did not affect the length of F-pili (Figure 5.1B). Although the Δ*traU* mutant nearly eliminated F-pilus synthesis, the remaining F-pili were about half as long (~1 μm) compared to the parental strain. Interestingly, the Δ*trbI* mutant had the opposite phenotype, with an average pilus length twice that of the parental strain. This observation is consistent with previous studies of *trbI* mutants that also exhibited unusually long F-pili under electron microscopy (99).

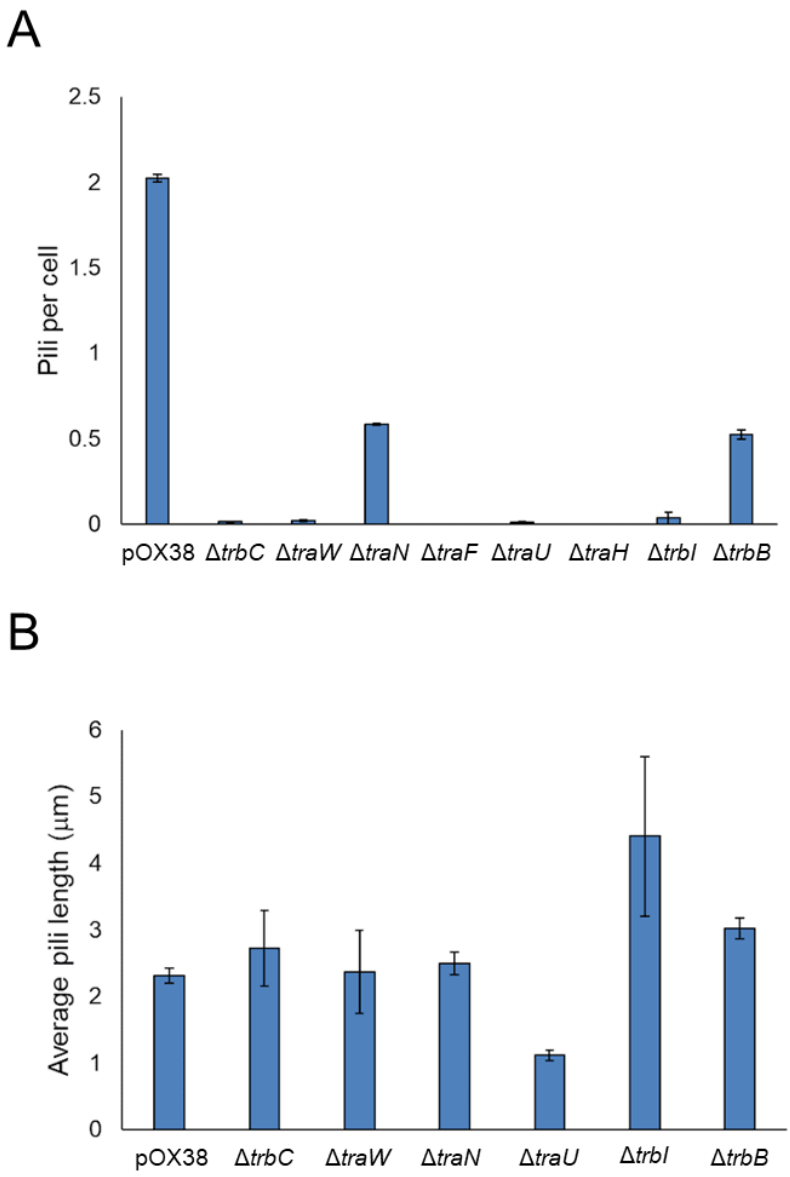

Figure 5.1 Quantification of F-pilus synthesis from F-T4SS deletion strains. Analysis of surface F-pili from pOX38 mutant variants as determined by MS2-GFP F-pilus labeling. (A) Quantification of the average number of F-pili per cell. (B) Quantification of F-pilus lengths from F-pili producing pOX38 mutant variants. Error bars represent standard deviation. At least 200 cells were analyzed per sample. The experiment was performed at least twice.

Quantification of F-pilus synthesis from misexpression of pOX38 genes

In addition to the conserved group of F-T4SS assembly components described above, there are several other *tra* genes that are broadly classified as assembly proteins (142). Many of these genes have not been examined for effects on F-pilus synthesis. To this end, we characterized a large collection of *tra/trb* genes by encoding them on L-arabinose inducible plasmids and quantifying the effects on F-pilus number and length during misexpression (Figure 5.2). Compared to the parental strain, overexpression of six different genes made more pili per cell (*traA*, *traC*, *traK*, *traL*, *traU*, and *traE*) (Figure 5.2A). Notably, both *traC* and *traE* overexpression caused the F-pili to be over 1 µm longer on average (Figure 5.2B). TraE cooperates with TraL to initiate pilus assembly by recruiting TraC, which facilitates pilus elongation in an ATP-dependent manner (95). This suggests that the concentration of intracellular TraC and TraE can alter the frequency and length of synthesized F-pili. Conversely, overexpression of several genes significantly reduced the pili per cell, with *traF, traT, trbB,* and *trbI* expression having the strongest F-pilus suppression phenotypes (Figure 5.2A). Many of these genes are suggested to play some role in F-pilus or T4SS assembly (95). Therefore, it is possible that overexpression of these genes disrupts proper assembly of the T4SS to subsequently produce normal levels of F-pili.

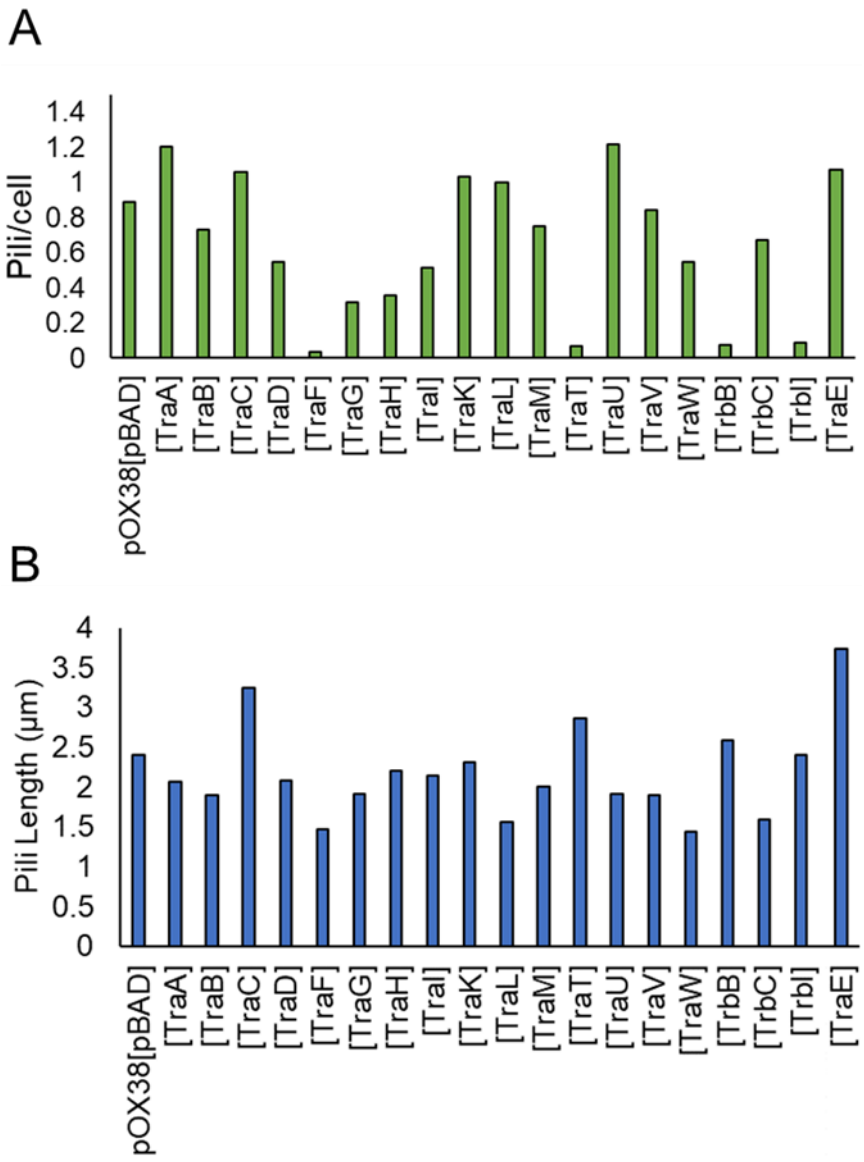

Figure 5.2 Quantification of F-pilus synthesis during overexpression of pOX38 genes.

(A) The average number of F-pili per cell from pOX38 carrying strains containing arabinose inducible plasmids encoding various *tra*/*trb* genes. (B) F-pilus length analysis from the same overexpression strains in (A). At least 200 cells were analyzed per sample. The experiment was performed once.

Direct visualization of F-pili dynamics

The use of MS2-GFP to detect and quantify F-pili has proven successful to obtain quantitative information from static images. However, this method is not ideal for visualizing F-pili dynamics under live-cell microscopy given that the labeled preparation of MS2 may still be infectious. Although F-pili dynamics were first visualized using the binding of fluorescent ssRNA phage R17 to detect F-pili, we were unable to visualize dynamic activity using these methods (24). We therefore employed a direct-labeling approach that has been used to observe type IV pili dynamics in several different bacterial strains (107, 129). This method requires the incorporation of a free Cys residue in the mature pilin monomer. Ideally, this substitution would target a surface exposed residue on the mature pilus filament to permit covalent modification by thiol specific, fluorescent maleimide dyes. We incorporated a Cys substitution at a surface exposed site towards the C-terminus of *traA* (A113C), using the Cryo-electron microscopy structure of the F-pilus filament as a guide to identify surface exposed residues (Figure 5.3A) (66). The *traA* sequence from the F-plasmid does not normally contain Cys residues, thus, cells expressing WT *traA* do not become fluorescent after treatment with Alexafluor 568 C5-maleimide (Figure 5.3B). However, after expressing *traA* (A113C) from an IPTG inducible plasmid, cells treated with the same dye appear to exhibit brightly labeled fluorescent F-pili (Figure 5.3B). As a control, we added MS2-GFP to ensure that the cells were producing F-pili. Interestingly, we found that MS2-GFP is capable of binding maleimide labeled F-pili (Figure 5.3B).

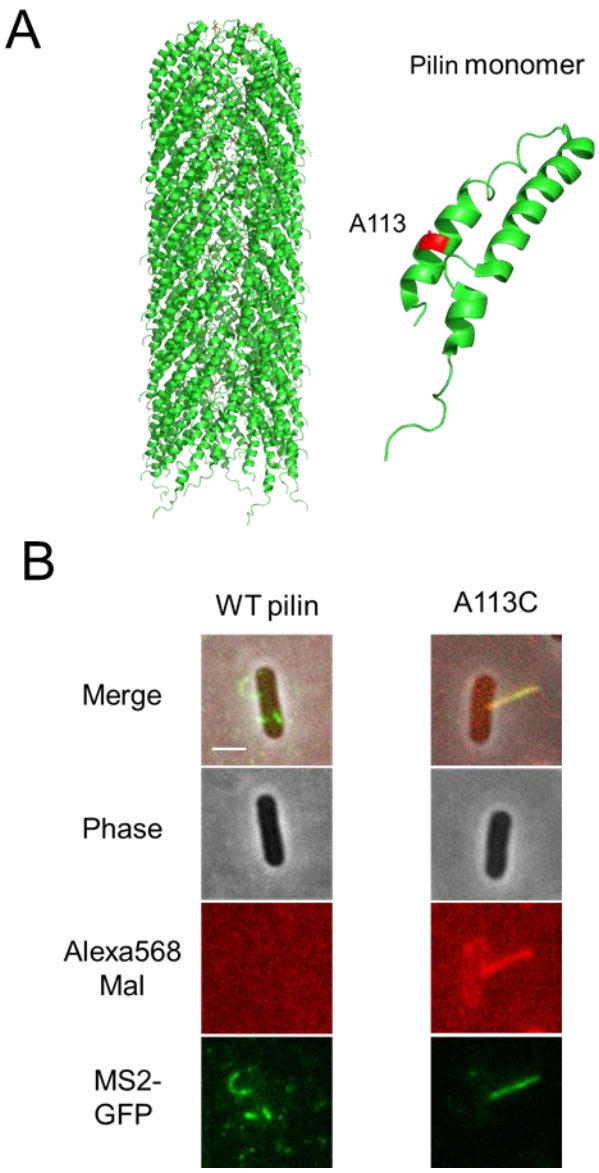

Figure 5.3 Direct labeling of cysteine modified F-pili.
(A) Ribbon diagram of the F-pilus filament as determined by cryo-electron microscopy. An individual pilin monomer is shown with the site of the surface exposed residue targeted for cysteine modification (right). PDB ID: 5LER. (B) Representative images of cells expressing WT or A113C modified TraA after treatment with Alexafluor 568 C5-maleimide and MS2-GFP. Scale bar = 1 µm.

Having established this system to directly label F-pili, we next sought to visualize F-pili dynamics under live-cell microscopy. Capturing the motion of F-pili requires the cells to be suspended in liquid to allow the F-pili to move freely (24). Consequently, cells may also move about freely, which makes it difficult to observe a specific group of cells over time. This was accomplished by using an *E. coli* K-12 derivative strain containing deletions of the *motAB* genes, which inactivates the flagella motor (190). There is also a 57 residue deletion and 6 residue substitution in the center of the *fliC* gene, encoding for flagellin, which causes the flagella to be sticky (191, 192). This strain adheres well to glass surfaces, permitting visualization under live-cell microscopy (193). This strain was made F^+ through conjugation and transformed with the IPTG inducible plasmid encoding *traA* (A113C) to observe F-pili dynamics in a homemade glass flow cell.

F-pilus retraction could be readily observed using this method (Figure 5.4A). Each of the 13 retraction events observed was continuous, meaning once F-pili retraction initiated, the pilus retracted completely without an observable extension event. Notably, we observed an average retraction rate of 51 ± 30 nm/s, which was about 3 times faster than previously reported values using fluorescently labeled R17 (24). There appeared to be a correlation between the initial F-pilus length and the average retraction rate of the F-pilus, where longer F-pili at the onset of retraction appeared to retract at a faster rate (Figure 5.4B). Overall, the direct labeling of F-pili appears to permit faster retraction events, suggesting that this method may be a less disruptive alternative to observe F-pili dynamics.

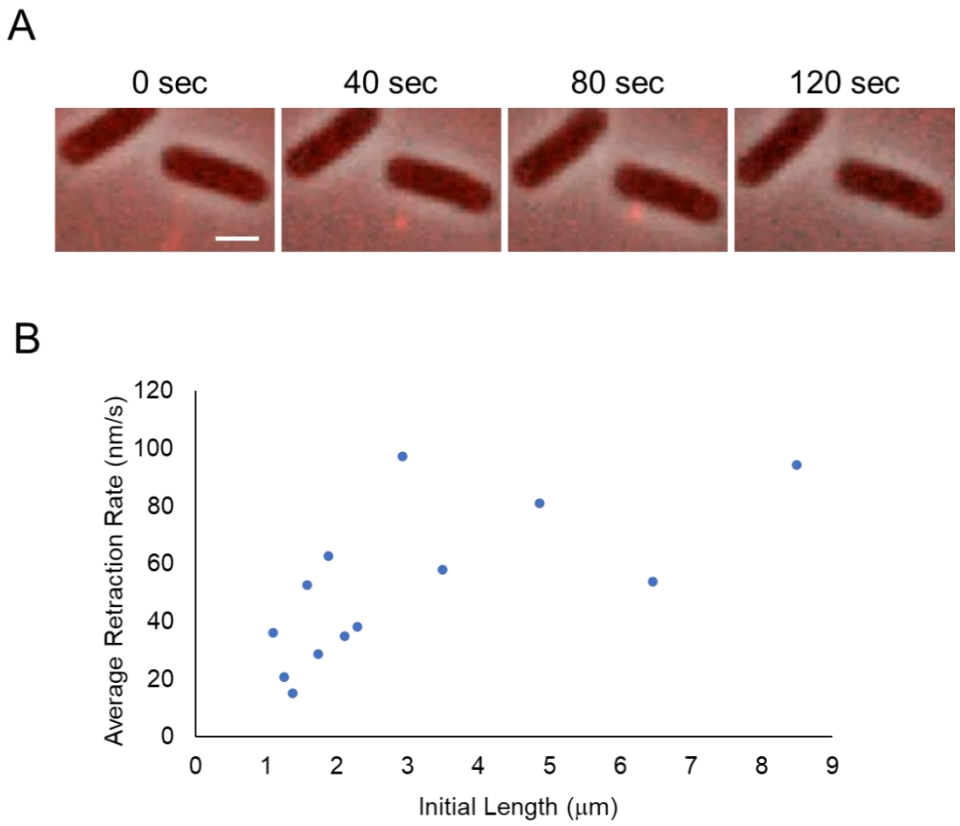

Figure 5.4 Live-cell visualization and quantification of F-pili dynamics.
(A) Representative time lapse image sequence of Alexafluor 568 C5-maleimide labeled LZ2662 cells. The F-pilus (red) retracts towards the cell body. (B) Comparison between F-pilus length and average retraction rate. Initial lengths of F-pili were measured immediately before the onset of retraction to correlate the rate of retraction and F-pilus length. For B, retraction rates were measured from live-cell movies using 30 sec imaging intervals. Scale bar = 1 μm. Individual measurements are displayed from at least two experiments.

Discussion

In this study, we investigated the F-pilus phenotypes resulting from deletion and overexpression of several different *tra*/*trb* genes to better understand how each factor contributes to the synthesis of F-pili. Generally, we found that deletions of genes that are considered to play a role in F-T4SS assembly inhibit synthesis of surface F-pili as observed through MS2-GFP binding. These results support the classification of these genes as contributors to F-T4SS assembly (95). Alternatively, overexpression of genes that were thought to promote F-pilus synthesis (i.e. *traE and traC*) lead to elevated levels of surface F-pili with longer average lengths. However, overexpression of several F-T4SS assembly proteins reduced the levels of surface F-pili. These findings suggest that some functions of *tra*/*trb* proteins are concentration-dependent, where artificial increases through induction can either promote or disrupt F-pilus synthesis.

Additionally, we developed a novel fluorescent labeling approach to detect and quantify F-pili dynamics under live-cell microscopy. Although F-pili dynamics were first observed using fluorescently labeled R17 binding, we were unable to reproduce this method under our conditions (24). While this method was useful for establishing the precedent for F-pili dynamics, it is unfortunately limited by the necessity of ssRNA phage binding and therefore cannot be applied to pilus systems lacking known ssRNA phages. Additionally, it is unclear whether the F-pilus behaviors reported previously (e.g., pilus supercoiling) are native to the system or are artifacts resulting from a high number of R17 particles decorating each pilus. As well, it is possible that the binding of R17 particles can alter the kinetics of dynamic activity, especially with high enough

numbers to bind along the entire length of the F-pilus. Indeed, we observed that F-pili tend to retract at faster rates compared to the previously reported value of 16 nm/s (24). However, we were unable to observe F-pilus extension. It is possible that extension can be stimulated through some extracellular interaction, such as ssRNA phage binding to the F-pilus, or if cells expressing F-pili are mixed with potential recipient cells to mimic conjugation. Therefore, while this system may still need optimization, it provides a powerful new tool for labeling conjugative pili and prompts its use in exploring genetic and environmental determinants affecting F-pilus assembly and dynamic activity.

CHAPTER VI

CONCLUSIONS

Early work exploring the physiology of ssRNA phages helped establish key findings related to cell penetration, including identification of pili as host receptors for ssRNA phages, the role of the Mat protein in host recognition, and RNAase sensitivity during RNA entry. Historically, however, researchers have consistently noted the mysterious nature of the cell penetration process, which gave rise to several models, each with little supporting evidence. Revisiting these earlier findings using new, high-resolution techniques have revealed important phenomena and provided new mechanistic details describing the function of host pili systems in permitting ssRNA phage cell penetration.

The role of F-pili in facilitating ssRNA phage penetration

The pilus was first proposed to be a hollow tube that the phage could potentially penetrate directly and have its gRNA passage through the pilus lumen (65). This model was later replaced with the pilus retraction model which has been evidenced by pilus shortening after PP7 infection of *P. aeruginosa* as observed by electron microscopy (67). Similar findings were reported during infection of *E. coli* cells by R17, however, an increase in the ability for the supernatant to adsorb R17 phages after infection was also noted (62). The authors interpreted this finding by suggesting that R17 infection can cause cells to secrete and release new F-pili, or that infection causes F-pilus fragmentation. However, direct evidence, as well as the molecular mechanism for F-pilus release resulting from ssRNA phage infection had yet to be established. The work presented in Chapter II outlines new methods for measuring and detecting F-pili. These

methods were used to directly observe F-pilus detachment, as well as determine that detachment likely results from F-pilus retraction.

Although the F-pilus detachment phenomenon is consistent, several questions remain. First, it is unclear whether every instance of phage entry results in F-pilus detachment or if some phages enter the cell without eliciting pilus detachment at all. This could be addressed using the live-cell fluorescence microscopy approach involving dual-labeling of the F-pilus and the infecting MS2 particle described in Chapter V. Theoretically, the fluorescently labeled MS2 virion could be visualized on the labeled F-pilus during dynamic activity. The number of infecting phage particles per pilus and the frequency of pilus retraction and subsequent detachment can be quantified using this technique. Additionally, direct observation of cytosolic gRNA penetration coupled to F-pilus detachment can be achieved by labeling gRNA upon entry. MS2 Coat proteins fused to a fluorescent reporter, such as GFP, have been used in multiple instances to detect RNAs modified to contain high affinity stem loop regions (194). It may be possible to use a similar approach to detect incoming MS2 gRNA under live-cell microscopy. Alternatively, the MS2 genome could be modified to contain fluorogenic RNA aptamers, which bind and activate the fluorescent properties of an otherwise non-fluorescent molecule (195).

F-pilus retraction is a key stage in the pilus detachment model, however, the mechanism of F-pilus retraction has perplexed researchers since its discovery. Direct evidence for F-pilus retraction was first obtained using fluorescent R17 particles to detect F-pili by proxy of phage binding. F-pili were observed to extend and retract at

random, with a pilus retraction event typically completing within 5 minutes of initiation. However, it is unclear whether this method of F-pilus detection affects the kinetics or behavior. The presumably less disruptive labeling method described in Chapter V, combined with mutational analysis of *tra* genes known to affect F-pilus assembly could provide clues about the nature of F-pilus retraction.

Pilus detachment is present in diverse pilus-phage systems

The pilus detachment phenomenon is thought to provide infecting phages with a selective advantage through two means: first, by directly removing and inhibiting the biogenesis of host receptors, and second, by releasing F-pili into the medium which can reversibly bind free phage to promote their distribution. Both mechanisms work to promote superinfection exclusion and provide fitness advantages to the phage population. We therefore expanded into a completely different pilus-phage system to determine the scope of pilus detachment. Our work with the ssRNA phage PP7 as it infects *P. aeruginosa* demonstrated that PP7 cell penetration results in the detachment of T4P. Pilus detachment translated into a disruption in further T4P biosynthesis, as well as an inhibition of T4P mediated twitching motility. Additionally, T4P retraction, and specifically the force generated through the retraction ATPase, PilU, was found to be essential for T4P detachment and subsequent PP7 cell penetration. These findings exemplified that the pilus detachment phenomenon is widespread and therefore, may be present among other ssRNA phages that use retractile pili to facilitate infection.

Beyond PP7 and its host *P. aeruginosa*, many other species of gram-negative bacteria secrete diverse types of pili which also facilitate important host functions.

Although ssRNA phages have not been identified for every pilus-producing species, presumably any bacterial strain producing a retractile pilus can serve as a host for a ssRNA phage. Therefore, the question of consistency (and differences) across systems remains. An investigation into the known ssRNA phage-pilus systems is warranted, such as the interaction between ssRNA phage AP205 and the T4P of host *Acinetobacter spp.* Additionally, the functionally unrelated Tad pili of *C. crescentus* serve as host receptors for the ssRNA phage ΦCb5. These studies would further enrich our understanding of pilus-phage systems and pilus detachment resulting from ssRNA phage infection.

Function of coupling proteins in ssRNA phage penetration

Tremendous contributions by William Paranchych, Charles Brinton, and several others helped establish the pilus retraction model through foundational results that describe the early interactions between ssRNA phages and their respective pili (196). The results described in chapters II and III help supplement this model by explaining how pilus retraction contributes to pilus detachment. However, while the pilus retraction model may explain how the infecting phage reaches the cell surface, it does not cover subsequent cell penetration involving passage through the cell envelope. The use of transfer-deficient amber mutants in the coupling protein, *traD*, provided some clues about the cell penetration process. These *traD* mutants created normal levels of F-pili, but were completely resistant to the group I ssRNA phages. Interestingly, the mutants were still sensitive to the male-specific ssRNA phage Qβ and ssDNA filamentous phages (161, 196). Therefore, it was thought that the *traD* gene product played some role in the infection cycle at a step post-ejection of the gRNA.

Experiments using a temperature-sensitive mutant of *traD* showed that MS2 RNA replication was inhibited by a temperature shift to 42 °C (197). However, it is unclear whether this mutant permitted penetration of the gRNA into the cytoplasm to allow replication to occur. Later, infection of phage R17 was found to be reliant on the docking of the conjugative R1 relaxosome, facilitated by an interaction between the relaxase, TraI, and TraD (186). These studies helped to establish the requirement for TraD in permitting productive infection of F-piliated *E. coli* by group I ssRNA phages, albeit still by an unknown mechanism. The work presented in chapters II and IV use fluorescent microscopy and genetic techniques to establish TraD as a gatekeeper for cytoplasmic penetration of MS2 gRNA. A Δ*traD* mutant failed to uptake MS2 gRNA, yet still permitted ejection and subsequently, F-pilus detachment. These findings were critical to determine that F-pilus detachment occurs extracellularly after the MS2 virion engages with the distal end of the T4SS basal body.

While the work in chapter II helped clarify the role of TraD in the infection cycle, the molecular mechanism is still mysterious. The findings in the R1 plasmid system suggested that conjugative plasmid transfer competency is a determining factor for successful infection. This prompted the work in chapter IV, where the use of *traD* mutants and restricted expression backgrounds helped elucidate possible details about the interaction between TraD and MS2. Experimental adaptation of an MS2 population infecting cells expressing basal levels of TraD gave rise to a mutant variant with improved plaquing efficiency. A single base change (G1192T) giving rise to an amino acid substitution in the Mat protein (A355S) was sufficient to elicit a clear plaque

phenotype on the basal TraD strain. Additional findings showing that the nucleotide relaxosome binding domains of TraD promote infection by MS2 suggested that the activity, and possibly recruitment of TraD to the conjugative pore, are important for cell penetration.

While the findings presented in chapter IV provide some details describing the function of coupling proteins in permitting cell penetration, the exact molecular mechanism is still unclear. The Mat protein mutation identified in the evolved MS2 population could suggest a relationship between Mat and TraD, however, this would still need to be established. Direct interactions between TraD and Mat could possibly be investigated through crosslinking and immunoprecipitation (177). Additionally, the interaction could be observed using a fluorescent TraD fusion protein expressed in a Δ*traD* background. TraD is known to interact transiently with the conjugative pore, therefore, a live-cell microscopy approach, combining the labeling schemes proposed above, could be used to observe the recruitment of TraD to site of infection. These methods could outline differences between the WT and evolved MS2 in recruiting TraD.

Lastly, the rationale for the dependence on functional coupling proteins by group I ssRNA phages is quite mysterious. Interestingly, the ssRNA phage Qβ does not require TraD for infection. It seems intuitive that the differences would lie in the Mat-pilin interactions, since the gRNA is thought to denature during entry, making the Mat-gRNA complexes between ssRNA phages similar in terms of composition. MS2 is thought to bind F-pili much more readily compared to Qβ, as Qβ particles only sparsely bind free F-pili under electron microscopy (59). It is possible that MS2 entry into the host cytosol

requires additional energy from the ATPase activity of TraD to pull the incoming gRNA from the conjugative pore, while the weaker Mat-pilin interactions of Qβ do not require this additional input. Mutation of the known F-pilin residues that contact the MS2 Mat could reduce the binding affinity of MS2, mimicking the Qβ-pilin interaction, and may attenuate the TraD requirement (58).

The advantages and justification for why the group I ssRNA phages have evolved to exploit the mechanics of coupling proteins are unclear. The requirement for a coupling protein engaged with the relaxosome likely benefits the host by limiting its phage sensitivity to occasions when the conjugative plasmid is being transferred (186). In contrast, given the transient association of the coupling proteins with the conjugative pore, the presence of coupling proteins is an indicator of a functional mating channel and possibly the metabolic state of the cell (90). Thus, the reliance on coupling proteins may indicate to the phage gRNA, awaiting passage into the cytosol, that the cell is healthy and will yield a productive infection once penetration is complete.

REFERENCES

1. Comeau, A.M. and H.M. Krisch, *War is peace--dispatches from the bacterial and phage killing fields.* Curr Opin Microbiol, 2005. **8**(4): p. 488-94.
2. Brussow, H., C. Canchaya, and W.D. Hardt, *Phages and the evolution of bacterial pathogens: from genomic rearrangements to lysogenic conversion.* Microbiol Mol Biol Rev, 2004. **68**(3): p. 560-602, table of contents.
3. Touchon, M., J.A. Moura de Sousa, and E.P. Rocha, *Embracing the enemy: the diversification of microbial gene repertoires by phage-mediated horizontal gene transfer.* Curr Opin Microbiol, 2017. **38**: p. 66-73.
4. Fernandez, L., A. Rodriguez, and P. Garcia, *Phage or foe: an insight into the impact of viral predation on microbial communities.* ISME J, 2018. **12**(5): p. 1171-1179.
5. King, A.M., et al., *Virus Taxonomy : Ninth Report of the International Committee on Taxonomy of Viruses*. 2011, St. Louis, UNITED STATES: Elsevier.
6. Bertozzi Silva, J., Z. Storms, and D. Sauvageau, *Host receptors for bacteriophage adsorption.* FEMS Microbiol Lett, 2016. **363**(4).
7. Wenzel, S., et al., *The Central Spike Complex of Bacteriophage T4 Contacts PpiD in the Periplasm of Escherichia coli.* Viruses, 2020. **12**(10).
8. Arisaka, F., et al., *The tail lysozyme complex of bacteriophage T4.* Int J Biochem Cell Biol, 2003. **35**(1): p. 16-21.

9. Cumby, N., et al., *The phage tail tape measure protein, an inner membrane protein and a periplasmic chaperone play connected roles in the genome injection process of E. coli phage HK97.* Mol Microbiol, 2015. **96**(3): p. 437-47.

10. Hay, I.D. and T. Lithgow, *Filamentous phages: masters of a microbial sharing economy.* EMBO Rep, 2019. **20**(6).

11. International Committee on Taxonomy of Viruses. and A.M.Q. King, *Virus taxonomy : classification and nomenclature of viruses : ninth report of the International Committee on Taxonomy of Viruses*. 2012, London ; Waltham, MA: Academic Press. x, 1327 p.

12. Sun, L., M.G. Rossmann, and B.A. Fane, *High-resolution structure of a virally encoded DNA-translocating conduit and the mechanism of DNA penetration.* J Virol, 2014. **88**(18): p. 10276-9.

13. Mai-Prochnow, A., et al., *'Big things in small packages: the genetics of filamentous phage and effects on fitness of their host'.* FEMS Microbiol Rev, 2015. **39**(4): p. 465-87.

14. Khalil, A.S., et al., *Single M13 bacteriophage tethering and stretching.* Proc Natl Acad Sci U S A, 2007. **104**(12): p. 4892-7.

15. Mao, C., et al., *Virus-based toolkit for the directed synthesis of magnetic and semiconducting nanowires.* Science, 2004. **303**(5655): p. 213-7.

16. Brodel, A.K., M. Isalan, and A. Jaramillo, *Engineering of biomolecules by bacteriophage directed evolution.* Curr Opin Biotechnol, 2018. **51**: p. 32-38.

17. Loh, B., et al., *The Transmembrane Morphogenesis Protein gp1 of Filamentous Phages Contains Walker A and Walker B Motifs Essential for Phage Assembly.* Viruses, 2017. **9**(4).

18. Park, I.W., et al., *Recent Developments and Prospects of M13- Bacteriophage Based Piezoelectric Energy Harvesting Devices.* Nanomaterials (Basel), 2020. **10**(1).

19. Russel, M. and P. Model, *Genetic analysis of the filamentous bacteriophage packaging signal and of the proteins that interact with it.* J Virol, 1989. **63**(8): p. 3284-95.

20. Gerding, M.A., et al., *The trans-envelope Tol-Pal complex is part of the cell division machinery and required for proper outer-membrane invagination during cell constriction in E. coli.* Mol Microbiol, 2007. **63**(4): p. 1008-25.

21. Eckert, B., et al., *Prolyl isomerization as a molecular timer in phage infection.* Nat Struct Mol Biol, 2005. **12**(7): p. 619-23.

22. Click, E.M. and R.E. Webster, *The TolQRA proteins are required for membrane insertion of the major capsid protein of the filamentous phage f1 during infection.* J Bacteriol, 1998. **180**(7): p. 1723-8.

23. Bennett, N.J. and J. Rakonjac, *Unlocking of the filamentous bacteriophage virion during infection is mediated by the C domain of pIII.* J Mol Biol, 2006. **356**(2): p. 266-73.

24. Clarke, M., et al., *F-pili dynamics by live-cell imaging.* Proc Natl Acad Sci U S A, 2008. **105**(46): p. 17978-81.

25. Lubkowski, J., et al., *Filamentous phage infection: crystal structure of g3p in complex with its coreceptor, the C-terminal domain of TolA.* Structure, 1999. **7**(6): p. 711-22.

26. Higashitani, N., A. Higashitani, and K. Horiuchi, *Nucleotide sequence of the primer RNA for DNA replication of filamentous bacteriophages.* J Virol, 1993. **67**(4): p. 2175-81.

27. Smeal, S.W., et al., *Simulation of the M13 life cycle I: Assembly of a genetically-structured deterministic chemical kinetic simulation.* Virology, 2017. **500**: p. 259-274.

28. Russel, M. and P. Model, *Filamentous Phage*, in *The Bacteriophages*, R. Calendar, Editor. 2006, Oxford University Press: New York. p. 146-160.

29. Smeal, S.W., et al., *Simulation of the M13 life cycle II: Investigation of the control mechanisms of M13 infection and establishment of the carrier state.* Virology, 2017. **500**: p. 275-284.

30. Vidaver, A.K., R.K. Koski, and J.L. Van Etten, *Bacteriophage phi6: a Lipid-Containing Virus of Pseudomonas phaseolicola.* J Virol, 1973. **11**(5): p. 799-805.

31. Roine, E., et al., *Characterization of type IV pilus genes in Pseudomonas syringae pv. tomato DC3000.* Mol Plant Microbe Interact, 1998. **11**(11): p. 1048-56.

32. Frilander, M., M. Poranen, and D.H. Bamford, *The large genome segment of dsRNA bacteriophage phi6 is the key regulator in the in vitro minus and plus strand synthesis.* RNA, 1995. **1**(5): p. 510-8.

33. Olkkonen, V.M. and D.H. Bamford, *The nucleocapsid of the lipid-containing double-stranded RNA bacteriophage phi 6 contains a protein skeleton consisting of a single polypeptide species.* J Virol, 1987. **61**(8): p. 2362-7.

34. Juuti, J.T. and D.H. Bamford, *RNA binding, packaging and polymerase activities of the different incomplete polymerase complex particles of dsRNA bacteriophage phi 6.* J Mol Biol, 1995. **249**(3): p. 545-54.

35. Paatero, A.O., J.E. Syvaoja, and D.H. Bamford, *Double-stranded RNA bacteriophage phi 6 protein P4 is an unspecific nucleoside triphosphatase activated by calcium ions.* J Virol, 1995. **69**(11): p. 6729-34.

36. Qiao, J., X. Qiao, and L. Mindich, *In vivo studies of genomic packaging in the dsRNA bacteriophage Phi8.* BMC Microbiol, 2005. **5**: p. 10.

37. Olkkonen, V.M., P.M. Ojala, and D.H. Bamford, *Generation of infectious nucleocapsids by in vitro assembly of the shell protein on to the polymerase complex of the dsRNA bacteriophage phi 6.* J Mol Biol, 1991. **218**(3): p. 569-81.

38. Mindich, L., *Phages with Segmented Double-Stranded RNA Genomes*, in *The Bacteriophages*, R. Calendar, Editor. 2006, Oxford University Press, New York. p. 197-207.

39. Mindich, L., et al., *Isolation of additional bacteriophages with genomes of segmented double-stranded RNA.* J Bacteriol, 1999. **181**(15): p. 4505-8.

40. Romantschuk, M. and D.H. Bamford, *Function of pili in bacteriophage phi 6 penetration.* J Gen Virol, 1985. **66 (Pt 11)**: p. 2461-9.

41. Bamford, D.H., M. Romantschuk, and P.J. Somerharju, *Membrane fusion in prokaryotes: bacteriophage phi 6 membrane fuses with the Pseudomonas syringae outer membrane.* EMBO J, 1987. **6**(5): p. 1467-73.

42. Pei, J. and N.V. Grishin, *The P5 protein from bacteriophage phi-6 is a distant homolog of lytic transglycosylases.* Protein Sci, 2005. **14**(5): p. 1370-4.

43. Dessau, M., et al., *Selective pressure causes an RNA virus to trade reproductive fitness for increased structural and thermal stability of a viral enzyme.* PLoS Genet, 2012. **8**(11): p. e1003102.

44. Bamford, D.H. and E.T. Palva, *Structure of the lipid-containing bacteriophage phi 6. Disruption by Triton X-100 treatment.* Biochim Biophys Acta, 1980. **601**(2): p. 245-59.

45. Mindich, L. and J. Lehman, *Cell wall lysin as a component of the bacteriophage phi 6 virion.* J Virol, 1979. **30**(2): p. 489-96.

46. Qiao, X., J. Qiao, and L. Mindich, *Stoichiometric packaging of the three genomic segments of double-stranded RNA bacteriophage phi6.* Proc Natl Acad Sci U S A, 1997. **94**(8): p. 4074-9.

47. Gottlieb, P., J. Strassman, and L. Mindich, *Protein P4 of the bacteriophage phi 6 procapsid has a nucleoside triphosphate-binding site with associated nucleoside triphosphate phosphohydrolase activity.* J Virol, 1992. **66**(10): p. 6220-2.

48. Juuti, J.T., et al., *Structure and NTPase activity of the RNA-translocating protein (P4) of bacteriophage phi 6.* J Mol Biol, 1998. **279**(2): p. 347-59.

49. Butcher, S.J., et al., *A mechanism for initiating RNA-dependent RNA polymerization.* Nature, 2001. **410**(6825): p. 235-40.

50. Lyytinen, O.L., D. Starkova, and M.M. Poranen, *Microbial production of lipid-protein vesicles using enveloped bacteriophage phi6.* Microb Cell Fact, 2019. **18**(1): p. 29.

51. Johnson, M.D., 3rd and L. Mindich, *Isolation and characterization of nonsense mutations in gene 10 of bacteriophage phi 6.* J Virol, 1994. **68**(4): p. 2331-8.

52. Callanan, J., et al., *Expansion of known ssRNA phage genomes: From tens to over a thousand.* Sci Adv, 2020. **6**(6): p. eaay5981.

53. Atkins, J.F., et al., *Binding of mammalian ribosomes to MS2 phage RNA reveals an overlapping gene encoding a lysis function.* Cell, 1979. **18**(2): p. 247-56.

54. Klovins, J., et al., *Nucleotide sequence of a ssRNA phage from Acinetobacter: kinship to coliphages.* J Gen Virol, 2002. **83**(Pt 6): p. 1523-1533.

55. Bernhardt, T.G., et al., *A protein antibiotic in the phage Qbeta virion: diversity in lysis targets.* Science, 2001. **292**(5525): p. 2326-9.

56. Hofstetter, H., H.J. Monstein, and C. Weissmann, *The readthrough protein A1 is essential for the formation of viable Q beta particles.* Biochim Biophys Acta, 1974. **374**(2): p. 238-51.

57. Ghigo, J.M., *Natural conjugative plasmids induce bacterial biofilm development.* Nature, 2001. **412**(6845): p. 442-5.

58. Meng, R., et al., *Structural basis for the adsorption of a single-stranded RNA bacteriophage.* Nat Commun, 2019. **10**(1): p. 3130.

59. Manchak, J., K.G. Anthony, and L.S. Frost, *Mutational analysis of F-pilin reveals domains for pilus assembly, phage infection and DNA transfer.* Mol Microbiol, 2002. **43**(1): p. 195-205.

60. Paranchych, W., P.M. Krahn, and R.D. Bradley, *Stages in phage R17 infection.* Virology, 1970. **41**(3): p. 465-73.

61. Valentine, R.C. and H. Wedel, *The extracellular stages of RNA bacteriophage infection.* Biochem Biophys Res Commun, 1965. **21**(2): p. 106-12.

62. Paranchych, W., et al., *Stages in phage R17 infection. V. Phage eclipse and the role of F pili.* Virology, 1971. **45**(3): p. 615-28.

63. Paranchych, W., *Stages in phage R17 infection: the role of divalent cations.* Virology, 1966. **28**(1): p. 90-9.

64. Krahn, P.M., R.J. O'Callaghan, and W. Paranchych, *Stages in phage R17 infection. VI. Injection of A protein and RNA into the host cell.* Virology, 1972. **47**(3): p. 628-37.

65. Brinton, C.C., Jr., *The structure, function, synthesis and genetic control of bacterial pili and a molecular model for DNA and RNA transport in gram negative bacteria.* Trans N Y Acad Sci, 1965. **27**(8): p. 1003-54.

66. Costa, T.R.D., et al., *Structure of the Bacterial Sex F Pilus Reveals an Assembly of a Stoichiometric Protein-Phospholipid Complex.* Cell, 2016. **166**(6): p. 1436-1444 e10.

67. Bradley, D.E., *Shortening of Pseudomonas aeruginosa pili after RNA-phage adsorption.* J Gen Microbiol, 1972. **72**(2): p. 303-19.

68. Van Duin, J. and N. Tsarena, *Single-stranded RNA Phages*, in *The Bacteriophages*, R. Calendar, Editor. 2006, Oxford University Press: New York. p. 175-196.

69. Blumenthal, T., T.A. Landers, and K. Weber, *Bacteriophage Q replicase contains the protein biosynthesis elongation factors EF Tu and EF Ts.* Proc Natl Acad Sci U S A, 1972. **69**(5): p. 1313-7.

70. Wahba, A.J., et al., *Subunit I of G beta replicase and 30 S ribosomal protein S1 of Escherichia coli. Evidence for the identity of the two proteins.* J Biol Chem, 1974. **249**(10): p. 3314-6.

71. van Meerten, D., G. Girard, and J. van Duin, *Translational control by delayed RNA folding: identification of the kinetic trap.* RNA, 2001. **7**(3): p. 483-94.

72. Adhin, M.R. and J. van Duin, *Scanning model for translational reinitiation in eubacteria.* J Mol Biol, 1990. **213**(4): p. 811-8.

73. Kamen, R., *Structure and function of the Qβ RNA replicase*, in *RNA Phages*, N.D. Zinder, Editor. 1975, Cold Spring Harbor Laboratory: Cold Spring Harbor, NY. p. 203-234.

74. Vasilyev, N.N., et al., *Ribosomal protein S1 functions as a termination factor in RNA synthesis by Qbeta phage replicase.* Nat Commun, 2013. **4**: p. 1781.

75. Dai, X., et al., *In situ structures of the genome and genome-delivery apparatus in a single-stranded RNA virus.* Nature, 2017. **541**(7635): p. 112-116.

76. Valegard, K., et al., *Crystal structure of an RNA bacteriophage coat protein-operator complex.* Nature, 1994. **371**(6498): p. 623-6.

77. Witherell, G.W., J.M. Gott, and O.C. Uhlenbeck, *Specific interaction between RNA phage coat proteins and RNA.* Prog Nucleic Acid Res Mol Biol, 1991. **40**: p. 185-220.

78. Chamakura, K. and R. Young, *Phage single-gene lysis: Finding the weak spot in the bacterial cell wall.* J Biol Chem, 2019. **294**(10): p. 3350-3358.

79. Chamakura, K.R., J.S. Tran, and R. Young, *MS2 Lysis of Escherichia coli Depends on Host Chaperone DnaJ.* J Bacteriol, 2017. **199**(12).

80. Chamakura, K.R., G.B. Edwards, and R. Young, *Mutational analysis of the MS2 lysis protein L.* Microbiology (Reading), 2017. **163**(7): p. 961-969.

81. Bradley, D.E., *The Structure and Infective Process of a Pseudomonas aeruginosa Bacteriophage Containing Ribonucleic Acid.* J Gen Microbiol, 1966. **45**: p. 83-96.

82. Pourcel, C., et al., *A carrier state is established in Pseudomonas aeruginosa by phage LeviOr01, a newly isolated ssRNA levivirus.* J Gen Virol, 2017. **98**(8): p. 2181-2189.

83. Schmidt, J.M. and R.Y. Stanier, *Isolation and Characterization of Bacteriophages Active against Stalked Bacteria.* J Gen Microbiol, 1965. **39**: p. 95-107.

84. Sangermani, M., et al., *Tad Pili Play a Dynamic Role in Caulobacter crescentus Surface Colonization.* mBio, 2019. **10**(3).

85. Burrows, L.L., *Pseudomonas aeruginosa twitching motility: type IV pili in action.* Annu Rev Microbiol, 2012. **66**: p. 493-520.

86. Rumnieks, J. and K. Tars, *Diversity of pili-specific bacteriophages: genome sequence of IncM plasmid-dependent RNA phage M.* BMC Microbiol, 2012. **12**: p. 277.

87. Paranchych, W. and L.S. Frost, *The physiology and biochemistry of pili.* Adv Microb Physiol, 1988. **29**: p. 53-114.

88. Tomoeda, M., M. Inuzuka, and T. Date, *Bacterial sex pili.* Prog Biophys Mol Biol, 1975. **30**(1): p. 23-56.

89. Armstrong, G.D., et al., *Comparative biochemical studies on F and EDP208 conjugative pili.* J Bacteriol, 1980. **141**(1): p. 333-41.

90. Hu, B., P. Khara, and P.J. Christie, *Structural bases for F plasmid conjugation and F pilus biogenesis in Escherichia coli.* Proc Natl Acad Sci U S A, 2019. **116**(28): p. 14222-14227.

91. Hu, B., et al., *In Situ Molecular Architecture of the Helicobacter pylori Cag Type IV Secretion System.* mBio, 2019. **10**(3).

92. Harris, R.L., et al., *Interaction between the F plasmid TraA (F-pilin) and TraQ proteins.* Mol Microbiol, 1999. **34**(4): p. 780-91.

93. Majdalani, N. and K. Ippen-Ihler, *Membrane insertion of the F-pilin subunit is Sec independent but requires leader peptidase B and the proton motive force.* J Bacteriol, 1996. **178**(13): p. 3742-7.

94. Moore, D., et al., *The Escherichia coli K-12 F plasmid gene traX is required for acetylation of F pilin.* J Bacteriol, 1993. **175**(5): p. 1375-83.

95. Lawley, T.D., et al., *F factor conjugation is a true type IV secretion system.* FEMS Microbiol Lett, 2003. **224**(1): p. 1-15.

96. Harris, R.L., V. Hombs, and P.M. Silverman, *Evidence that F-plasmid proteins TraV, TraK and TraB assemble into an envelope-spanning structure in Escherichia coli.* Mol Microbiol, 2001. **42**(3): p. 757-66.

97. Harris, R.L. and P.M. Silverman, *Tra proteins characteristic of F-like type IV secretion systems constitute an interaction group by yeast two-hybrid analysis.* J Bacteriol, 2004. **186**(16): p. 5480-5.

98. Novotny, C.P. and P. Fives-Taylor, *Retraction of F pili.* J Bacteriol, 1974. **117**(3): p. 1306-11.

99. Maneewannakul, S., K. Maneewannakul, and K. Ippen-Ihler, *Characterization, localization, and sequence of F transfer region products: the pilus assembly gene product TraW and a new product, TrbI.* J Bacteriol, 1992. **174**(17): p. 5567-74.

100. Beck, C.M., et al., *The F pilus mediates a novel pathway of CDI toxin import.* Mol Microbiol, 2014. **93**(2): p. 276-90.

101. Anthony, K.G., et al., *Comparison of proteins involved in pilus synthesis and mating pair stabilization from the related plasmids F and R100-1: insights into the mechanism of conjugation.* J Bacteriol, 1999. **181**(17): p. 5149-59.

102. Herrero, M., V. de Lorenzo, and K.N. Timmis, *Transposon vectors containing non-antibiotic resistance selection markers for cloning and stable chromosomal insertion of foreign genes in gram-negative bacteria.* J Bacteriol, 1990. **172**(11): p. 6557-67.

103. Byrd, D.R. and S.W. Matson, *Nicking by transesterification: the reaction catalysed by a relaxase.* Mol Microbiol, 1997. **25**(6): p. 1011-22.

104. Moncalian, G. and F. de la Cruz, *DNA binding properties of protein TrwA, a possible structural variant of the Arc repressor superfamily.* Biochim Biophys Acta, 2004. **1701**(1-2): p. 15-23.

105. Llosa, M., et al., *Bacterial conjugation: a two-step mechanism for DNA transport.* Mol Microbiol, 2002. **45**(1): p. 1-8.

106. Draper, O., et al., *Site-specific recombinase and integrase activities of a conjugative relaxase in recipient cells.* Proc Natl Acad Sci U S A, 2005. **102**(45): p. 16385-90.

107. Koch, M.D., et al., *Competitive binding of independent extension and retraction motors explains the quantitative dynamics of type IV pili.* Proc Natl Acad Sci U S A, 2021. **118**(8).

108. Wang, F., et al., *Cryoelectron Microscopy Reconstructions of the Pseudomonas aeruginosa and Neisseria gonorrhoeae Type IV Pili at Sub-nanometer Resolution.* Structure, 2017. **25**(9): p. 1423-1435 e4.

109. Aas, F.E., et al., *Substitutions in the N-terminal alpha helical spine of Neisseria gonorrhoeae pilin affect Type IV pilus assembly, dynamics and associated functions.* Mol Microbiol, 2007. **63**(1): p. 69-85.

110. Ayers, M., P.L. Howell, and L.L. Burrows, *Architecture of the type II secretion and type IV pilus machineries.* Future Microbiol, 2010. **5**(8): p. 1203-18.

111. Ellison, C.K., et al., *A bifunctional ATPase drives tad pilus extension and retraction.* Sci Adv, 2019. **5**(12): p. eaay2591.

112. Nguyen, Y., et al., *Pseudomonas aeruginosa minor pilins prime type IVa pilus assembly and promote surface display of the PilY1 adhesin.* J Biol Chem, 2015. **290**(1): p. 601-11.

113. Graham, K., *The Regulation and Dynamics of Type IV Pili in Pseudomonas Aeruginosa*, in *Biochemistry and Biomedical Sciences*. 2021, McMaster University: Hamilton, Ontario. p. 106.

114. Chang, Y.W., et al., *Architecture of the type IVa pilus machine.* Science, 2016. **351**(6278): p. aad2001.

115. Strom, M.S., D.N. Nunn, and S. Lory, *A single bifunctional enzyme, PilD, catalyzes cleavage and N-methylation of proteins belonging to the type IV pilin family.* Proc Natl Acad Sci U S A, 1993. **90**(6): p. 2404-8.

116. Giltner, C.L., et al., *Evolutionary and functional diversity of the Pseudomonas type IVa pilin island.* Environ Microbiol, 2011. **13**(1): p. 250-264.

117. Cisneros, D.A., et al., *Minor pseudopilin self-assembly primes type II secretion pseudopilus elongation.* EMBO J, 2012. **31**(4): p. 1041-53.

118. Giltner, C.L., M. Habash, and L.L. Burrows, *Pseudomonas aeruginosa minor pilins are incorporated into type IV pili.* J Mol Biol, 2010. **398**(3): p. 444-61.

119. Bertrand, J.J., J.T. West, and J.N. Engel, *Genetic analysis of the regulation of type IV pilus function by the Chp chemosensory system of Pseudomonas aeruginosa.* J Bacteriol, 2010. **192**(4): p. 994-1010.

120. Belete, B., H. Lu, and D.J. Wozniak, *Pseudomonas aeruginosa AlgR regulates type IV pilus biosynthesis by activating transcription of the fimU-pilVWXY1Y2E operon.* J Bacteriol, 2008. **190**(6): p. 2023-30.

121. Baker, M.D., P.M. Wolanin, and J.B. Stock, *Signal transduction in bacterial chemotaxis.* Bioessays, 2006. **28**(1): p. 9-22.

122. Borkovich, K.A., L.A. Alex, and M.I. Simon, *Attenuation of sensory receptor signaling by covalent modification.* Proc Natl Acad Sci U S A, 1992. **89**(15): p. 6756-60.

123. Muok, A.R., A. Briegel, and B.R. Crane, *Regulation of the chemotaxis histidine kinase CheA: A structural perspective.* Biochim Biophys Acta Biomembr, 2020. **1862**(1): p. 183030.

124. DeLange, P.A., et al., *PilJ localizes to cell poles and is required for type IV pilus extension in Pseudomonas aeruginosa.* Curr Microbiol, 2007. **55**(5): p. 389-95.

125. Whitchurch, C.B., et al., *Characterization of a complex chemosensory signal transduction system which controls twitching motility in Pseudomonas aeruginosa.* Mol Microbiol, 2004. **52**(3): p. 873-93.

126. McCallum, M., et al., *The molecular mechanism of the type IVa pilus motors.* Nat Commun, 2017. **8**: p. 15091.

127. McCallum, M., et al., *Multiple conformations facilitate PilT function in the type IV pilus.* Nat Commun, 2019. **10**(1): p. 5198.

128. Ellison, C.K., et al., *Real-time microscopy and physical perturbation of bacterial pili using maleimide-conjugated molecules.* Nat Protoc, 2019. **14**(6): p. 1803-1819.

129. Ellison, C.K., et al., *Retraction of DNA-bound type IV competence pili initiates DNA uptake during natural transformation in Vibrio cholerae.* Nat Microbiol, 2018. **3**(7): p. 773-780.

130. Bradley, D.E., *A study of pili on Pseudomonas aeruginosa.* Genet. Res., 1972. **19**: p. 39-51.

131. Maier, B., et al., *Single pilus motor forces exceed 100 pN.* Proc Natl Acad Sci U S A, 2002. **99**(25): p. 16012-7.

132. Biais, N., et al., *Cooperative retraction of bundled type IV pili enables nanonewton force generation.* PLoS Biol, 2008. **6**(4): p. e87.

133. Semmler, A.B., C.B. Whitchurch, and J.S. Mattick, *A re-examination of twitching motility in Pseudomonas aeruginosa.* Microbiology (Reading), 1999. **145 (Pt 10)**: p. 2863-73.

134. Tala, L., et al., *Pseudomonas aeruginosa orchestrates twitching motility by sequential control of type IV pili movements.* Nat Microbiol, 2019. **4**(5): p. 774-780.

135. Huang, B., C.B. Whitchurch, and J.S. Mattick, *FimX, a multidomain protein connecting environmental signals to twitching motility in Pseudomonas aeruginosa.* J Bacteriol, 2003. **185**(24): p. 7068-76.

136. Pamp, S.J. and T. Tolker-Nielsen, *Multiple roles of biosurfactants in structural biofilm development by Pseudomonas aeruginosa.* J Bacteriol, 2007. **189**(6): p. 2531-9.

137. Holz, C., et al., *Multiple pilus motors cooperate for persistent bacterial movement in two dimensions.* Phys Rev Lett, 2010. **104**(17): p. 178104.

138. Gorzelnik, K.V., et al., *Asymmetric cryo-EM structure of the canonical Allolevivirus Qbeta reveals a single maturation protein and the genomic ssRNA in situ.* Proc Natl Acad Sci U S A, 2016. **113**(41): p. 11519-11524.

139. Kannoly, S., Y. Shao, and I.N. Wang, *Rethinking the evolution of single-stranded RNA (ssRNA) bacteriophages based on genomic sequences and characterizations of two R-plasmid-dependent ssRNA phages, C-1 and Hgal1*. J Bacteriol, 2012. **194**(18): p. 5073-9.

140. Stockley, P.G., N.J. Stonehouse, and K. Valegard, *Molecular mechanism of RNA phage morphogenesis.* Int J Biochem, 1994. **26**(10-11): p. 1249-60.

141. Koning, R.I., et al., *Asymmetric cryo-EM reconstruction of phage MS2 reveals genome structure in situ.* Nat Commun, 2016. **7**: p. 12524.

142. Arutyunov, D. and L.S. Frost, *F conjugation: back to the beginning.* Plasmid, 2013. **70**(1): p. 18-32.

143. O'Callaghan, R., R. Bradley, and W. Paranchych, *The effect of M13 phage infection upon the F pili of E. coli.* Virology, 1973. **54**(1): p. 220-9.

144. Bradley, D.E. and J. Whelan, *Escherichia coli tolQ mutants are resistant to filamentous bacteriophages that adsorb to the tips, not the shafts, of conjugative pili.* J Gen Microbiol, 1989. **135**(7): p. 1857-63.

145. Guzman, L.M., et al., *Tight regulation, modulation, and high-level expression by vectors containing the arabinose PBAD promoter.* J Bacteriol, 1995. **177**(14): p. 4121-30.

146. Datsenko, K.A. and B.L. Wanner, *One-step inactivation of chromosomal genes in Escherichia coli K-12 using PCR products.* Proc Natl Acad Sci U S A, 2000. **97**(12): p. 6640-5.

147. Guyer, M.S., et al., *Identification of a sex-factor-affinity site in E. coli as gamma delta.* Cold Spring Harb Symp Quant Biol, 1981. **45**: p. 135-40.

148. Strauss, J.H., Jr. and R.L. Sinsheimer, *Purification and properties of bacteriophage MS2 and of its ribonucleic acid.* J Mol Biol, 1963. **7**: p. 43-54.

149. Baba, T., et al., *Construction of Escherichia coli K-12 in-frame, single-gene knockout mutants: the Keio collection.* Mol Syst Biol, 2006. **2**: p. 2006 0008.

150. Danziger, R.E. and W. Paranchych, *Stages in phage R17 infection. 3. Energy requirements for the F-pili mediated eclipse of viral infectivity.* Virology, 1970. **40**(3): p. 554-64.

151. Skinner, S.O., et al., *Measuring mRNA copy number in individual Escherichia coli cells using single-molecule fluorescent in situ hybridization.* Nat Protoc, 2013. **8**(6): p. 1100-13.

152. Biebricher, C.K. and E.M. Duker, *Light-microscopic visualization of F and type 1 pili.* J Gen Microbiol, 1984. **130**(4): p. 941-9.

153. Daehnel, K., et al., *Fluorescence assays for F-pili and their application.* Microbiology, 2005. **151**(Pt 11): p. 3541-8.

154. Zeng, L., et al., *Decision making at a subcellular level determines the outcome of bacteriophage infection.* Cell, 2010. **141**(4): p. 682-91.

155. Zhang, K., R. Young, and L. Zeng, *Bacteriophage P1 does not show spatial preference when infecting Escherichia coli.* Virology, 2020. **542**: p. 1-7.

156. Moore, D., B.A. Sowa, and K. Ippen-Ihler, *The effect of tra mutations on the synthesis of the F-pilin membrane polypeptide.* Mol Gen Genet, 1981. **184**(2): p. 260-4.

157. Brinton, C.C., Jr., P. Gemski, Jr., and J. Carnahan, *A New Type of Bacterial Pilus Genetically Controlled by the Fertility Factor of E. Coli K 12 and Its Role in Chromosome Transfer.* Proc Natl Acad Sci U S A, 1964. **52**: p. 776-83.

158. Brinton, C.C., Jr. and H. Beer, *The Interaction of Male-Specific Bacteriophages with F Pili.* The Molecular Biology of Viruses, 1967: p. 251-289.

159. Lang, S., et al., *An activation domain of plasmid R1 TraI protein delineates stages of gene transfer initiation.* Mol Microbiol, 2011. **82**(5): p. 1071-85.

160. Willetts, N. and M. Achtman, *Genetic analysis of transfer by the Escherichia coli sex factor F, using P1 transductional complementation.* J Bacteriol, 1972. **110**(3): p. 843-51.

161. Achtman, M., N. Willetts, and A.J. Clark, *Beginning a genetic analysis of conjugational transfer determined by the F factor in Escherichia coli by isolation and characterization of transfer-deficient mutants.* J Bacteriol, 1971. **106**(2): p. 529-38.

162. Bidlack, J.E. and P.M. Silverman, *An active type IV secretion system encoded by the F plasmid sensitizes Escherichia coli to bile salts.* J Bacteriol, 2004. **186**(16): p. 5202-9.

163. Shiba, T. and T. Miyake, *New type of infectious complex of E. coli RNA phage.* Nature, 1975. **254**(5496): p. 157-8.

164. Harb, L., et al., *ssRNA Phage Penetration Triggers Detachment of the F-Pilus* Proc Natl Acad Sci U S A, 2020.

165. Oliveira, N.M., K.R. Foster, and W.M. Durham, *Single-cell twitching chemotaxis in developing biofilms.* Proc Natl Acad Sci U S A, 2016. **113**(23): p. 6532-7.

166. Kuhn, M.J., et al., *Mechanotaxis directs Pseudomonas aeruginosa twitching motility.* Proc Natl Acad Sci U S A, 2021. **118**(30).

167. Adams, D.W., et al., *The type IV pilus protein PilU functions as a PilT-dependent retraction ATPase.* PLoS Genet, 2019. **15**(9): p. e1008393.

168. Stern, A. and R. Sorek, *The phage-host arms race: shaping the evolution of microbes.* Bioessays, 2011. **33**(1): p. 43-51.

169. Suttle, C.A., *Marine viruses--major players in the global ecosystem.* Nat Rev Microbiol, 2007. **5**(10): p. 801-12.

170. Fuhrman, J.A., *Marine viruses and their biogeochemical and ecological effects.* Nature, 1999. **399**(6736): p. 541-8.

171. Danovaro, R., et al., *Marine viruses and global climate change.* FEMS Microbiol Rev, 2011. **35**(6): p. 993-1034.

172. Worden, R.P., *A speed limit for evolution.* J Theor Biol, 1995. **176**(1): p. 137-52.

173. Chao, L., C.U. Rang, and L.E. Wong, *Distribution of Spontaneous Mutants and Inferences about the Replication Mode of the RNA Bacteriophage φ6.* Journal of Virology, 2002. **76**(7): p. 3276-3281.

174. Bull, J.J., et al., *Experimental Molecular Evolution of Bacteriophage T7.* Evolution, 1993. **47**(4): p. 993-1007.

175. Lazaro, E., et al., *Evolutionary adaptation of an RNA bacteriophage to the simultaneous increase in the within-host and extracellular temperatures.* Sci Rep, 2018. **8**(1): p. 8080.

176. Garcia-Villada, L. and J.W. Drake, *Experimental selection reveals a trade-off between fecundity and lifespan in the coliphage Qss.* Open Biol, 2013. **3**(6): p. 130043.

177. Haft, R.J., et al., *In vivo oligomerization of the F conjugative coupling protein TraD.* J Bacteriol, 2007. **189**(18): p. 6626-34.

178. Lu, J., et al., *Structural basis of specific TraD-TraM recognition during F plasmid-mediated bacterial conjugation.* Mol Microbiol, 2008. **70**(1): p. 89-99.

179. Alvarez-Rodriguez, I., et al., *Conjugative Coupling Proteins and the Role of Their Domains in Conjugation, Secondary Structure and in vivo Subcellular Location.* Front Mol Biosci, 2020. **7**: p. 185.

180. Errington, J., J. Bath, and L.J. Wu, *DNA transport in bacteria.* Nat Rev Mol Cell Biol, 2001. **2**(7): p. 538-45.

181. Lu, J., et al., *Analysis and characterization of the IncFV plasmid pED208 transfer region.* Plasmid, 2002. **48**(1): p. 24-37.

182. Al Mamun, A.A.M., K. Kishida, and P.J. Christie, *Protein Transfer through an F Plasmid-Encoded Type IV Secretion System Suppresses the Mating-Induced SOS Response.* mBio, 2021. **12**(4): p. e0162921.

183. Lang, S. and E.L. Zechner, *General requirements for protein secretion by the F-like conjugation system R1.* Plasmid, 2012. **67**(2): p. 128-38.

184. Fernandez-Lopez, R., et al., *Comparative Genomics of the Conjugation Region of F-like Plasmids: Five Shades of F.* Front Mol Biosci, 2016. **3**: p. 71.

185. Wong, J.J., et al., *Structural basis of cooperative DNA recognition by the plasmid conjugation factor, TraM.* Nucleic Acids Res, 2011. **39**(15): p. 6775-88.

186. Lang, S., et al., *Common requirement for the relaxosome of plasmid R1 in multiple activities of the conjugative type IV secretion system.* J Bacteriol, 2014. **196**(11): p. 2108-21.

187. Rice, P., I. Longden, and A. Bleasby, *EMBOSS: the European Molecular Biology Open Software Suite.* Trends Genet, 2000. **16**(6): p. 276-7.

188. Schoulaker, R. and H. Engelberg-Kulka, *Escherichia coli mutant temperature sensitive for group I RNA bacteriophages.* J Virol, 1978. **25**(1): p. 433-5.

189. Zechner, E.L., S. Lang, and J.F. Schildbach, *Assembly and mechanisms of bacterial type IV secretion machines.* Philos Trans R Soc Lond B Biol Sci, 2012. **367**(1592): p. 1073-87.

190. Yonekura, K., S. Maki-Yonekura, and M. Homma, *Structure of the flagellar motor protein complex PomAB: implications for the torque-generating conformation.* J Bacteriol, 2011. **193**(15): p. 3863-70.

191. Scharf, B.E., et al., *Control of direction of flagellar rotation in bacterial chemotaxis.* Proc Natl Acad Sci U S A, 1998. **95**(1): p. 201-6.

192. Kuwajima, G., *Construction of a minimum-size functional flagellin of Escherichia coli.* J Bacteriol, 1988. **170**(7): p. 3305-9.

193. Yang, J., et al., *Biphasic chemotaxis of Escherichia coli to the microbiota metabolite indole.* Proc Natl Acad Sci U S A, 2020. **117**(11): p. 6114-6120.

194. Querido, E. and P. Chartrand, *Using fluorescent proteins to study mRNA trafficking in living cells.* Methods Cell Biol, 2008. **85**: p. 273-92.

195. Filonov, G.S., et al., *Broccoli: rapid selection of an RNA mimic of green fluorescent protein by fluorescence-based selection and directed evolution.* J Am Chem Soc, 2014. **136**(46): p. 16299-308.

196. Zinder, N.D., *RNA phages*. Cold Spring Harbor monograph series. 1975, Cold Spring Harbor, N.Y.: Cold Spring Harbor Laboratory. viii, 428 p.

197. Schoulaker-Schwarz, R. and H. Engelberg-Kulka, *Effect of an Escherichia coli traD (ts) mutation on MS2 RNA replication.* J Gen Virol, 1983. **64 (Pt 1)**: p. 207-10.